Universidad de Concepción
Dirección de Postgrado
Facultad de Ciencias Físicas y Matemáticas
Programa de Doctorado en Ciencias Aplicadas
con Mención en Ingeniería Matemática

MÉTODOS DE GALERKIN DISCONTINUO HIBRIDIZABLE ADAPTIVOS Y DE ALTO ORDEN EN MECÁNICA DE FLUIDOS

(ADAPTIVE AND HIGH ORDER HYBRIDIZABLE DISCONTINUOUS GALERKIN METHODS IN FLUID MECHANICS)

Tesis para optar al grado de Doctor en Ciencias
Aplicadas con mención en Ingeniería Matemática

Patrick Andrés Vega Román
concepción-chile
2018

Profesor Guía: Manuel Solano Palma
CI²MA y Departamento de Ingeniería Matemática
Universidad de Concepción, Chile

Cotutor 1: Rodolfo Araya Durán
CI²MA y Departamento de Ingeniería Matemática
Universidad de Concepción, Chile

Cotutor 2: Weifeng Qiu
Department of Mathematics
City University of Hong Kong, Hong Kong, China

Adaptive and High Order Hybridizable Discontinuous Galerkin Methods in Fluid Mechanics

Patrick Andrés Vega Román

Director de Tesis:	Prof. Manuel Solano, Universidad de Concepción, Chile.
Codirectores de Tesis:	Prof. Rodolfo Araya, Universidad de Concepción, Chile.
	Prof. Weifeng Qiu, City University of Hong Kong, Hong Kong, China.
Director de Programa:	Prof. Rodolfo Rodríguez, Universidad de Concepción, Chile.

Comisión evaluadora

Prof. Bernardo Cockburn, University of Minnesota, USA.

Prof. Alexandre Ern, Université Paris-Est, ENPC and INRIA, France.

Prof. Guosheng Fu, Brown University, USA.

Prof. Francisco-Javier Sayas, University of Delaware, USA.

Prof. Wujun Zhang, Rutgers University, USA.

Comisión examinadora

Firma: _____
Prof. Rodolfo Araya, Universidad de Concepción, Chile.

Firma: _____
Prof. Rommel Bustinza, Universidad de Concepción, Chile.

Firma: _____
Prof. Norbert Heuer, Pontificia Universidad Católica de Chile, Chile.

Firma: _____
Prof. Luis Gatica, Universidad Católica de la Santísima Concepción, Chile.

Firma: _____
Prof. Manuel Solano, Universidad de Concepción, Chile.

Calificación: _____

Concepción, 28 de Noviembre de 2018

Abstract

The aim of this thesis is to contribute to the development of hybridizable discontinuous Galerkin (HDG) methods to solve partial differential equations arising from fluid mechanics.

First, we propose a novel technique to solve elliptic problems involving a non-polygonal interface/boundary. It is based on a high order HDG method where the mesh does not exactly fit the domain. We first study the case of a curved-boundary value problem with mixed boundary conditions. On the computational boundary, the Dirichlet data is approximated by using a transferring technique and the treatment of the Neumann data is based on extrapolating the approximation of the gradient. We then extend these ideas to curved interfaces. We provide numerical results suggesting that optimal high order convergence is achieved if the computational domain is constructed by interpolating the boundary/interface using piecewise linear segments.

Next, we introduce and analyze an HDG method for the gradient-velocity-pressure formulation of the Brinkman problem. We present an *a priori* error analysis of the method, showing optimal order of convergence of the error. We also introduce an *a posteriori* error estimator, of the residual type, which helps us to improve the quality of the numerical solution. We establish reliability and local efficiency of our estimator for the natural norms, with constants written explicitly in terms of the physical parameters and independent of the meshsize. In particular, our results are also valid for the Stokes problem. Finally, we provide numerical experiments showing the quality of our adaptive scheme.

At last, we propose a residual type *a posteriori* error estimator for an HDG method applied to the Oseen problem with unknowns as in the Brinkman problem. Similarly to the Brinkman problem, we prove reliability and local efficiency keeping track on the parameters dependence. For both Brinkman and Oseen problems we use the approximation properties of the Oswald interpolation operator and, for the last one, we employ a weighted function technique to control the L^2-error of the velocity. Numerical experiments in three dimensions illustrate the quality of our adaptive scheme.

Resumen

El objetivo de esta tesis es contribuir al desarrollo de métodos de Galerkin discontinuo hibridizables (HDG por su sigla en inglés) para resolver ecuaciones diferenciales parciales provenientes de la mecánica de fluidos.

En primer lugar, proponemos una técnica novedosa para resolver problemas elípticos que involucran una interfaz/frontera no poligonal. Se basa en un método HDG de alto orden en el que la malla no se ajusta exactamente al dominio. Primero estudiamos el caso de un problema de valor de frontera curva con condiciones de borde mixtas. En la frontera computacional, el dato Dirichlet se aproxima utilizando una técnica de transferencia y el tratamiento del dato Neumann se basa en la extrapolación de la aproximación del gradiente. Luego, extendemos estas ideas a interfaces curvas. Proporcionamos resultados numéricos que sugieren orden de convergencia óptimo, de alto orden, si el dominio computacional es construido mediante la interpolación de la frontera/interfaz utilizando segmentos lineales por trozos.

A continuación, presentamos y analizamos un método HDG para la formulación gradiente-velocidad-presión del problema Brinkman. Realizamos un análisis de error *a priori* del método, que muestra el orden óptimo de convergencia del error. También presentamos un estimador de error *a posteriori*, del tipo residual, que nos ayuda a mejorar la calidad de la solución numérica. Establecemos confiabilidad y eficiencia local de nuestro estimador para las normas naturales con constantes escritas explícitamente en términos de los parámetros físicos e independientes del tamaño de la malla. En particular, nuestros resultados también son válidos para el problema de Stokes. Finalmente, proporcionamos experimentos numéricos que muestran la calidad de nuestro esquema adaptivo.

Por último, proponemos un estimador de error *a posteriori* residual para un método HDG aplicado al problema de Oseen con ingógnitas como las del problema de Brinkman. Al igual que en el problema de Brinkman, probamos confiabilidad y la eficiencia local restreando la dependencia en los parámetros. Tanto para el problema de Brinkman como para el de Oseen usamos las propiedades de aproximación del operador de interpolación Oswald y, para el último, empleamos una técnica de función ponderada para controlar el error L^2 de la velocidad. Experimentos numéricos en tres dimensiones ilustran la calidad de nuestro esquema de adaptación.

Agradecimientos

En primer lugar, agradezco a Dios por ser quien guía mis pasos y me da la fuerza para seguir adelante en lo que me proponga. A mis padres, Elsa y Patricio, porque sin la formación que me dieron y el amor que siempre me han dado, nada de esto sería posible.

A Daniela, Iván, Yolanda, Carol, Maite, Gustavo, Tomás y a todos quienes son parte de mi familia, por ser parte de mis alegrías cada vez que visito mi tierra natal. A mi abuelita Raquel, que partió mientras escribía esta tesis, por todo lo que nos diste a mi y mi familia.

A mi director de tesis, el profesor Manuel Solano, por su infinita paciencia, su buena disposición, por ser un ejemplo de como seguir este camino que estoy comenzando, siendo un gran investigador, un gran docente y, por sobre todo, una gran persona. Gracias por confiar en mi al aceptar dirigir esta tesis.

Al profesor Rodolfo Araya, mi cotutor, quien ha sido un apoyo fundamental en el desarrollo de esta tesis. Por su paciencia, consejos y buen humor, que junto al apoyo y confianza puesta en mi han sido vitales durante el desarrollo de esta tesis. Siento que formamos un buen equipo.

To professor Weifeng Qiu, also my co-advisor, for his hospitality during my research visit to the City University of Hong Kong. Thanks for his advices and constructive criticisms.

I would like to thank professors Bernardo Cockburn, Alexandre Ern, Guosheng Fu, Francisco-Javier Sayas and Wujun Zhang for being on my evaluating committee. I am also very thankful to professors Rommel Bustinza, Norbert Heuer and Luis F. Gatica for being on my examination committee. Thanks to them for constructive criticism leading to a better presentation of the material in this thesis.

A Ernesto, Vanessa, Cristóbal y Sebastián, quienes han sido mi familia en Concepción. Gracias por hacer todo más llevadero con su apoyo en las buenas, las malas, por cada recuerdo, cada tarde-noche-mañana que compartimos. Un abrazo a Ernesto a la distancia.

A mis amigos Belén, Pancha, Darío, Julio, Nayda, Fepo, Jimmy, Víctor (Osoreh), Gabriel, Gabi, Raúl, Ale y quienes se me queden en el tintero, por cada vez que podemos compartir un buen momento, o uno malo, da igual, la cosa es compartirlo.

A mis compañeros del CI^{2}MA, en especial, además de los ya mencionados, a Elvis, Daniel, Joaquín, Felipe Vargas, Cinthya, Sergio y David, con quienes compartí discusiones académicas y tantos otros buenos momentos. De una u otra forma fueron un apoyo para mi.

A Yazmina Rojas, por ser un pilar fundamental en mi vida, en su momento.

Al profesor Gabriel Gatica, en su calidad de director del CI^{2}MA, por hacer más cómodo nuestro

trabajo y por el apoyo que se nos ha dado durante nuestro paso por dicho centro. Al profesor Raimund Bürger, en su calidad de director de programa durante gran parte de mis estudios, por sus gestiones y dedicación en la realización de dicha labor. Al profesor Rodolfo Rodríguez, con quien trabajé en mi tesis de pregrado, por guiarme en mis primeros pasos. Al profesor Freddy Paiva por sus consejos y buen sentido del humor.

Al personal administrativo del CI^{2}MA y el Departamento de Ingeniería Matemática, por su buena disposición, en especial a la Sra. Lorena Carrasco y a José Parra.

Finalmente, pero no por esomenos importantes, a las instituciones que apoyaron y financiaron mis estudios doctorales. A la Comisión Nacional de Investigación y Tecnologiía (CONICYT) del gobierno de Chile quien a través de la beca PCHA/Doctorado Nacional/2014-21140137 y el proyecto AFB170001 del programa PIA: Concurso Apoyo a Centros Científicos y Tecnológicos de Excelencia con Financiamiento Basal. A la Universidad de Concepción, en particular al Centro de Investigación en Ingeniería Matemática (CI^{2}MA) por el espacio físico y financiamiento complementario, al Departamento de Ingeniería Matemática, por apoyo financiero para asistencia a eventos, y a la Dirección de Postgrado por cursos de inglés y de perfeccionamiento docente.

Patrick Andrés Vega Román

Contents

List of Tables

List of Figures

Introduction

Applications in areas such as biology, engineering (mechanical, civil, chemical, biomedical), geophysics and astrophysics, to name a few, motivate the development of mathematical tools to solve partial differential equations (PDEs). In particular, we are interested in problems arising from fluid mechanics, which is the branch of continuum mechanics that studies the behavior of fluids (liquids, gases and plasmas) and the forces that act on them.

The complexity of these problems, from the mathematical point of view, can be translated into the impossibility of their resolution through purely analytic tools, opening a way to the development and study of numerical methods for their resolution. Among them, the finite element method and the finite volume method. The first is particularly useful when the geometry of the problem is complex and when the exact solution is sufficiently regular, but presents difficulties both in the treatment of interior and boundary layers and in the discontinuities of solutions of non-linear hyperbolic equations. On the other hand, the finite volume method can deal with the above mentioned problems, through piecewise constant and discontinuous approximations, which in turn constitutes a disadvantage for its low order accuracy.

The *discontinuous Galerkin* (DG) method, introduced by Reed and Hill in 1973 [98], uses the ideas of finite element and finite volume methods to solve PDEs numerically, based on piecewise polynomial and discontinuous approximations, which are robust and have high order precision, being able to deal with interior and boundary layers, discontinuous solutions or with steep gradients. The above features make the DG methods suitable for problems that arise, in particular, from fluid mechanics. Moreover, the DG method gives us flexibility in the design of the mesh (hanging nodes, non-conformity, anisotropy), the use of variable polynomial degree by element, adaptive schemes and parallelization of the calculations in its computational implementation. A more detailed bibliographic discussion on the DG method can be found in [52, 53].

Let us briefly describe the historic perspective of the development of hybridizable discontinuous Galerkin (HDG) methods. The main criticism of DG methods is due to the fact that they have too many globally coupled degrees of freedom. In order to overcome this drawback, Cockburn, Gopalakrishnan and Lazarov [32] introduced a unifying framework for hybridization of DG methods for diffusion problems, where the only globally coupled degrees of freedom are those of the numerical traces on the inter-element boundaries. The remaining unknowns are then obtained by solving local problems on each element. To be more precise, at the continuous level, the intra-element variables can be written in terms of the unknowns in the skeleton of the triangulation. These problems, called local solvers, can be discretized by a DG method, generating a family of schemes named HDG methods. In particular, if the local solvers are approximated by the local discontinuous Galerkin (LDG) method introduced in

[40], the resulting scheme is called LDG-hybridizable (LDG-H) as explained in [32].

In the literature, the most commonly used HDG schemes are, indeed, the LDG-H methods. Using a special projection, Cockburn, Dong and Guzmán [28] proved optimal order of convergence for a type of LDG-H method where the stabilization parameter is set to be zero in all but one face of each element. In addition, they also provided an element-by-element postprocessing of the approximated solution having superconvergence properties. A larger class of LDG-H methods were analyzed in [36] by also using special projections. Later, [34] simplified the analysis of these methods by using a technique based on a suitable designed projection inspired by the form of the numerical traces.

Besides diffusion equations, in the context of fluid mechanics, HDG methods have been developed for a wide variety of problems such as convection-diffusion equation [17, 24, 25, 29, 42, 62, 76, 87, 88, 95], Stokes flow [31, 33, 38, 89], quasi-Newtonian Stokes flow [65, 66], Stokes-Darcy coupling [67], Brinkman problem [61, 68], Oseen problem [21] and Navier–Stokes equations [22, 69, 90, 93, 94, 96, 99], just to name a few. In addition, hybrid high-order (HHO) methods have appeared recently [48]; these methods are closely related to HDG methods as shown in [30].

On the other hand, in the context of adaptivity, few contributions on the development of *a posteriori* error estimators for HDG methods can be found in the literature. Certainly, *a posteriori* error analyses of DG methods have been extensively studied. Indeed, in the context of error control in energy-like norms, we refer to [1, 3, 11, 27, 54, 57, 58, 59, 60] for equilibrated error estimators, [10, 16, 74, 78, 79, 105] for residual type estimators, [46, 47] for estimators based on gradient recovery by averaging and [83] for functional *a posteriori* error estimates. *A posteriori* error estimates to control the L^2-error of the scalar variable can be found in [20, 100]. In addition, unified frameworks of error control have been developed in [19, 86]. The first *a posteriori* error analysis for HDG methods was carried out in [43] for an LDG-H method applied to a diffusion problem. There, the authors proposed an efficient and reliable residual-based estimator that controls the error in $\boldsymbol{q}$, the gradient of the scalar variable u, which only depends on the data oscillation and on the difference between the trace of the approximation of u and its corresponding numerical trace. The construction of this estimator relies in two key ingredients. The first one is the use of an element-by-element postprocessing of the scalar variable u having superconvergence properties. The second ingredient is the Oswald interpolation operator [12, 56, 92] that provides a continuous approximation of a discontinuous piecewise polynomial function. Based on this technique, [44] presented a unified *a posteriori* error analysis for diffusion problems. There, the authors provided an efficient and reliable error estimator for the L^2-norm of $\boldsymbol{q} - \widetilde{\boldsymbol{q}}_h$, where $\widetilde{\boldsymbol{q}}_h$ is any approximation of the flux $\boldsymbol{q}$ satisfying certain conditions (see Section 2.3.1 in [44] for details). That framework is employed to obtain *a posteriori* error indicators for a wide class of method and recover well-known error estimates for mixed methods and the continuous Galerkin method. In the context of the convection-dominated diffusion equation, [23] proposed a reliable and locally efficient residual-based error estimator for the HDG method presented in [62], that controls the error measured in an energy norm. This estimator is robust in the sense of that the bounds of error are uniform with respect to the diffusion coefficient. The authors also employed the Oswald interpolant and considered a weighted auxiliary function technique to control the L^2-norm of the scalar solution. However, they did not use the postprocessing technique mentioned above since there is no superconvergence result for the HDG methods when the diffusion parameter is too small. When we bounding the error in the energy norm, the standard approach is to use the global inf-sup condition associated to the continuous

variational formulation which makes possible to directly bound the error in terms of the residuals. This needs to be done carefully if applied to HDG methods since the spaces are not necessarily conforming. In this direction, [66] proposed an error estimator for an augmented HDG method applied to a class of quasi-Newtonian Stokes flows in velocity gradient-pseudostress-velocity formulation. There, in order to be able to use the global inf-sup condition of the continuous problem, the numerical trace of the velocity is eliminated from the scheme by expressing it in terms of the intra-element unknowns, obtaining an equivalent discrete formulation. Moreover, the discontinuous approximation is postprocessed to construct an $\mathrm{H}(\mathrm{div}, \Omega)$-conforming approximation of the pseudostress that is used to construct an efficient and reliable residual-based error estimator. In addition, [68] employed similar techniques to propose an error estimator for an HDG method applied to the Brinkman problem in a pseudostress-velocity formulation. Furthermore, the first fully computable *a posteriori* error bounds for HDG methods have been recently presented in [2].

The present work is organized as follows. In Chapter 1, we propose a technique to numerically solve second order elliptic problems in domains Ω which are not necessarily polygonal. In addition, we deal with domains divided in two regions by a curved interface Σ. In particular we use an HDG method where the computational domain does not exactly fit the curved boundary or interface. The main motivation of this technique is being able to achieve high order accuracy avoiding the use of meshes with curved elements.

This work focuses, first, on the treatment of part of the boundary where a Neumann data is prescribed. It is important to understand this situation in order to extend the ideas to problems having a curved interface. In fact, the transmission conditions at the interface involve jumps of the scalar variable and jumps of the normal component of the flux. The jump of the scalar variable can be treated considering the *transferring* technique of [41] and the jump of the normal component of the flux can be handled using the *extrapolation* method for the Neumann data that we will describe in the following sections.

Since most of the methods based on linear fitting of the boundary/interface are only second order accurate, we believe our method constitutes a competitive alternative.

The contents of this chapter were published in the following work:

[97] Qiu W., Solano M. and Vega P., *A high order HDG method for curved-interface problems via approximation from straight triangulations.* **J. Sci. Comput.**, vol. 69, 3, pp. 1384–1407, (2016).

In Chapter 2, we introduce an HDG method for Brinkman equations, where the unknowns are the velocity, pressure and the gradient of the velocity, and its *a priori* and *a posteriori* error analysis. Even though the Stokes case has been introduced and analyzed in [33], without an *a posteriori* analysis, for the sake of completeness of this manuscript, we use the procedure in [33] to analyse the Brinkman problem. In the *a posteriori* error analysis we propose a reliable and locally efficient residual-based *a posteriori* error estimator for both Brinkman and Stokes problems, using the Oswald interpolation operator and a postprocessing technique. As we will see in Section 2.1.2, we propose a *new* postprocessed approximation of the velocity suited to the Brinkman problem, that will helps us in the construction of the estimator. In addition, all the constants in the estimates are written explicitly in terms of the physical parameters α and ν.

The contents of this chapter have been recently published in the following work:

[4] Araya, R., Solano, M. and Vega, P., *Analysis of an adaptive HDG method for the Brinkman problem.* **IMA J. Numer. Anal.**, dry031, (2018).

In Chapter 3, we propose a reliable and locally efficient residual-based *a posteriori* error estimator applied to an HDG method for Oseen equations, where the unknowns are the velocity, pressure and the gradient of the velocity. For this, we use the Oswald interpolation operator, a postprocessing technique and a weighted function technique to control the L^2- error of the velocity. Additionally, we keep track the dependence on the physical parameters ν and $\boldsymbol{\beta}$.

The contents of this chapter can be found in the following preprint, and it has been submitted to a peer-reviewed journal:

[5] Araya, R., Solano, M. and Vega, P., *A posteriori error analysis of an HDG method for the Oseen problem.* Preprint 2018-40, Centro de Investigación en Ingeniería Matemática (CI^{2}MA), Universidad de Concepción, Chile.

The two-dimensional numerical implementation of the methods presented in this work was completely developed in `MATLAB`. For simulations in three dimensions, we used as a base the tools in [63]. `Paraview` was employed for visualization.

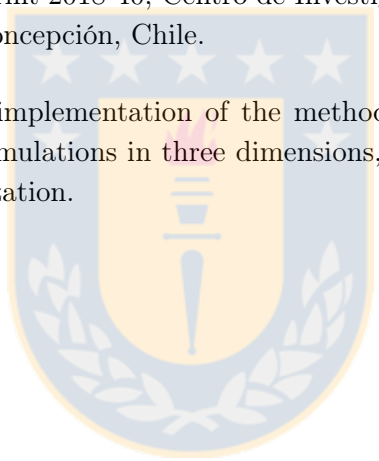

Introducción

Aplicaciones en áreas tales como biología, ingeniería (mecánica, civil química, biomédica), geofísica y astrofísica, por nombrar unas pocas, motivan el desarrollo de herramientas matemáticas para resolver ecuaciones diferenciales parciales (PDEs por su sigla en inglés). En particular, estamos interesados in problemas provenientes de la mecánica de fluidos, que es una rama de la mecánica de medios continuos que estudia el comportamiento de los fluidos (líquidos, gases y plasmas) y las fuerzas que actuan sobre ellos.

La complejidad de estos problemas, desde el punto de vista matemático, puede traducirse en la imposibilidad de su resolución mediante herramientas puramente analíticas, dando paso así al desarrollo y estudio de métodos numéricos para su resolución. Entre ellos el método de elementos finitos y el método de volúmenes finitos. El primero es particularmente útil cuando la geometría del problema es compleja y cuando la solución exacta es suficientemente regular, pero presenta dificultades tanto en el tratamiento de capas interiores y límites como en las discontinuidades propias de soluciones de ecuaciones hiperbolicas no-lineales. Por otro lado, el método de volumenes finitos puede lidiar con los problemas antes mencionados, a través de aproximaciones por constantes a trozos y discontinuas, que a su vez contituye una desventaja por su precisión de bajo orden.

El *método de Galerkin discontinuo* (DG por su sigla en inglés), introducido por Reed y Hill en 1973 [98], usa las ideas de los métodos de elementos finitos y volumenes finitos para resolver PDEs numéricamente, basados en aproximaciones polinomiales a trozos y discontinuas, que son robustas y con precisión de alto orden, permitiendo tratar con capas interiores y límites, soluciones discontinuas o con gradientes escarpados. Las características anteriores hacen que el método DG sea apropiado para tratar problemas que surgen, en particular, de la mecánica de fluidos. Además, el método nos da flexibilidad en el diseño de la malla (nodos colgantes, no-conformidad, anisotropía), el uso de grado polinomial variable por elemento, esquemas adaptivos y paralelización de los cálculos en su implementación computacional. Una discusión bibliográfica más detallada sobre el método DG puede ser encontrada en [52, 53].

Describamos brevemente la perspectiva histórica del desarrollo de los métodos de Galerkin discontinuo hybridizable (HDG por su sigla en inglés). La principal crítica de los métodos DG se debe al hecho de que tienen demasiados grados de libertad globalmente acoplados. Para superar este inconveniente, Cockburn, Gopalakrishnan y Lazarov [32] introdujeron un marco unificado para la hibridación de métodos DG para problemas de difusión, donde los únicos grados de libertad acoplados globalmente son los de las trazas numéricas en las fronteras entre elementos. Las incógnitas restantes se obtienen resolviendo problemas locales en cada elemento. Para ser más precisos, a nivel continuo, las variables dentro del elemento se pueden escribir en términos de incógnitas en el esqueleto de la triangulación.

Estos problemas, llamados *local solvers*, se pueden discretizar mediante un método DG, generando una familia de esquemas llamados métodos HDG. En particular, si los *local solvers* son aproximados por el método de Galerkin discontinuo local (LDG por su sigla en inglés) introducido en [40], el esquema resultante se llama LDG-hibridizable (LDG-H) como se explica en [32].

En la literatura, los esquemas HDG más comúnmente utilizados son, de hecho, los métodos LDG-H. Utilizando una proyección especial, Cockburn, Dong y Guzmán [28] demostraron orden óptimo de convergencia para un tipo de método LDG-H donde el parámetro de estabilización se fija como distinto de cero en una cara de cada elemento y cero en el resto. Además, proporcionaron también un postproceso elemento por elemento de la solución aproximada que tiene propiedades de superconvergencia. Una clase más amplia de métodos LDG-H fue analizada en [36] utilizando también proyecciones especiales. Más tarde, [34] simplificó el análisis de estos métodos mediante el uso de una técnica basada en una proyección, adecuadamente diseñada, inspirada en la forma de los trazas numéricas.

Además de las ecuaciones de difusión, en el contexto de la mecánica de fluidos, los métodos HDG han sido desarrollados para una amplia variedad de problemas, como la ecuación de convección-difusión [17, 24, 25, 29, 42, 62, 76, 87, 88, 95], flujo de Stokes [31, 33, 38, 89], flujo de Stokes cuasi-Newtoniano [65, 66], acoplamiento de Stokes-Darcy [67], problema de Brinkman [61, 68], problema de Oseen [21] y Navier-Stokes [22, 69, 90, 93, 94, 96, 99], por nombrar algunos. Adicionalmente, métodos híbridos de alto orden (HHO por su sigla en inglés) han aparecido recientemente [48]; estos métodos están cercanamente relacionados con lo métodos HDG como se muestra en [30].

Por otro lado, en el contexto de la adaptidad, pocas contribuciones sobre el desarrollo de estimadores de errores *a posteriori* para los métodos HDG pueden encontrarse en la literatura. Ciertamente, los análisis de error *a posteriori* de los métodos DG han sido ampliamente estudiados. De hecho, en el contexto del control de errores en normas similares a la de la energía, referimos a [1, 3, 11, 27, 54, 57, 58, 59, 60] para estimadores de error equilibrados, [10, 16, 74, 78, 79, 105] para estimadores de tipo residual, [46, 47] para estimadores basados en la recuperación del gradiente vía promediación y [83] para estimaciones de error *a posteriori* funcionales. Estimaciones de error de *a posteriori* para controlar el error L^2 de la variable escalar se pueden encontrar en [20, 100]. Además, se han desarrollado marcos unificados de control del error en [19, 86]. El primer análisis de error *a posteriori* para los métodos HDG se llevó a cabo en [43] para un método LDG-H aplicado a un problema de difusión. Allí, los autores propusieron un estimador residual eficiente y confiable que controla el error en $\boldsymbol{q}$, el gradiente de la variable escalar u, que sólo depende de la oscilación de datos y de la diferencia entre la traza de la aproximación de u y su correspondiente traza numérica. La construcción de este estimador se basa en dos ingredientes clave. El primero es el uso de un postprocesamiento elemento por elemento de la variable escalar u que tiene propiedades de superconvergencia. El segundo es el operador de interpolación de Oswald [12, 56, 92] que proporciona una aproximación continua de una función polinomial discontinua a trozos. Basado en esta técnica, [44] presentó un análisis de error *a posteriori* unificado para problemas de difusión. Allí, los autores proporcionaron un estimador de error eficiente y confiable para la norma L^2 de $\boldsymbol{q}-\widetilde{\boldsymbol{q}}_h$, donde $\widetilde{\boldsymbol{q}}_h$ es una aproximación del flujo $\boldsymbol{q}$ que cumple ciertas condiciones (ver Sección 2.3.1 en [44] para más detalles). Ese marco es empleado para obtener indicadores de error *a posteriori* para una amplia clase de métodos y también recuperar estimaciones de error conocidas para métodos mixtos y el método de Galerkin continuo. En el contexto de la ecuación de difusión con convección dominante, [23] propuso un estimador de error, basado en residuos, confiable y

localmente eficiente para el método HDG presentado en [62], que controla el error medido en una norma de energía. Este estimador es robusto en el sentido que las cotas de error son uniformes con respecto al coeficiente de difusión. Los autores también emplearon el interpolante de Oswald y consideraron una técnica de función auxiliar ponderada para controlar la norma L^2 de la solución escalar. Sin embargo, no utilizaron la técnica de posprocesamiento mencionada anteriormente, ya que no existe un resultado de superconvergencia para los métodos HDG cuando el parámetro de difusión es demasiado pequeño. Cuando acotamos el error en la norma de la energía, el enfoque estándar es usar la condición inf-sup global asociada a la formulación variacional continua que hace posible acotar directamente el error en términos de los residuos. Esto debe hacerse con cuidado si se aplica a los métodos HDG ya que los espacios no son necesariamente conformes. En esta dirección, [66] propuso un estimador de error para un método HDG aumentado aplicado a una clase de flujos de Stokes cuasi-Newtonianos en formulación gradiente de velocidad-pseudoesfuerzo-velocidad. Allí, para poder usar la condición inf-sup global del problema continuo, la traza numérica de la velocidad se elimina del esquema expresándola en términos de las incógnitas dentro del elemento, obteniendo una formulación discreta equivalente. Además, la aproximación discontinua se postprocesa para construir una aproximación $\mathrm{H}(\mathrm{div}, \Omega)$-conforme del pseudoesfuerzo que es usada para construir un estimador de error residual eficiente y confiable. Además, [68] empleó técnicas similares para proponer un estimador de error para zun método HDG aplicado al problema de Brinkman en una formulación de pseudoesfuerzo-velocidad. Por último, las primeras cotas de error *a posteriori* totalmente computables para métodos HDG han sido presentadas recientemente en [2].

El presente trabajo está organizado de la siguiente manera. En el Capítulo 1, proponemos una técnica para resolver numéricamente problemas elípticos de segundo orden en dominios Ω que son no necesariamente poligonales. Además, tratamos dominios divididos en dos regiones por una interfaz curva Σ. En particular, utilizamos un método HDG donde el dominio computacional no se ajusta exactamente a la frontera o interfaz curva. La principal motivación de esta técnica es lograr precisión de alto orden evitando el uso de mallas con elementos curvos.

Este trabajo se enfoca, primero, en el tratamiento de parte de la frontera donde se prescriben los datos de Neumann. Es importante entender esta situación para extender las ideas a los problemas que tienen una interfaz curva. De hecho, las condiciones de transmisión en la interfaz implican saltos de la variable escalar y saltos del componente normal del flujo. El salto de la variable escalar se puede tratar considerando la técnica de *transferencia* de [41] y el salto del componente normal del flujo se puede manejar utilizando el método *extrapolación* para los datos de Neumann que describiremos en las siguientes secciones.

Dado que la mayoría de los métodos basados en el ajuste lineal de la frontera/interfaz son sólo de presición de segundo orden, creemos que nuestro método constituye una alternativa competitiva.

El contenido de este capítulo fue publicado en el siguiente artículo:

[97] Qiu W., Solano M. and Vega P., *A high order HDG method for curved-interface problems via approximation from straight triangulations*. **J. Sci. Comput.**, vol. 69, 3, pp. 1384–1407, (2016).

En el Capítulo 2, presentamos un método HDG para la ecuación de Brinkman, donde las incógnitas son la velocidad, la presión y el gradiente de la velocidad, y su análisis de error *a priori* y *a*

posteriori. Si bien el caso de Stokes se ha introducido y analizado en [33], sin un análisis *a posteriori*, para completitud de esta tesis utilizaremos el procedimiento en [33] para analizar el problema de Brinkman. En el análisis de error *a posteriori*, proponemos un estimador de error residual confiable y localmente eficiente para los problemas de Brinkman y Stokes, utilizando el operador de interpolación de Oswald y una técnica de posprocesamiento. Como veremos en la Sección 2.1.2, proponemos una *nueva* aproximación posprocesada de la velocidad adecuada para el problema de Brinkman, que nos ayudará en la construcción del estimador. Además, todas las constantes en las estimaciones se escriben explícitamente en términos de los parámetros físicos α y ν.

El contenido de este capítulo ha sido publicado recientemente en siguiente artículo:

[4] Araya, R., Solano, M. and Vega, P., *Analysis of an adaptive HDG method for the Brinkman problem*. **IMA J. Numer. Anal.**, dry031, (2018).

En el Capítulo 3, proponemos un estimador de error *a posteriori*, basado en residuos, confiable y localmente eficiente, aplicado a un método HDG para las ecuaciones de Oseen, donde las incógnitas son la velocidad, presión y el gradiente de velocidad. Para ello, usamos el operador de interpolación de Oswald, una técnica de postprocesamiento y una técnica de función ponderada para controlar el error L^2 de la velocidad. Además, seguimos la dependencia de los parámetros físicos ν y $\boldsymbol{\beta}$.

El contenido de este capítulo puede ser encontrado en la siguiente pre-publicación, y ha sido sometido a una revista revisada por pares:

[5] Araya, R., Solano, M. and Vega, P., *A posteriori error analysis of an HDG method for the Oseen problem*. Preprint 2018-40, Centro de Investigación en Ingeniería Matemática (CI^{2}MA), Universidad de Concepción, Chile.

La implementación computacional bidimensional de los métodos presentados en este trabajo fueron completamente desarrolladas en `MATLAB`. Para las simulaciones en tres dimensiones, usamos como base las herramientas en [63]. `Paraview` fue empleado para visualización.

Preliminaries: notation and review of known results

We start by introducing common notations used throughout this thesis.

Let $\Omega \subseteq \mathbb{R}^d$, $d \in \{2,3\}$, denote a bounded domain with boundary $\Gamma = \overline{\Gamma}_D \cup \overline{\Gamma}_N$, with Γ_D, Γ_N, the Dirichlet and Neumann parts of Γ, respectively, such that $\Gamma_D \cap \Gamma_N = \emptyset$ and $|\Gamma_D| > 0$. In Chapter 1, Ω is not necessarily polygonal and we consider a polygonal domain Ω_h that approximates Ω and does not necessarily fit its boundary. Its boundary $\Gamma^h = \overline{\Gamma}_D^h \cup \overline{\Gamma}_N^h$ satisfies $\Gamma_D^h \cap \Gamma_N^h = \emptyset$ and $|\Gamma_D^h| > 0$, where Γ_D^h, Γ_N^h are parts of Γ^h with prescribed Dirichlet and Neumann data, respectively. We denote by $d(\Gamma, \Gamma^h)$ the distance between Γ and Γ^h. In the remaining chapters, Ω will be polygonal or polyhedral domain as appropriate.

Let $\{\mathcal{T}_h\}_{h>0}$ be a family of conforming triangulations, made of simplexes K, of the domain Ω (Chapter 2 and 3) or Ω_h (Chapter 1) that verifies the shape-regularity condition, i.e. there exists a positive constant σ such that $h_K/\rho_K \leq \sigma$ for all $K \in \mathcal{T}_h$ and for all $h := \max_{K\in\mathcal{T}_h} h_K > 0$, where h_K and ρ_K denote the diameter of K and the diameter of the largest ball inside K, respectively. Let h_e be the diameter of a face/edge e. From now on, we will use the word "face" even in the context of dimension two. We denote by $\mathcal{E}_h^i$ and by $\mathcal{E}_h^\partial$ the set of interior and boundary faces, respectively. We set $\mathcal{E}_h := \mathcal{E}_h^i \cup \mathcal{E}_h^\partial$, $\partial\mathcal{T}_h := \{\partial K : K \in \mathcal{T}_h\}$, $\omega_e := \{K \in \mathcal{T}_h : e \subset \partial K\}$.

We use the notation $(\cdot,\cdot)_K$ for the L^2-inner product on $K \in \mathcal{T}_h$, $\langle\cdot,\cdot\rangle_{\partial K}$ for the L^2-inner product on ∂K, and $\langle\cdot,\cdot\rangle_e$ for the L^2-inner product on $e \in \mathcal{E}_h$. Thus, for ξ and ψ we define

$$(\xi,\psi)_S = \sum_{K\in S}(\xi,\psi)_K, \quad \langle\xi,\psi\rangle_{\partial S} = \sum_{K\in S}\langle\xi,\psi\rangle_{\partial K} \quad \text{and} \quad \langle\xi,\psi\rangle_S = \sum_{e\in F}\langle\xi,\psi\rangle_e,$$

for $S \subseteq \mathcal{T}_h$ and $F \subseteq \mathcal{E}_h$. We will use bold and Roman letters to denote vector- and tensor-valued variables, respectively. For a tensor-valued function G and a vector-valued functions $\boldsymbol{v} = (v_i)_{i=1,d}$, $\boldsymbol{w} = (w_i)_{i=1,d}$, we set the gradient, divergence, tensor product and jump operators, as

$$\nabla\boldsymbol{v} := \left(\frac{\partial v_i}{\partial x_j}\right)_{i,j=1,d}, \qquad \nabla\cdot\boldsymbol{v} := \sum_{j=1}^{d}\frac{\partial v_j}{\partial x_j}, \qquad \boldsymbol{v}\otimes\boldsymbol{w} := (v_i w_j)_{i,j=1,d},$$

$$[\![\mathrm{G}]\!] := \begin{cases} \mathrm{G}^-\boldsymbol{n}^- + \mathrm{G}^+\boldsymbol{n}^+, & e \in \mathcal{E}_h \setminus \mathcal{E}_h^\partial \\ \mathbf{0}, & e \in \mathcal{E}_h^\partial \end{cases} \quad \text{and} \quad [\![\boldsymbol{v}]\!] := \begin{cases} \boldsymbol{v}^+ - \boldsymbol{v}^-, & e \in \mathcal{E}_h \setminus \mathcal{E}_h^\partial \\ \boldsymbol{v} - \boldsymbol{u}_D, & e \in \mathcal{E}_h^\partial \end{cases},$$

where $\boldsymbol{n}$ denotes the outward unit normal vector to ∂K. We note that the divergence operator for a tensor-valued function G is the above divergence operator acting along the rows of G. Let us also define, for $D \subseteq \mathcal{T}_h$,

$$|\!|\!| \boldsymbol{v} |\!|\!|_{1,D} := \left(\gamma\|\boldsymbol{v}\|_{0,D}^2 + \nu|\boldsymbol{v}|_{1,D}^2\right)^{1/2},$$

where $\|\cdot\|_{0,D}$ and $|\cdot|_{1,D}$ denote the L^2-norm and H^1-seminorm, respectively. Here, $\nu > 0$ will be the viscosity of the fluid (in Chapters 2-3) and $\gamma > 0$ is a coefficient that will be specified on each chapter. $\mathbb{P}_k(D)$ will denote the space of polynomials of total degree no greater than $k \in \mathbb{N} \cup \{0\}$, with D being a simplex or a face as appropriate. In addition, we introduce the broken polynomial and Sobolev spaces $\mathbb{P}_k(\mathcal{T}_h) := \{v \in L^2(\Omega) : v|_K \in \mathbb{P}_1(K) \ \ \forall K \in \mathcal{T}_h\}$ and $H^1(\mathcal{T}_h) := \{v \in L^2(\Omega) : v|_K \in H^1(K) \ \ \forall K \in \mathcal{T}_h\}$, respectively.

Finally, to simplify the notation, in what follows, we will use $a \preceq b$ to denote $a \leq Cb$, where C is a generic constant depending only on the shape regularity constant σ, the domain Ω and the polynomial degree k, but independent of h and the physical parameters of the equations.

As we will see, Chapters 2 and 3 are related. That is why, in the remaining of this section we summarize the common ingredients that we will need to prove the main results of these chapters.

First, in the context of the *a priori* error estimates in Chapter 2, we recall the projection Π_h defined in [33], that will allow us split the error into an approximation error plus a projection of the error. To be more precise, let $(\mathrm{L}, \boldsymbol{u}, p) \in [H^1(\mathcal{T}_h)]^{d\times d} \times [H^1(\mathcal{T}_h)]^d \times H^1(\mathcal{T}_h)$. Then, $\Pi_h(\mathrm{L}, \boldsymbol{u}, p) := (\Pi_{\mathrm{G}}\mathrm{L}, \Pi_{\boldsymbol{V}}\boldsymbol{u}, \Pi_P p) \in [\mathbb{P}_k(\mathcal{T}_h)]^{d\times d} \times [\mathbb{P}_k(\mathcal{T}_h)]^d \times \mathbb{P}_k(\mathcal{T}_h)$ is defined as the only solution of

$$
\begin{aligned}
(\Pi_{\mathrm{G}}\mathrm{L}, \mathrm{G})_K &= (\mathrm{L}, \mathrm{G})_K && \forall \mathrm{G} \in [\mathbb{P}_{k-1}(K)]^{d\times d}, && \text{(1a)}\\
(\Pi_{\boldsymbol{V}}\boldsymbol{u}, \boldsymbol{v})_K &= (\boldsymbol{u}, \boldsymbol{v})_K && \forall \boldsymbol{v} \in [\mathbb{P}_{k-1}(K)]^d, && \text{(1b)}\\
(\Pi_P p, q)_K &= (p, q)_K && \forall q \in \mathbb{P}_{k-1}(K), && \text{(1c)}\\
(\mathrm{tr}\ \Pi_{\mathrm{G}}\mathrm{L}, q)_K &= (\mathrm{tr}\ \mathrm{L}, q)_K && \forall q \in \mathbb{P}_k(K), && \text{(1d)}\\
\langle \nu\Pi_{\mathrm{G}}\mathrm{L}\boldsymbol{n} - \Pi_P p\boldsymbol{n} - \nu\Pi_{\boldsymbol{V}}\boldsymbol{u}, \boldsymbol{\mu}\rangle_e &= \langle \nu\mathrm{L}\boldsymbol{n} - p\boldsymbol{n} - \nu\boldsymbol{u}, \boldsymbol{\mu}\rangle_e && \forall \boldsymbol{\mu} \in [\mathbb{P}_k(e)]^d, && \text{(1e)}
\end{aligned}
$$

for all $K \in \mathcal{T}_h$ and $e \subset \partial K$. This projection has the following approximation properties.

Lemma 0.1. *Let $\ell_{\boldsymbol{u}}$, ℓ_σ, ℓ_{L}, $\ell_p \in [0, k]$. On each $K \in \mathcal{T}_h$ it holds*

$$
\begin{aligned}
\|\Pi_{\boldsymbol{V}}\boldsymbol{u} - \boldsymbol{u}\|_{0,K} &\preceq h_K^{\ell_{\boldsymbol{u}}+1}|\boldsymbol{u}|_{\ell_{\boldsymbol{u}}+1,K} + h_K^{\ell_\sigma+1}\nu^{-1}|\nabla\cdot(\nu\mathrm{L} - p\mathrm{I})|_{\ell_\sigma,K},\\
\|\Pi_{\mathrm{G}}\mathrm{L} - \mathrm{L}\|_{0,K} &\preceq h_K^{\ell_{\mathrm{L}}+1}|\mathrm{L}|_{\ell_{\mathrm{L}}+1,K} + \|\Pi_{\boldsymbol{V}}\boldsymbol{u} - \boldsymbol{u}\|_{0,K} + h_K^{\ell_{\boldsymbol{u}}+1}|\boldsymbol{u}|_{\ell_{\boldsymbol{u}}+1,K},\\
\|\Pi_P p - p\|_{0,K} &\preceq h_K^{\ell_p+1}|p|_{\ell_p+1,K} + \nu\|\Pi_{\mathrm{G}}\mathrm{L} - \mathrm{L}\|_{0,K} + h_K^{\ell_{\mathrm{L}}+1}\nu|\mathrm{L}|_{\ell_{\mathrm{L}}+1,K}.
\end{aligned}
$$

Proof. See Theorems 2.1 and 2.3 in [33]. □

Now, for the *a posteriori* error analyses in Chapters 2-3, we present estimates employed to prove our main results.

First, we recall the approximation properties of the Clément interpolation operator $\mathcal{C}_h : L^1(\Omega) \to V_h^{1,c} \cap H_0^1(\Omega)$, introduced in [26], as

$$
\mathcal{C}_h w := \sum_{z\in\mathcal{N}_h^i} \left(\frac{1}{|\Omega_z|}\int_{\Omega_z} w \ \mathrm{d}x\right)\phi_z,
$$

where ϕ_z is the $\mathbb{P}_1$ nodal basis functions associated to the interior vertex z, $\Omega_z := \mathrm{supp}\ \phi_z$, $\mathcal{N}_h^i$ is the set of all the interior vertices, and $V_h^{1,c} := \{w \in \mathcal{C}(\Omega) : w|_K \in \mathbb{P}_1(K),\ K \in \mathcal{T}_h\}$.

In the following two lemmas, the positive constants θ_K and θ_e will be specified in the respective chapters.

Lemma 0.2. *For any $K \in \mathcal{T}_h$, $e \in \mathcal{E}_h^i$ and $0 \le m \le 1$, the following estimates hold for any $w \in H_0^1(\Omega)$:*

$$\|\mathcal{C}_h w\|_{m,\Omega} \preceq \|w\|_{m,\Omega}, \quad \|w - \mathcal{C}_h w\|_{0,K} \preceq \theta_K |\!|\!| w |\!|\!|_{1,\Delta_K}, \quad \|w - \mathcal{C}_h w\|_{0,e} \preceq \nu^{-1/4}\theta_e^{1/2} |\!|\!| w |\!|\!|_{1,\Delta_e},$$

where $\Delta_K := \{K' \in \mathcal{T}_h : \overline{K'} \cap \overline{K} \neq \emptyset\}$ for $K \in \mathcal{T}_h$ and $\Delta_e := \{K' \in \mathcal{T}_h : \overline{K'} \cap \overline{e} \neq \emptyset\}$ for $e \in \mathcal{E}_h$.

Proof. See Lemma 3.2 in [103]. □

In order to prove the local efficiency of the *a posteriori* error estimators, we need to construct suitable local cut-off functions which will allow us to localize the error analysis. More precisely, let $B_K := \Pi_{i=1}^{d+1}\lambda_i$ be the element-bubble function associated to $K \in \mathcal{T}_h$, where $\{\lambda_i\}_{i=1}^{d+1}$ are the barycentric coordinates of K. We define the face-bubble function B_e associated to the face $e \subset \partial K$ as follows: let j be the index such that λ_j vanishes on e, then $B_e := \Pi_{\substack{i=1\\ i\neq j}}^{d+1}\lambda_i$.

Lemma 0.3. *Let $K \in \mathcal{T}_h$ and $e \in \mathcal{E}_h$. The following estimates hold for all $\boldsymbol{v} \in [\mathbb{P}_k(K)]^d$, $\boldsymbol{\mu} \in [\mathbb{P}_k(e)]^d$:*

$$\|\boldsymbol{v}\|_{0,K}^2 \preceq (\boldsymbol{v}, B_K\boldsymbol{v})_K, \qquad \|B_K\boldsymbol{v}\|_{0,K} \preceq \|\boldsymbol{v}\|_{0,K}, \qquad |\!|\!| B_K\boldsymbol{v} |\!|\!|_{1,K} \preceq \theta_K^{-1}\|\boldsymbol{v}\|_{0,K},$$
$$\|\boldsymbol{\mu}\|_{0,e}^2 \preceq (\boldsymbol{\mu}, B_e\boldsymbol{\mu})_e, \qquad \|B_e\boldsymbol{\mu}\|_{0,\omega_e} \preceq \nu^{1/4}\theta_e^{1/2}\|\boldsymbol{\mu}\|_{0,e}, \qquad |\!|\!| B_e\boldsymbol{\mu} |\!|\!|_{1,\omega_e} \preceq \nu^{1/4}\theta_e^{-1/2}\|\boldsymbol{\mu}\|_{0,e}.$$

Proof. The proof is an extension of Lemma 3.3 in [103]. □

The next result shows that an element $\boldsymbol{w}$ of $[\mathbb{P}_l(\mathcal{T}_h)]^d$, $l \ge 1$, can be approximated by a continuous function $\widetilde{\boldsymbol{w}} \in [\mathbb{P}_l(\mathcal{T}_h)]^d$, its Oswald interpolant, and that the approximation error can be controlled by the size of the inter-element jumps of $\boldsymbol{w}$.

Lemma 0.4. *Let D^ρ be the row-wise gradient or identity operator (for $|\rho| = 1$ or $|\rho| = 0$, respectively). For any $\boldsymbol{w}_h \in [\mathbb{P}_l(\mathcal{T}_h)]^d$, $l \ge 1$, and any multi-index ρ with $|\rho| = 0, 1$ the following approximation result holds: Let $\boldsymbol{g}$ be the restriction to Γ of a function in $[\mathbb{P}_l(\mathcal{T}_h)]^d \cap [H^1(\Omega)]^d$. Then there exists a function $\widetilde{\boldsymbol{w}}_h \in [\mathbb{P}_l(\mathcal{T}_h)]^d \cap [H^1(\Omega)]^d$ satisfying $\widetilde{\boldsymbol{w}}_h|_\Gamma = \boldsymbol{g}$ and*

$$\sum_{K\in\mathcal{T}_h} \|D^\rho(\boldsymbol{w}_h - \widetilde{\boldsymbol{w}}_h)\|_{0,K}^2 \preceq \sum_{e\in\mathcal{E}_h^i} h_e^{1-2|\rho|} \|\,[\![\boldsymbol{w}_h]\!]\,\|_{0,e}^2 + \sum_{e\in\mathcal{E}_h^\partial} h_e^{1-2|\rho|}\|\boldsymbol{g} - \boldsymbol{w}_h\|_{0,e}^2.$$

Proof. See Lemma 4.3 in [56]. □

We also recall the approximation property of P_k, the L^2-projection onto $\mathbb{P}_k(\mathcal{T}_h)$.

Lemma 0.5. *For all $0 \le l \le k+1$, $1 \le p \le \infty$, and $v \in W^{l,p}(\Omega)$,*

$$\|v - \mathsf{P}_k v\|_{0,p,\Omega} \preceq h^l |v|_{l,p,\Omega}.$$

Proof. See Proposition 1.135 in [55]. □

Finally, in Chapters 2-3, to avoid nonessential technical difficulties, we make the following assumption

Assumption H: We assume that the Dirichlet boundary data $\boldsymbol{u}_D$ is the trace of a continuous function in $[\mathbb{P}_k(\mathcal{T}_h)]^d$ and the source term $\boldsymbol{f}$ is a piecewise polynomial function. Otherwise, high order terms associated to oscillations involving $\boldsymbol{u}_D$ and $\boldsymbol{f}$ will appear.

CHAPTER 1

A high order HDG method for curved-interface problems via approximations from straight triangulations

In this chapter we propose a novel technique to solve elliptic problems involving a non-polygonal interface/boundary to develop a high order method based on a triangulation of the domain involving only straight elements. As we will discuss, the boundary/interface must be interpolated by piecewise linear function in order to obtain the expected rates of convergence.

1.1 Introduction

In this chapter we propose a technique to numerically solve second order elliptic problems in domains Ω which are not necessarily polygonal and, in addition, we deal with domains divided in two regions by a curved interface Σ.

One of the first ideas in this direction was introduced by [35] for the one-dimensional case and then extended to higher space dimensions for pure diffusion [37, 41] and convection-diffusion [41] equations. In their work, the mesh does not fit the domain and the distance between the computational domain and the boundary $\Gamma := \partial\Omega$ is of only order $O(h)$, making this method attractive from a computational point of view. In addition, [39] applied this method to couple boundary element and HDG methods to solve exterior diffusion problems. However, only Dirichlet boundary value problems have been considered since Neumann data can not be handled in the same way as we will explain later. We will see that for the Neumann boundary case the proposed technique works properly if the computational domain is order $O(h^2)$ away from the actual boundary.

One of the first methods that approximate Neumann boundary conditions on curved domains considering non-fitted meshes was introduced by [7]. There, a piecewise linear finite element method was considered and optimal convergence in the H^1-norm was shown. In addition, the same authors solved a semi-definite Neumann problem on curved domains using a similar technique [8]. They showed optimal behavior of the errors in H^1 and L^2-norms using again piecewise linear elements. On the other hand, higher order approximation finite element methods require to properly fit the boundary in order to keep high order accuracy. For instance, isoparametric elements can be considered [8, 84]. In the case of elliptic interface problems, usually the curve describing the interface is interpolated by a piecewise linear computational interface. Hence, super-parametric elements near the interface must be considered

in order to achieve high order accuracy [75].

Recently, the cut finite element method (CutFEM) and the hybrid high-order method (HHO) have appeared as new alternatives to solve elliptic interface problems. CutFEM [14, 73] has seen a lot of developments to treat elliptic interface problems making the discretization as independent as possible of the geometric description of the domain and minimizing the complexity of mesh generation, but retaining desirable properties of a standard finite element method as the accuracy and robustness. In that approach, the boundary of a given domain is represented on a background grid that is also used to represent the approximate solution of the involved PDEs, turning the mesh generation in requiring only a low-quality and even non-conform surface mesh representation of the computational geometry. An overview of literature and state of the art of the CutFEM can be found in [14]. On the other hand, [15] introduced an unfitted HHO method for elliptic interface problems. That approach consists of doubling the unknowns in the cut cells and the cut faces, in a spirit similar to unfitted finite element methods and combines the ideas of HHO methods (and more broadly HDG methods) with those from [72] concerning Nitsche's formulation, but with material dependent weights rather than cut-dependent weights, and those from [77] to handle unfavorable cuts by a local cell-agglomeration procedure. The cell-agglomeration procedure takes full advantage of the fact that the HHO method supports general meshes with polyhedral cells.

1.2 Boundary value problem with mixed boundary conditions

We consider the following model problem:

$$\begin{aligned} \nabla \cdot \boldsymbol{q} &= f \text{ in } \Omega, && \text{(1.1a)}\\ \boldsymbol{q} + \mathbf{K}\nabla u &= 0 \text{ in } \Omega, && \text{(1.1b)}\\ u &= g_D \text{ on } \Gamma_D, && \text{(1.1c)}\\ \boldsymbol{q}\cdot\boldsymbol{n} &= g_N \text{ on } \Gamma_N. && \text{(1.1d)} \end{aligned}$$

Here $g_D \in H^{1/2}(\Gamma_D)$ and $g_N \in H^{-1/2}(\Gamma_N)$ are given data at the border, $f \in L^2(\Omega)$ is a source term and $\mathbf{K} \in [L^\infty(\Omega)]^{2\times 2}$ is a symmetric and positive definite tensor.

In the computational domain Ω_h, problem (1.1) can be written as follows:

$$\begin{aligned} \nabla \cdot \boldsymbol{q} &= f \text{ in } \Omega_h, && \text{(1.2a)}\\ \boldsymbol{q} + \mathbf{K}\nabla u &= 0 \text{ in } \Omega_h, && \text{(1.2b)}\\ u &= \widetilde{g}_D \text{ on } \Gamma_D^h, && \text{(1.2c)}\\ \boldsymbol{q}\cdot\boldsymbol{n} &= \widetilde{g}_N \text{ on } \Gamma_N^h. && \text{(1.2d)} \end{aligned}$$

Here $\widetilde{g}_D$ and $\widetilde{g}_N$ are unknowns. As we mentioned before, $\widetilde{g}_D$ can be calculated following [35, 39, 41], i.e.,

$$\widetilde{g}_D(\boldsymbol{x}) := g_D(\bar{\boldsymbol{x}}) + \int_{\sigma(\boldsymbol{x})} \mathbf{K}^{-1}\boldsymbol{q}\cdot\boldsymbol{m}\, ds, \tag{1.3}$$

where $\sigma(\boldsymbol{x})$, is a path starting at $\boldsymbol{x} \in \Gamma_D^h$ and ending at $\bar{\boldsymbol{x}} \in \Gamma_D$; and $\boldsymbol{m} := \bar{\boldsymbol{x}} - \boldsymbol{x}$ is the tangent vector to $\sigma(\boldsymbol{x})$. This expression comes from integrating (1.1b) along the path $\sigma(\boldsymbol{x})$ (see [41] for details).

In principle, any kind of numerical method using polygonal domains can be used to solve the equations in Ω_h. However, it is desirable to consider those methods where an accurate approximation of $\boldsymbol{q}$ is obtained, since the boundary condition (1.3) depends on that flux. We also notice from (1.3) that the same idea will not work for $\widetilde{g}_N$ since a similar expression will involve derivatives of $\boldsymbol{q}$ which are not well approximated by the numerical method.

1.2.1 The HDG method

The method seeks an approximation $(\boldsymbol{q}_h, u_h, \widehat{u}_h)$ of the exact solution $(\boldsymbol{q}, u, u|_{\mathcal{E}_h})$ in the space $\boldsymbol{V}_h \times W_h \times M_h$ given by

$$\boldsymbol{V}_h = \{\boldsymbol{v} \in [L^2(\mathcal{T}_h)]^2 : \quad \boldsymbol{v}|_K \in [\mathbb{P}_k(K)]^2 \quad \forall K \in \mathcal{T}_h\}, \tag{1.4a}$$

$$W_h = \{w \in L^2(\mathcal{T}_h) : \quad w|_K \in \mathbb{P}_k(K) \quad \forall K \in \mathcal{T}_h\}, \tag{1.4b}$$

$$M_h = \{\mu \in L^2(\mathcal{E}_h) : \quad \mu|_e \in \mathbb{P}_k(e) \quad \forall e \in \mathcal{E}_h\}. \tag{1.4c}$$

It is defined by requiring that it satisfies the equations

$$-(\boldsymbol{q}_h, \nabla w)_{\mathcal{T}_h} + \langle \widehat{\boldsymbol{q}}_h \cdot \boldsymbol{n}, w\rangle_{\partial\mathcal{T}_h} = (f, w)_{\mathcal{T}_h} \tag{1.5a}$$

$$(\mathbf{K}^{-1}\boldsymbol{q}_h, \boldsymbol{v})_{\mathcal{T}_h} - (u_h, \nabla \cdot \boldsymbol{v})_{\mathcal{T}_h} + \langle \widehat{u}_h, \boldsymbol{v} \cdot \boldsymbol{n}\rangle_{\partial\mathcal{T}_h} = 0, \tag{1.5b}$$

$$\langle \mu, \widehat{\boldsymbol{q}}_h \cdot \boldsymbol{\nu}\rangle_{\partial\mathcal{T}_h \setminus \Gamma^h} = 0, \tag{1.5c}$$

$$\langle \mu, \widehat{u}_h\rangle_{\Gamma_D^h} = \langle \mu, g_D^h\rangle_{\Gamma_D^h}, \tag{1.5d}$$

$$\langle \mu, \widehat{\boldsymbol{q}}_h\rangle_{\Gamma_N^h} = \langle \mu, g_N^h\rangle_{\Gamma_N^h}, \tag{1.5e}$$

for all $(\boldsymbol{v}, w, \mu) \in \boldsymbol{V}_h \times W_h \times M_h$. Here g_D^h is the approximation of $\widetilde{g}_D$ proposed by [41]. More precisely, let $K \in \mathcal{T}_h$. We define the operator $E^K : [\mathbb{P}_k(K)]^2 \to [\mathbb{P}_k(\mathbb{R}^2)]^2$ such that $E^K(\boldsymbol{v}) = \boldsymbol{v}$ for all $\boldsymbol{v} \in [\mathbb{P}_k(K)]^2$. Then, for $\boldsymbol{x} \in e \subset \Gamma_D^h$,

$$\widetilde{g}_D(\boldsymbol{x}) \approx g_D^h(\boldsymbol{x}) := g_D(\bar{\boldsymbol{x}}) + \int_{\sigma(\boldsymbol{x})} \mathbf{K}^{-1} E^{K_e}(\boldsymbol{q}_h) \cdot \boldsymbol{m}\, ds, \tag{1.5f}$$

where K_e is the triangle where e belongs. In other words, E^{K_e} is the standard extension of a polynomial to the whole $\mathbb{R}^2$ space. On the other hand, g_N^h is an approximation of $\widetilde{g}_N$ which is still unknown. In Subsection 1.2.3 we propose to replace (1.5e) by an equation involving known quantities at the right hand side.

Finally, to complete the definition of the HDG method we must specify the definition of numerical trace $\widehat{\boldsymbol{q}}_h$ on $\partial\mathcal{T}_h$, which we takes of the form

$$\widehat{\boldsymbol{q}}_h = \boldsymbol{q}_h + \tau(u_h - \widehat{u}_h)\boldsymbol{n}, \tag{1.5g}$$

where $\tau : \partial\mathcal{T}_h \to (0, \infty)$ is a stabilization parameter that guaranties solvability of (1.5) and can be set as $\tau|_K = \|\mathbf{K}\|_{L^\infty(K)}$ on each element K (see [32, 87]). Here $\|\mathbf{K}\|_{L^\infty(K)}$ is the L^∞-norm of the tensor $\mathbf{K}$ in the element K.

1.2.2 Definition of the family of paths

The representation of g_D^h in (1.5f) is independent on the integration path. Let $\boldsymbol{x}$ be a point on a boundary edge e and K_e the element where it belongs. Previous work has proposed two ways to determine a point $\bar{\boldsymbol{x}}$ in Γ and hence construct $\sigma(\boldsymbol{x})$:

(P1) Let $\boldsymbol{x}_i$ $(i = 1, 2)$ be the vertices of e. The authors in [41] suggest three conditions on $\sigma(\boldsymbol{x}_i)$:

(a) The paths $\sigma(\boldsymbol{x}_1)$ and $\sigma(\boldsymbol{x}_2)$ cannot intersect inside Ω. This will avoid overlapping between $E^{K_e}(\boldsymbol{q}_h)$ and the extrapolated polynomials from neighboring elements.

(b) The paths $\sigma(\boldsymbol{x}_1)$ and $\sigma(\boldsymbol{x}_2)$ cannot intersect the interior of the computational domain Ω_h. Otherwise the extrapolated polynomials from neighboring elements would overlap the polynomial $\boldsymbol{q}_h|_{K_e}$.

(c) The length of the segments $\sigma(\boldsymbol{x}_i)$ must be at least of order h.

A detailed construction of the segments $\sigma(\boldsymbol{x}_i)$ satisfying the above requirements can be found in Section 2.4.2 of [41]. Moreover, Figure 3 in [41] illustrate the procedure.
Now, let $\boldsymbol{x}$ an interior point of e. For $\theta \in [0, 1]$ we write $\boldsymbol{x} = \boldsymbol{x}_1 + (1 - \theta)(\boldsymbol{x}_2 - \boldsymbol{x}_1)$ and define $\widetilde{\boldsymbol{m}} := \boldsymbol{m}_1 + (1 - \theta)(\boldsymbol{m}_2 - \boldsymbol{m}_1)$, where $\boldsymbol{m}_i$ $(i = 1, 2)$ are the tangent vectors to $\sigma(\boldsymbol{x}_i)$. Then, we define $\bar{\boldsymbol{x}}$ as the intersection between the boundary Γ and the ray starting at $\boldsymbol{x}$ whose tangent vector is $\widetilde{\boldsymbol{m}}$. Thus, the segment $\sigma(\boldsymbol{x})$ is the one joining $\boldsymbol{x}$ and $\bar{\boldsymbol{x}}$. For the Dirichlet boundary value problem, the authors in [41] numerically showed optimal rates of convergence with this choice of $\sigma(\boldsymbol{x})$ when $d(\Gamma, \Gamma^h)$ is of order h, that is, order $k + 1$ for u_h and $\boldsymbol{q}_h$ and order $k + 2$ for the numerical trace $\widehat{u}_h$.

(P2) On the other hand, [37] analyzed the case where $\bar{\boldsymbol{x}}$ is determined such that $\boldsymbol{m}$ is normal to the edge e. In this case these authors theoretically proved that if $d(\Gamma, \Gamma^h)$ is of order h, the order of convergence for u_h and $\boldsymbol{q}_h$ is indeed $k + 1$, but the order for $\widehat{u}_h$ is only $k + 3/2$. However, if $d(\Gamma, \Gamma^h)$ is of order $h^{5/4}$ the numerical trace also superconverges with order $k+2$. Moreover, they also showed numerical evidence indicating that the numerical trace optimally superconverges even though $d(\Gamma, \Gamma^h)$ is of order h.

Let e be a boundary edge with vertices $\boldsymbol{x}_1$ and $\boldsymbol{x}_2$. We denote by Γ_e the part of Γ determined by $\bar{\boldsymbol{x}}_1$ and $\bar{\boldsymbol{x}}_2$ as it is shown in Fig. 1.1. In this paper we assume that if $e \subset \Gamma_D^h$ (or $e \subset \Gamma_N^h$) then $\Gamma_e \subset \Gamma_D$ ($\Gamma_e \subset \Gamma_N$). The algorithm in **(P1)** can be easily modified to satisfy this assumption. On the other hand, the paths defined in **(P2)** will not always satisfy this condition.

1.2.3 Approximation of the Neumann boundary condition

Let $e \subset \Gamma_N^h$ be a Neumann boundary face and $\Gamma_e \subset \Gamma_N$ the part of Γ_N associated to e. We denote by K_e the element of the triangulation where e belongs.

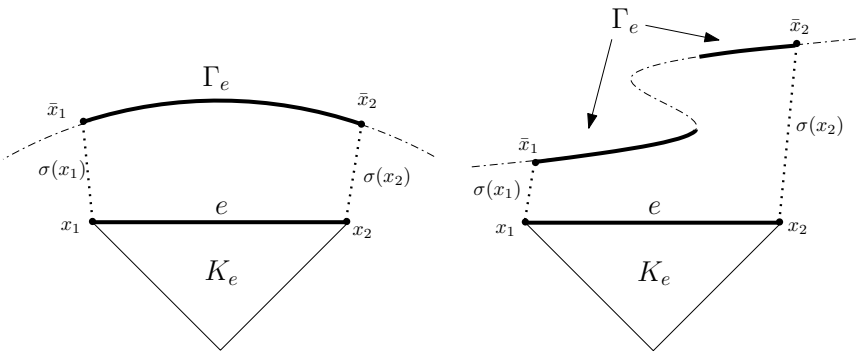

Figure 1.1: Examples of a boundary edge e with vertices $\boldsymbol{x}_1$ and $\boldsymbol{x}_2$. Γ_e is the segment of Γ_N determined by $\bar{\boldsymbol{x}}_1$ and $\bar{\boldsymbol{x}}_2$. (Fuente: Elaboración propia)

The main idea is to characterize Γ_e using the parameterization *induced* by the family of paths. More precisely, let $e = \{\boldsymbol{x} : \boldsymbol{x}(\theta) = (\boldsymbol{x}_2 - \boldsymbol{x}_1)\theta + \boldsymbol{x}_1, \theta \in [0,1]\}$. Then

$$\Gamma_e = \{\bar{\boldsymbol{x}} = \boldsymbol{\phi}(\theta) : \boldsymbol{\phi}(\theta) = \boldsymbol{x}(\theta) + |\sigma(\boldsymbol{x}(\theta))|\boldsymbol{m}(\theta), \theta \in [0,1]\}, \tag{1.6}$$

where we recall that $|\sigma(\boldsymbol{x}(\theta))|$ and $\boldsymbol{m}(\theta)$ are the length and tangent vector of the segment joining $\boldsymbol{x}(\theta)$ and $\bar{\boldsymbol{x}}(\theta)$. We define the space

$$M_{\boldsymbol{\phi}}(\Gamma_e) := \left\{ \mu \in L^2(\Gamma_e) : \mu = \frac{\tilde{\mu} \circ \boldsymbol{\phi}^{-1}}{\|\boldsymbol{\phi}' \circ \boldsymbol{\phi}^{-1}\|_2} \text{ with } \tilde{\mu} \in \mathbb{P}_k([0,1]) \right\}, \tag{1.7}$$

where $\|\cdot\|_2$ is the Euclidean norm.

Equation (1.5e) is then replaced by imposing the following condition over $\boldsymbol{q}_h$:

$$\langle E^{K_e}(\boldsymbol{q}_h) \cdot \boldsymbol{n}, \mu \rangle_{\Gamma_e} = \langle g_N, \mu \rangle_{\Gamma_e} \quad \forall \mu \in M_{\boldsymbol{\phi}}(\Gamma_e). \tag{1.8}$$

In the standard HDG method, the Neumann boundary condition is imposed in the numerical flux $\widehat{\boldsymbol{q}}_h \cdot \boldsymbol{n}$, which depends on $\boldsymbol{q}_h$, u_h and $\widehat{u}_h$. The variables $\boldsymbol{q}_h$ and u_h can be extrapolated since they are piecewise polynomial on K_e. However, $\widehat{u}_h$ is a polynomial over the edge e; then, it cannot be extrapolated to a two dimensional region in order to achieve the boundary Γ_e. This is why we impose the Neumann data on $\boldsymbol{q}_h \cdot \boldsymbol{n}$ instead of $\widehat{\boldsymbol{q}}_h \cdot \boldsymbol{n}$. Perhaps it would be interesting to think of a way of finding a polynomial in Γ_e, say p, using the information provided by $\widehat{u}_h$ in order to impose the Neumann condition on $E^{K_e}(\boldsymbol{q}_h) \cdot \boldsymbol{n} + \tau(E^{K_e}(u_h) - p)$ for a suitable stabilization parameter τ. Since this is not the scope of this paper, we leave this question open and it could lead to an alternative approach in a future work.

Notice that (1.8) becomes

$$\int_0^1 \left(E^{K_e}(\boldsymbol{q}_h) \cdot \boldsymbol{n}\right) \circ \boldsymbol{\phi})(\theta)\, \tilde{\mu}(\theta) d\theta = \int_0^1 (g_N \circ \boldsymbol{\phi})\, \tilde{\mu}(\theta) d\theta \tag{1.9}$$

for all $\tilde{\mu}(\theta) \in \mathbb{P}_k([0,1])$; hence, there is no need of computing the derivative of $\boldsymbol{\phi}$.

On the other hand, we observe that if $\boldsymbol{m}$ and σ were independent of θ (for example, if Γ_e were polygonal and $\boldsymbol{m}$ perpendicular to e), then $\|\boldsymbol{\phi}' \circ \boldsymbol{\phi}^{-1}\|_2$ would be a constant and hence $M_{\boldsymbol{\phi}}(\Gamma_e)$ becomes the standard space of polynomials through pulling back polynomials from the interval $[0,1]$. As we will see in the numerical experiments provided in next section, this technique performs optimally if $\boldsymbol{m}$ and $\boldsymbol{n}$ have the same direction.

1.2.4 Numerical results: Boundary-value problem

In this section we present numerical experiments showing the performance of the technique proposed in previous sections and the influence of the choice of paths. Since the size of the computational domain changes with h, we measure the errors $e_u := u - u_h$, $e_{\boldsymbol{q}} := \boldsymbol{q} - \boldsymbol{q}_h$ and $e_{\widehat{u}} := u - \widehat{u}_h$ by using the following norms:

$$\|e_u\|_{\text{int}} := \frac{\|e_u\|_{L^2(\Omega_h)}}{|\Omega_h|^{1/2}}, \quad \|e_{\boldsymbol{q}}\|_{\text{int}} := \frac{\|e_{\boldsymbol{q}}\|_{[L^2(\Omega_h)]^2}}{|\Omega_h|^{1/2}}, \quad \|e_{\hat{u}}\|_{\mathcal{E}_h} := \left(\frac{\sum_{K\in\Omega_h} h_K \|\mathsf{P}_\partial u - \hat{u}_h\|^2_{L^2(\partial K)}}{\sum_{K\in\Omega_h} h_k |\partial K|} \right)^{1/2}.$$

Here $|\Omega_h|$ denotes the area of the computational domain and P_∂ is the L^2-projection over $\mathbb{P}_k(e)$ with $e \subset \partial K$.

In addition we compute an element-by-element postprocessing, denoted by u_h^*, of the approximate solution u_h, which provides a better approximation for the scalar variable when $k \geq 1$ (see [34, 36]). Given an element K we construct $u_h^* = \bar{u}_h + \tilde{u}_h$ as the only function in $\mathbb{P}_{k+1}(K)$ such that

$$\bar{u}_h = \begin{cases} \frac{1}{3}\sum_{e\in\partial K} \widehat{u}_h|_e & \text{if } k = 0, \\ \frac{1}{|K|}\int_K u_h dx & \text{if } k > 0, \end{cases}$$

and $\tilde{u}_h$ is the polynomial in $\mathbb{P}_{k+1}(K)^0$ (set of functions in $\mathbb{P}_{k+1}(K)$ with mean zero) satisfying

$$(\nabla \tilde{u}_h, \nabla w)_K = -(\boldsymbol{q}_h, \nabla w)_K \quad \forall w \in \mathbb{P}_{k+1}(K).$$

In the purely diffusive case, this new approximation of u has been proven to converge with order $k+2$ for $k \geq 1$ when the domain is polygonal (see [34, 36]), and also when it has curved Dirichlet boundary (see [37, 41]).

We set $\mathbf{K} = \mathbf{I}$ in all the experiments of this section. In Subsection 1.2.4 we show that deteriorate convergence can happen if $d(\Gamma, \Gamma^h) = O(h)$. However, we will see in Subsection 1.2.4 that optimal convergence is obtained when $d(\Gamma, \Gamma^h) = O(h^2)$.

Computational domain at a distance $d(\Gamma, \Gamma^h) = O(h)$

In the following examples the computational domain is constructed in such a way that the distance $d(\Gamma, \Gamma^h)$ is of order h. Moreover, f, g_D and g_N are chosen in order that $u(x,y) = \sin(x)\sin(y)$ is solution the exact of (1.1).

Example 1.2.1. Our first example consist of approximating a squared domain $\Omega = (0,1)^2$ by a squared subdomain satisfying $d(\Gamma, \Gamma^h) = O(h)$ as Fig. 1.2 shows. Let $\Gamma_N = \{x : x = 0\}$, $\Gamma_D = \partial\Omega \setminus \Gamma_N$ and the family of paths is computed according to **(P2)**.

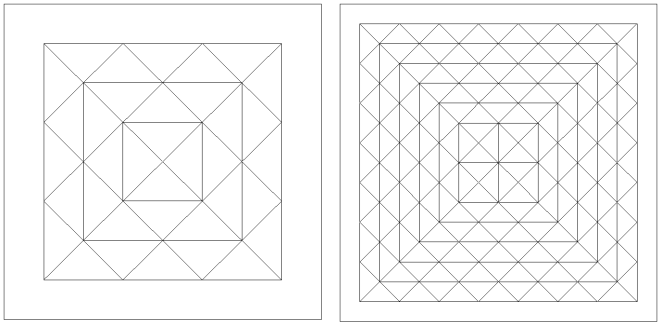

Figure 1.2: Two consecutive meshes ($h = 1/4$ and $h = 1/8$) approximating the domain of Example 1.2.1. (Figure obtained from [37])

In Table 1.1 we display the history of convergence for different polynomial degree ($k = 0, 1, 2$ and 3) and meshsizes ($h = 1/2, 1/4, 1/8, 1/16$ and $1/32$). We observe that the error of u and $\boldsymbol{q}$ behaves optimally with convergence rate of order $k+1$. Moreover the error of numerical trace and postprocessed solution also converge with order $k+1$, which is not optimal for the standard HDG method on polygonal domains. Even though, the errors e_{u^*} are always small than e_u. We attribute this lack of superconvergence to the fact that the Neumann condition (1.8) is being imposed on $\boldsymbol{q}_h$ and not on $\widehat{\boldsymbol{q}}_h$ as in the standard HDG method.

		$\|e_u\|_{\text{int}}$		$\|e_{\boldsymbol{q}}\|_{\text{int}}$		$\|e_{\widehat{u}}\|_{\mathcal{E}_h}$		$\|e_{u^*}\|_{\text{int}}$	
k	h	error	order	error	order	error	order	error	order
	1/2	4.58e-03	-	6.59e-02	-	2.13e-02	-	7.50e-03	-
	1/4	6.09e-03	-0.41	4.77e-02	0.46	5.75e-03	1.89	6.60e-03	0.18
0	1/8	4.62e-03	0.40	2.74e-02	0.80	1.75e-03	1.71	4.71e-03	0.49
	1/16	2.78e-03	0.73	1.46e-02	0.91	6.18e-04	1.51	2.80e-03	0.75
	1/32	1.52e-03	0.87	7.52e-03	0.96	2.51e-04	1.30	1.53e-03	0.88
	1/2	1.54e-03	-	9.89e-03	-	3.70e-03	-	1.67e-03	-
	1/4	5.67e-04	1.44	2.55e-03	1.96	6.31e-04	2.55	4.68e-04	1.84
1	1/8	1.69e-04	1.75	7.09e-04	1.85	1.50e-04	2.07	1.31e-04	1.83
	1/16	4.62e-05	1.86	1.94e-04	1.87	3.84e-05	1.97	3.60e-05	1.87
	1/32	1.21e-05	1.93	5.13e-05	1.92	9.83e-06	1.97	9.52e-06	1.92
	1/2	2.29e-04	-	1.20e-03	-	5.23e-04	-	2.17e-04	-
	1/4	2.82e-05	3.02	1.24e-04	3.28	3.36e-05	3.96	2.44e-05	3.16
2	1/8	3.43e-06	3.03	1.36e-05	3.19	3.22e-06	3.38	2.81e-06	3.12
	1/16	4.25e-07	3.01	1.63e-06	3.06	3.61e-07	3.16	3.38e-07	3.05
	1/32	5.28e-08	3.01	2.02e-07	3.01	4.26e-08	3.08	4.13e-08	3.03
	1/2	3.37e-05	-	1.51e-04	-	7.55e-05	-	3.39e-05	-
	1/4	2.30e-06	3.87	9.32e-06	4.02	3.12e-06	4.59	2.30e-06	3.88
3	1/8	1.55e-07	3.89	6.74e-07	3.79	1.78e-07	4.14	1.55e-07	3.89
	1/16	1.05e-08	3.89	4.76e-08	3.82	1.12e-08	3.99	1.05e-08	3.89
	1/32	6.90e-10	3.92	3.22e-09	3.89	7.13e-10	3.97	6.90e-010	3.92

Table 1.1: History of convergence of the approximation in Example 1.2.1. (Fuente: Elaboración propia)

Example 1.2.2. We now consider an annular domain $\Omega = \{(x, y) \in \mathbb{R}^2 : 14^2 < x^2 + y^2 < 20^2\}$ that

is being approximated by a polygonal subdomain satisfying $d(\Gamma, \Gamma^h) = O(h)$ as shown in Fig. 1.3. We consider Neumman data in the outer boundary $\Gamma_N = \{(x, y) \in \mathbb{R}^2 : x^2 + y^2 = 20^2\}$ and Dirichlet data in the inner boundary $\Gamma_D = \{(x, y) : x^2 + y^2 = 14^2\}$. Here the paths are computed according to **(P2)**.

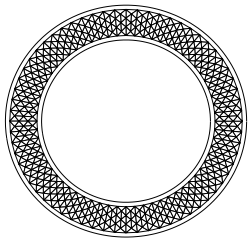

Figure 1.3: Annular domain and mesh in Example 1.2.2. (Fuente: Elaboración propia)

The behavior of the L^2-norm of the error displayed in Table 1.2 is similar to the one obtained in the previous example, i.e., the rate of convergence of the error in all the variables is of order $k+1$. Thus, this example suggests that our technique performs properly when the boundary is actually non-polygonal.

		$\|e_{\boldsymbol{u}}\|_{\text{int}}$		$\|e_{\boldsymbol{q}}\|_{\text{int}}$		$\|e_{\widetilde{u}}\|_{\mathcal{E}_h}$		$\|e_{\boldsymbol{u}^*}\|_{\text{int}}$	
k	h	error	order	error	order	error	order	error	order
	1.89	9.56e+00	-	8.79e+00	-	4.66e-01	-	9.80e+00	-
	0.96	8.47e+00	0.18	5.82e+00	0.61	3.72e-01	0.33	8.50e+00	0.21
0	0.49	5.72e+00	0.57	3.38e+00	0.79	2.42e-01	0.63	5.72e+00	0.56
	0.24	3.29e+00	0.81	1.82e+00	0.90	1.37e-01	0.83	3.29e+00	0.81
	0.12	1.76e+00	0.91	9.42e−01	0.91	7.26e−02	0.92	1.76e+00	0.91
	1.89	2.03e+01	-	7.85e+00	-	9.56e−01	-	2.04e+01	-
	0.96	5.94e+00	1.82	2.12e+00	1.94	2.58e−01	1.94	5.96e+00	1.82
1	0.49	1.43e+00	2.08	5.03e−01	2.10	6.00e−02	2.13	1.43e+00	2.08
	0.24	3.40e−01	2.09	1.20e−01	2.08	1.40e−02	2.11	3.40e−01	2.09
	0.12	8.19e−02	2.06	2.92e−02	2.06	3.35e−03	2.11	8.20e−02	2.06
	1.89	4.04e+00	-	1.82e+00	-	1.90e−01	-	4.04e+00	-
	0.96	6.80e−01	2.64	3.42e−01	2.46	2.95e−02	2.76	6.81e−01	2.64
2	0.49	1.41e−01	2.30	5.86e−02	2.58	5.89e−03	2.36	1.41e−01	2.30
	0.24	2.12e−02	2.75	8.33e−03	2.83	8.75e−04	2.77	2.12e−02	2.75
	0.12	2.88e−03	2.89	1.10e−03	2.93	1.16e−04	2.90	2.88e−03	2.93
	1.89	4.12e+00	-	1.52e+00	-	1.93e−01	-	4.12e+00	-
	0.96	3.17e−01	3.80	1.07e−01	3.93	1.37e−03	3.92	3.17e−01	3.80
3	0.49	1.89e−02	4.13	6.29e−03	4.15	7.89e−04	4.18	1.89e−02	4.13
	0.24	1.10e−03	4.13	3.70e−04	4.12	4.53e−05	4.15	1.10e−03	4.13
	0.12	6.56e−05	4.08	2.23e−05	4.07	2.68e−06	4.09	6.56e−05	4.08

Table 1.2: History of convergence of the approximation in Example 1.2.2. (Fuente: Elaboración propia)

Remark 1.2.1. *The construction of the family of paths according to* **(P1)** *in Examples 1.2.1 and 1.2.2 deliver similar results since the difference between* **(P1)** *and* **(P2)** *is not significant for these domains. That is why we do not display the convergence tables for this case. This numerical evidence indicates that the technique proposed provides optimal rate of convergence when* $d(\Gamma, \Gamma^h) = O(h)$ *and the family of paths is constructed according to* **(P1)** *or* **(P2)**. *However, in practice, this condition over*

the distance can not be satisfied in general, unless the mesh is constructed properly to do so.

A practical construction of the computational domain $\mathcal{T}_h$ was described in [41]. It consists of "immersing" the domain in a Cartesian background mesh and set $\mathcal{T}_h$ as the union of all the elements that are completely inside of Ω as it is shown in Fig. 1.4. Here $d(\Gamma, \Gamma^h) = O(h)$. In this case it is not convenient to construct the paths according to **(P2)**. *In fact, given a point $\boldsymbol{x} \in \mathcal{E}_h^{\partial}$ it might happen that $\bar{\boldsymbol{x}}$ is extremely far from $\boldsymbol{x}$, specially in parts of Γ where the domain is non-convex. Since both procedures deliver similar results in previous examples, we will consider from now on* **(P1)**.

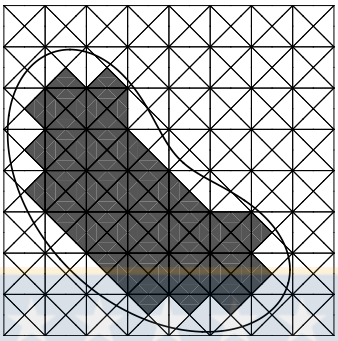

Figure 1.4: Left: Domain Ω, its boundary Γ (solid line), a background mesh $\mathcal{B}_h$ and the polygonal subdomain Ω_h (gray). Right: Dirichlet data g on Γ transferred to φ on Γ_h. (Figure taken from [41])

Example 1.2.3. In order to observe the performance of the method where the mesh satisfies $d(\Gamma, \Gamma^h) = O(h)$ and the paths are given by **(P1)**, we consider the ring $\Omega = \{(x, y) \in \mathbb{R}^2 : 0.25^2 < (x - 0.5)^2 + (y - 0.5)^2 < 1\}$ with $\Gamma_N = \{(x, y) \in \mathbb{R}^2 : x^2 + y^2 = 1\}$ and $\Gamma_D = \{(x, y) : x^2 + y^2 = 0.25^2\}$. In Fig. 1.5 we show a zoom at the upper-right corner of three consecutive meshes. We also plot the family paths from vertices and quadrature points on the boundary edges. In Table 1.3 we display the history of convergence. Even though the method is still convergent for $k = 0$, 1 and 2, the rates deteriorate. Moreover, there is no convergence when $k = 3$. For the Dirichlet boundary value problem this non-optimal behavior does not occur as [41] showed. This example suggests that in a practical situation (meshes satisfying $d(\Gamma, \Gamma^h) = O(h)$ and paths constructed using **(P1)**, the method does not perform properly. So, it seems that for Neumann boundary data, the family of paths needs to be build according to **(P2)**. Even though we have no theoretical support that explains this behavior, we believe it might be related to the oscillatory nature of high degree polynomials. In fact, for the Dirichlet problem, [37] showed error estimates where some of the constants depend on the polynomial degree. In addition, [42] numerically studied the robustness of this method applied to a convection-diffusion problem with Dirichlet boundary data. They concluded that, even though $d(\Gamma, \Gamma^h) = O(h)$, Γ and Γ^h must be "close enough' when $k \geq 1$.

One way of always being able to construct the paths using **(P2)** is to interpolate the boundary by a piecewise linear function. In this case $d(\Gamma, \Gamma^h) = O(h^2)$.

Remark 1.2.2. *In Example 1.2.3 it is not possible to construct the family of path by* **(P1)**. *In fact, a path perpendicular to an inner boundary edge might not intersect the inner ring . Moreover, a path perpendicular to an outer boundary edge might intersect the outer boundary extremely "far" as would*

happen in the third mesh of Fig. 1.5.

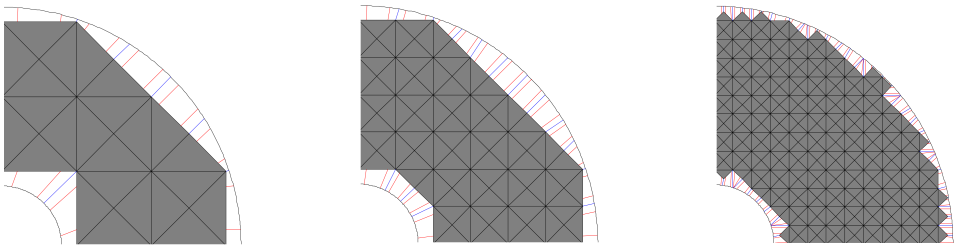

Figure 1.5: Zoom at the upper-right corner of three consecutive meshes of Example 1.2.3. Mesh (grey region) constructed considering the procedure in [41] and family of paths determined according to **(P1)**. Blue lines: paths from the vertices. Red lines: paths from quadrature points of the boundary edges ($k = 1$). (Fuente: Elaboración propia)

		$\|e_u\|_{\text{int}}$		$\|e_{\boldsymbol{q}}\|_{\text{int}}$		$\|e_{\widehat{u}}\|_{\mathcal{E}_h}$		$\|e_{u^*}\|_{\text{int}}$	
k	h	error	order	error	order	error	order	error	order
	0.312	4.12e−02	-	1.83e−01	-	4.40e−02	-	4.15e−02	-
	0.156	3.70e−02	0.16	1.27e−01	0.53	3.26e−02	0.43	3.69e−02	0.17
0	0.078	1.69e−02	1.13	1.37e−01	-0.11	1.50e−02	1.12	1.69e−02	1.13
	0.039	9.11e−03	0.89	7.00e−02	0.96	7.61e−03	0.97	9.11e−03	0.89
	0.019	8.50e−03	0.10	4.92e−02	0.51	5.66e−03	0.43	8.50e−03	0.10
	0.312	6.13e−03	-	1.82e−02	-	3.75e−03	-	5.71e−03	-
	0.156	3.44e−03	0.84	1.06e−02	0.77	2.18e−03	0.78	3.37e−03	0.76
1	0.078	3.86e−03	-0.17	9.41e−03	0.18	2.36e−03	-0.11	3.86e−03	-0.20
	0.039	1.16e−03	1.74	2.68e−03	1.81	6.88e−04	1.78	1.16e−03	1.73
	0.019	5.17e−04	1.16	1.16e−03	1.20	3.04e−04	1.18	5.16e−04	1.16
	0.312	4.68e−04	-	1.25e−03	-	3.03e−04	-	4.60e−04	-
	0.156	2.25e−04	1.06	5.89e−04	1.08	1.45e−04	1.06	2.24e−04	1.04
2	0.078	1.21e−04	0.89	3.24e−04	0.86	7.39e−05	0.97	1.21e−04	0.89
	0.039	1.31e−05	3.20	3.60e−05	3.17	7.79e−06	3.25	1.31e−05	3.21
	0.019	2.63e−06	2.32	7.03e−06	2.35	1.54e−06	2.33	2.63e−06	2.32
	0.312	3.02e−05	-	8.78e−05	-	1.98e−05	-	3.00e−05	-
	0.156	1.11e−05	1.44	3.45e−05	1.35	7.19e−06	1.45	1.10e−05	1.44
3	0.078	1.65e−06	2.75	5.37e−06	2.67	1.01e−06	2.83	1.65e−06	2.75
	0.039	6.69e−06	-	1.53e−05	-	3.98e−06	-	6.70e−06	-
	0.019	8.03e−03	-	2.26e−02	-	4.73e−03	-	8.04e−03	-

Table 1.3: History of convergence of the approximation in Example 1.2.3. (Fuente: Elaboración propia)

Computational domain at a distance $d(\Gamma, \Gamma^h) = O(h^2)$

Another practical construction of $\mathcal{T}_h$ is defining first Γ^h by interpolating Γ using piecewise linear segments. Then, $\mathcal{T}_h$ is the domain enclosed by Γ_h as Fig. 1.6 shows. In this case $d(\Gamma, \Gamma_h) = O(h^2)$ and the family of paths can be easily defined according to **(P2)**.

Example 1.2.4. We consider the domain $\Omega = \{(x,y) \in \mathbb{R}^2 : 1 < (x-0.5)^2 + (y-0.5)^2 < 4\}$ with $\Gamma_N = \{(x,y) \in \mathbb{R}^2 : x^2 + y^2 = 1\}$ and $\Gamma_D = \{(x,y) : x^2 + y^2 = 4\}$. In Table 1.4 we observe again that the order of convergence in all the variables in $k+1$. We point out that part of the computational domain is outside of Ω as it can be observed in the inner circle in Fig. 1.6. This was never the case in the examples provided by [41] and [37]. Thus, these results indicates that their technique also works when $\Omega^c \cap \mathcal{T}_h \neq \emptyset$. In Fig. 1.7 we show the approximated solution p_h considering $h = 1.10$ (left) and 0.55 (right) and using polynomials of degree $k = 0, 1$ and 2. We clearly see an improvement either when the mesh is refined or the polynomial degree increases.

		$\|e_u\|_{\text{int}}$		$\|e_{\boldsymbol{q}}\|_{\text{int}}$		$\|e_{\widehat{u}}\|_{\mathcal{E}_h}$		$\|e_{u^*}\|_{\text{int}}$	
k	h	error	order	error	order	error	order	error	order
	1.72	5.31e−01	-	2.14e+00	-	2.22e−01	-	6.63e−01	-
	1.10	2.87e−01	1.37	1.19e+00	1.3	1.14e−01	1.48	3.00e−01	1.77
0	0.55	1.45e−01	0.99	6.13e−01	0.95	5.76e−02	1.00	1.46e−01	1.04
	0.29	8.10e−02	0.89	3.31e−01	0.95	3.10e−02	0.95	8.05e−02	0.91
	0.15	4.36e−02	0.98	1.69e−01	1.07	1.60e−02	1.05	4.34e−02	0.98
	0.08	2.24e−02	0.99	8.48e−02	1.02	8.12e−03	1.01	2.23e−02	1.00
	1.72	2.59e−01	-	9.51e−03	-	9.51e−03	-	1.22e−01	-
	1.10	7.11e−02	2.89	1.61e−03	3.97	1.61e−03	3.97	1.80e−02	4.27
1	0.55	1.77e−02	2.01	2.50e−04	2.68	2.50e−04	2.68	2.54e−03	2.82
	0.29	4.45e−03	2.12	5.92e−05	2.22	5.92e−05	2.22	4.23e−04	2.76
	0.15	1.08e−03	2.26	1.43e−05	2.25	1.43e−05	2.25	9.03e−05	2.45
	0.08	2.66e−04	2.08	4.24e−06	1.81	4.24e−06	1.81	2.69e−05	1.80
	1.72	4.59e−02	-	6.22e−02	-	1.43e−03	-	1.04e−02	-
	1.10	6.55e−03	4.35	9.09e−03	4.29	1.95e−04	4.44	1.35e−03	4.56
2	0.55	8.37e−04	2.97	1.26e−03	2.85	1.10e−05	4.15	8.25e−05	4.03
	0.29	1.12e−04	3.09	1.71e−04	3.07	2.14e−06	2.52	1.44e−05	2.67
	0.15	1.42e−05	3.29	2.11e−05	3.32	2.01e−07	3.75	1.34e−06	3.77
	0.08	1.77e−06	3.10	2.63e−06	3.10	3.37e−08	2.66	2.22e−07	2.68
	1.72	5.61e−03	-	8.48e−03	-	0.57e−04	-	1.28e−03	-
	1.10	4.47e−04	5.65	6.59e−04	5.71	6.52e−06	7.11	4.82e−05	7.32
3	0.55	3.31e−05	3.75	4.77e−05	3.78	1.77e−07	5.20	1.42e−06	5.08
	0.29	2.26e−06	4.12	3.30e−06	4.11	1.51e−08	3.78	1.04e−07	4.01
	0.15	1.37e−07	4.46	2.12e−07	4.36	9.59e−10	4.39	6.42e−09	4.43
	0.08	8.47e−09	4.14	1.32e−08	4.13	9.52e−11	3.43	6.28e−10	3.46

Table 1.4: History of convergence of the approximation in Example 1.2.4. (Fuente: Elaboración propia)

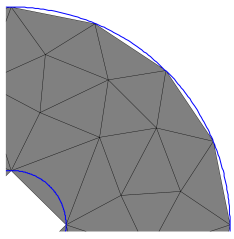

Figure 1.6: Zoom at the upper-right corner of Example 1.2.4. Blue line: boundary Γ. Grey region: mesh. (Fuente: Elaboración propia)

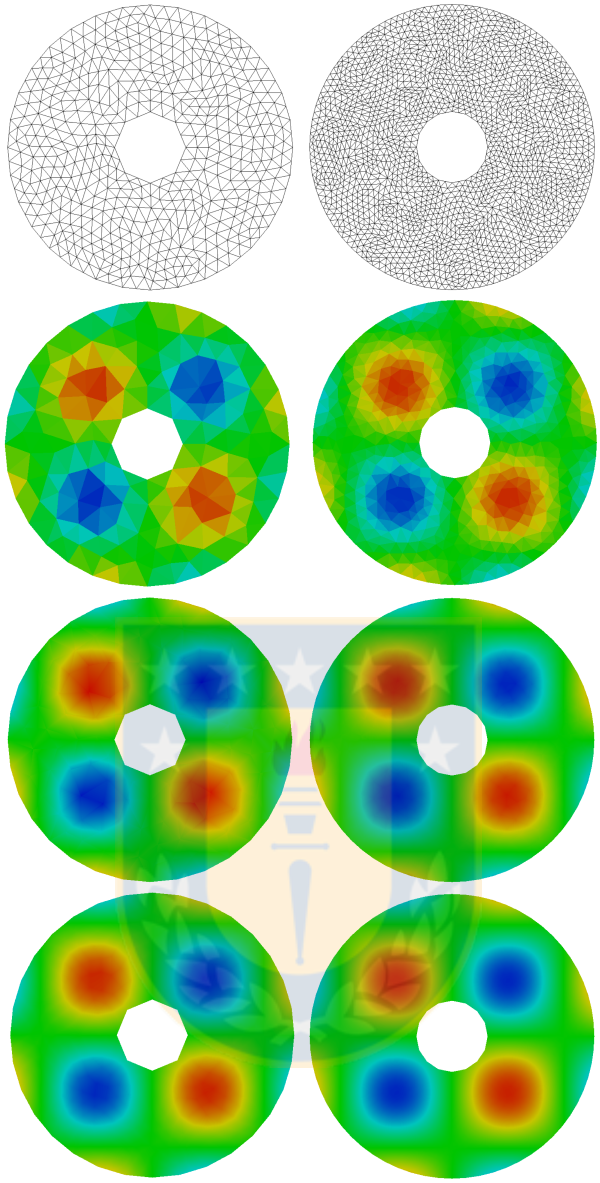

Figure 1.7: Approximation of the scalar variable in Example 1.2.4. Columns: meshsize $h = 1.10$ and 0.55. Rows: Polynomial of degree $k = 0, 1$ and 2. (Fuente: Elaboración propia)

Example 1.2.5. Now we test the performance of the method where Ω is a bounded domain exterior to an airfoil. This is the most difficult case in our examples since the domain has a boundary with a curved, re-entrant corner. The airfoil is obtained by using the Joukowsky transformation:

$$J(z) = z + \frac{\lambda^2}{z},$$

where $z \in \mathbb{C}$ and $\lambda \in \mathbb{R}$. It is well known that this transformation maps the disc centered at (s_1, s_2) of radius R to an airfoil when we set $\lambda = R - \sqrt{s_1^2 + s_2^2}$. Here, we take $R = 0.1605$ and $s_1 = s_2 = 0.01$. In Fig. 1.8 we show two triangulations of the domain with meshsizes $h = 0.143$ and 0.073. Neumann boundary conditions are imposed around the airfoil and Dirichlet data in the remaining part of the boundary.

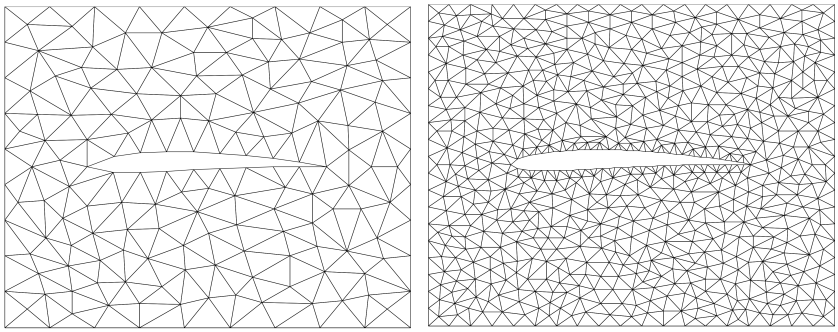

Figure 1.8: Meshes of Example 1.2.5. Meshsizes $h = 0.143$ and 0.073. (Fuente: Elaboración propia)

We consider the following two examples:

a) **Smooth solution**. We set f and g such that $u(x, y) = \sin(x)\sin(y)$ is the exact solution as in previous example. In Table 1.5 we observe that similar conclusions to those in previous examples can be drawn, even though in the case the domain is more complicated.

		$\|e_u\|_{\text{int}}$		$\|e_{\boldsymbol{q}}\|_{\text{int}}$		$\|e_{\widehat{u}}\|_{\mathcal{E}_h}$		$\|e_{u^*}\|_{\text{int}}$	
k	h	error	order	error	order	error	order	error	order
	0.143	5.69e−03	-	2.25e−02	-	1.35e−03	-	5.76e−03	-
	0.113	4.78e−03	0.75	1.71e−02	1.18	7.52e−04	2.50	4.81e−03	0.77
0	0.073	3.12e−03	0.98	1.05e−02	1.11	4.30e−04	1.29	3.14e−03	0.98
	0.038	1.59e−03	1.03	5.36e−03	1.04	1.97e−04	1.19	1.59e−03	1.04
	0.024	9.93e−04	1.02	3.25e−03	1.08	1.21e−04	1.06	9.94e−04	1.02
	0.143	1.41e−04	-	2.91e−04	-	1.46e−05	-	1.48e−05	-
	0.113	8.04e−05	2.38	1.68e−04	2.33	8.36e−06	2.39	8.46e−06	2.37
1	0.073	3.36e−05	2.01	6.72e−05	2.11	1.95e−06	3.35	1.96e−06	3.36
	0.038	8.51e−06	2.11	1.74e−05	2.07	5.30e−07	2.00	5.14e−07	2.05
	0.024	3.21e−06	2.11	6.50e−06	2.12	1.32e−07	3.00	1.28e−07	3.00
	0.143	1.89e−06	-	3.58e−06	-	1.92e−07	-	1.85e−07	-
	0.113	8.56e−07	3.37	1.55e−06	3.56	6.58e−08	4.56	6.34e−08	4.56
2	0.073	2.27e−07	3.06	4.06e−07	3.09	5.65e−09	5.65	5.67e−09	5.56
	0.038	2.96e−08	3.12	5.30e−08	3.12	6.17e−10	3.39	5.97e−10	3.45
	0.024	6.87e−09	3.15	1.24e−08	3.14	7.78e−11	4.47	7.57e−11	4.45
	0.143	2.13e−08	-	3.00e−08	-	1.04e−08	-	9.98e−10	-
	0.113	7.16e−09	4.64	1.06e−08	4.44	3.33e−09	4.86	3.20e−10	4.85
3	0.073	1.32e−09	3.89	1.80e−09	4.08	1.89e−10	6.61	1.83e−11	6.58
	0.038	8.65e−11	4.18	1.20e−10	4.14	1.47e−11	3.91	1.40e−12	3.95
	0.024	1.25e−11	4.17	1.75e−11	4.16	3.52e−12	3.09	3.32e−13	3.10

Table 1.5: History of convergence of the approximation in Example 1.2.5a) (smooth solution). (Fuente: Elaboración propia)

b) **Non-smooth solution**. We now consider a potential flow around the airfoil where the exact solution in polar coordinates is $u(r, \theta) = r\cos(\theta)\big(1 + R^2/r^2\big)$. Here $g_N = 0$ around the airfoil. In this case ∇u has singularities at the leading and trailing edges, hence we do not expect high order convergence rates. In fact, this can be seen on Table 1.6 where in all the cases u converges

with order one and $\boldsymbol{q}$ converges with order less than one. However, for a fixed mesh, the errors decrease when the polynomial degree increases. In Fig. 1.9 we show the approximation of the x-component of $\boldsymbol{q}$ considering $h = 0.143$ and 0.024 and $k = 0, 1$ and 2.

		$\|e_u\|_{\text{int}}$		$\|e_{\boldsymbol{q}}\|_{\text{int}}$		$\|e_{\widehat{u}}\|_{\mathcal{E}_h}$		$\|e_{u^*}\|_{\text{int}}$	
k	h	error	order	error	order	error	order	error	order
	0.143	2.49e−03	-	2.20e−02	-	1.40e−03	-	2.53e−0	-
	0.113	1.81e−03	1.35	1.62e−02	1.29	7.08e−04	2.92	1.84e−03	1.36
0	0.073	1.11e−03	1.11	1.10e−02	0.90	2.94e−04	2.02	1.12e−03	1.14
	0.038	5.75e−04	1.01	7.23e−03	0.64	1.63e−04	0.91	5.77e−04	1.02
	0.024	3.49e−04	1.08	5.73e−03	0.50	9.09e−05	1.26	3.50e−04	1.08
	0.143	4.04e−04	-	8.38e−03	-	4.29e−04	-	3.97e−04	-
	0.113	1.80e−04	3.45	5.60e−03	1.72	2.08e−04	3.09	1.89e−04	3.15
1	0.073	7.93e−05	1.88	3.38e−03	1.16	8.83e−05	1.97	8.07e−05	1.96
	0.038	4.52e−05	0.86	2.00e−03	0.80	4.82e−05	0.93	4.53e−05	0.88
	0.024	3.03e−05	0.86	1.63e−03	0.45	3.23e−05	0.87	3.03e−05	0.87
	0.143	1.55e−04	-	4.37e−03	-	1.77e−04	-	1.57e−04	-
	0.113	8.10e−05	2.78	3.02e−03	1.58	9.16e−05	2.81	8.12e−05	2.82
2	0.073	4.91e−05	1.15	1.72e−03	1.30	5.35e−05	1.24	4.91e−05	1.16
	0.038	2.70e−05	0.92	9.71e−04	0.87	2.87e−05	0.95	2.70e−05	0.92
	0.024	1.70e−05	0.99	8.32e−04	0.33	1.81e−05	0.99	1.70e−05	0.99
	0.143	7.94e−05	-	2.73e−03	-	9.13e−05	-	8.02e−05	-
	0.113	4.89e−05	2.06	1.84e−03	1.68	5.45e−05	2.19	4.92e−05	2.08
3	0.073	3.59e−05	0.71	1.09e−03	1.21	3.90e−05	0.77	3.60e−05	0.72
	0.038	1.79e−05	1.07	6.34e−04	0.83	1.90e−05	1.10	1.79e−05	1.07
	0.024	1.07e−05	1.10	5.15e−04	0.45	1.14e−05	1.10	1.08e−05	1.10

Table 1.6: History of convergence of the approximation in Example 1.2.5b) (non-smooth solution). (Fuente: Elaboración propia)

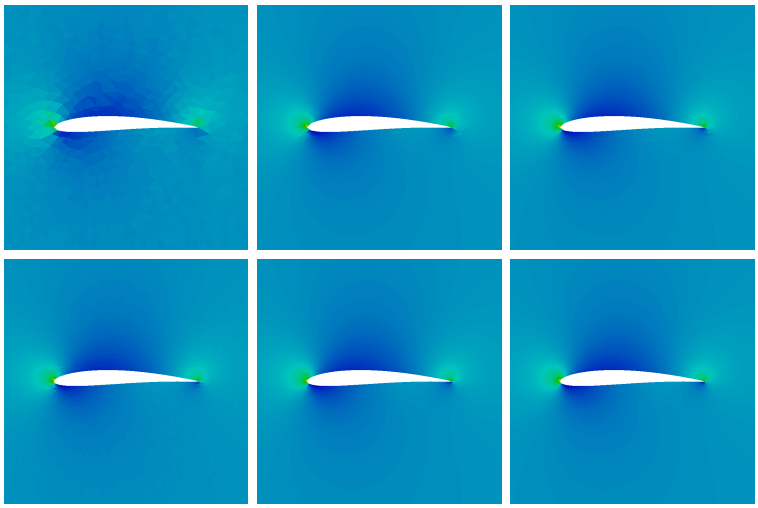

Figure 1.9: Approximation of the x-component of $\boldsymbol{q}$ Example 1.2.5 (non-smooth solution). Columns: Polynomial of degree $k = 0, 1$ and 2. Rows: meshsize $h = 0.143$ and 0.024. (Fuente: Elaboración propia)

1.3 Elliptic interface problem

Let us now consider an interface Σ that divides the domain Ω in two disjoint subdomains Ω^1 and Ω^2 as Figure 1.10 shows. Then, problem (1.1) becomes

$$\nabla \cdot \boldsymbol{q} = f \quad \text{in } \Omega, \tag{1.10a}$$
$$\boldsymbol{q} + \mathbf{K}\nabla u = 0 \quad \text{in } \Omega, \tag{1.10b}$$
$$u = g_D \text{ on } \Gamma_D, \tag{1.10c}$$
$$\boldsymbol{q} \cdot \boldsymbol{n} = g_N \text{ on } \Gamma_N, \tag{1.10d}$$
$$u|_{\Sigma^1} - u|_{\Sigma^2} = s_D \text{ on } \Sigma, \tag{1.10e}$$
$$\boldsymbol{q}|_{\Sigma^1} \cdot \boldsymbol{n^1} + \boldsymbol{q}|_{\Sigma^2} \cdot \boldsymbol{n^2} = s_N \text{ on } \Sigma. \tag{1.10f}$$

Here Σ^1 and Σ^2 are defined by

$$\Sigma^1 := \{\boldsymbol{x} - \epsilon \boldsymbol{n}^1 : \boldsymbol{x} \in \Sigma \text{ and } \epsilon \to 0\},$$
$$\Sigma^2 := \{\boldsymbol{x} - \epsilon \boldsymbol{n}^2 : \boldsymbol{x} \in \Sigma \text{ and } \epsilon \to 0\},$$

where $\boldsymbol{n}^j$ ($j \in \{1, 2\}$) is the unit outward normal unit vector of the subdomain Ω^j, $s_D \in H^{1/2}(\Sigma)$ and $s_N \in H^{-1/2}(\Sigma)$ are prescribed jumps at the interface. At Σ we adopt the convention $\boldsymbol{n} := \boldsymbol{n}^1$.

For the sake of simplicity we assume $\partial\Omega$ to be polygonal (if not, we apply the technique explained in previous section). However, the interface Σ is not necessarily piecewise flat. The numerical results provided in Section 1.2.4 for a boundary value problem, suggested that the distance between the computational domain and the boundary should be of order $O(h^2)$ with a family of paths normal to the computational boundary. That is why we interpolate the interface Σ by piecewise linear segments. The computational interface, denoted by Σ_h, divides the computational domain Ω_h in two disjoint unions of elements Ω_h^1 and Ω_h^2. Σ_h^j ($j \in \{1, 2\}$) is defined as $\Sigma_h^j := \{\boldsymbol{x} - \epsilon \boldsymbol{n}_h^j : \boldsymbol{x} \in \Sigma_h \text{ and } \epsilon \to 0\}$, where $\boldsymbol{n}_h^j$ is the unit outward normal vector of the computational domain Ω_h^j.

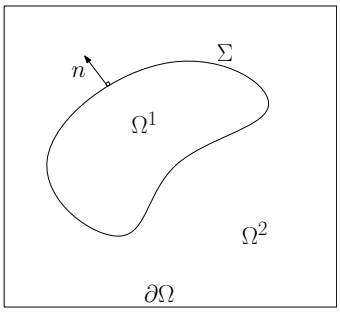

Figure 1.10: Example domain Ω divided in two regions Ω^1 and Ω^2 by an interface Σ. (Fuente: Elaboración propia)

Let s_D^h be an approximation of the jump of the discrete scalar variable in Σ_h. In Section 1.3.1 we will justify a proper choice of s_D^h. On the other hand, the jump s_N will be imposed at Σ by using the idea explained in Section 1.2.3.

Following the approach by [75], the method HDG applied to the interface problem seeks an approximation $(\boldsymbol{q}_h, u_h, \lambda_h) \in \boldsymbol{V}_h \times W_h \times M_h$ such that

$$(\mathbf{K}^{-1}\boldsymbol{q}_h, \boldsymbol{v})_{\mathcal{T}_h} - (u_h, \nabla_h \cdot \boldsymbol{v})_{\mathcal{T}_h} + \langle \lambda_h, \boldsymbol{v}\cdot\boldsymbol{n}\rangle_{\partial\mathcal{T}_h} = 0, \tag{1.11a}$$

$$(w, \nabla_h \cdot \boldsymbol{q}_h)_{\mathcal{T}_h} + \langle (\widehat{\boldsymbol{q}}_h - \boldsymbol{q}_h)\cdot\boldsymbol{n}, w\rangle_{\partial\mathcal{T}_h} = (f, w)_{\mathcal{T}_h}, \tag{1.11b}$$

$$\langle \widehat{\boldsymbol{q}}_h \cdot \boldsymbol{n}, \mu\rangle_{\partial\mathcal{T}_h\setminus(\Gamma\cup\Sigma_h)} = 0, \tag{1.11c}$$

$$\langle \lambda_h, \mu\rangle_{\Gamma_D} = \langle g_D, \mu\rangle_{\Gamma_D}, \tag{1.11d}$$

$$\langle \widehat{\boldsymbol{q}}_h \cdot \boldsymbol{n}, \mu\rangle_{\Gamma_N} = \langle g_N, \mu\rangle_{\Gamma_N}, \tag{1.11e}$$

for all $(\boldsymbol{v}, w, \mu) \in \boldsymbol{V}_h \times W_h \times M_h$. The jump of the normal component of $\boldsymbol{q}_h$ at Σ_h will be specified in Section 1.3.2.

Here λ_h is a single-valued function, however the approximation of u must be double-valued on Σ_h. Then, similarly to [75], we let λ_h be the approximation of $u_h|_{\Sigma_h^2}$ and consider $\lambda_h + s_D^h$ as an approximation of $u_h|_{\Sigma_h^1}$. Thus, we define

$$\widehat{u}_h := \lambda_h + \delta_{\Sigma_h} s_D^h, \tag{1.11f}$$

where δ_{Σ_h}, defined on $\partial\mathcal{T}_h$, satisfies

$$\delta_{\Sigma_h} = \begin{cases} 1 & \text{on } \partial K \cap \Sigma_h, \text{ if } \partial K \cap \Sigma_h \neq \emptyset \text{ and } K \in \Omega_h^1, \\ 0 & \text{otherwise.} \end{cases} \tag{1.12}$$

To complete the method we define the numerical flux as usual

$$\widehat{\boldsymbol{q}}_h := \boldsymbol{q}_h - \tau(u_h - \widehat{u}_h)\boldsymbol{n} \quad \text{on} \quad \partial\mathcal{T}_h.$$

1.3.1 Approximation s_D^h

In order to define the approximation s_D^h, we use the same *transferring* technique used for the Dirichlet data on a curved boundary (1.3). Let $e \subset \Sigma_h$ such that $e = \partial K_1 \cap \partial K_2$ and, without loss of generality, assume that e lies completely inside of Ω^2. We denote by $(\boldsymbol{q}_h^j, u_h^j)$ the approximation $(\boldsymbol{q}_h, u_h)$ restricted to the domain Ω_h^j. Now, for each $\boldsymbol{x} \in e$, we observe that $\sigma(\boldsymbol{x}) \subset K_1 \cap \Omega^2$ and then, according to the approximation given in (1.5f),

$$u_h^2(\boldsymbol{x}) \approx u_h^2(\bar{\boldsymbol{x}}) + \int_{\sigma(\boldsymbol{x})} \mathbf{K}^{-1} E^{K_2}(\boldsymbol{q}_h^2)\cdot\boldsymbol{m}, \tag{1.13}$$

where $E^{K_2}(\boldsymbol{q}_h^2)$ is the standard extrapolation of $\boldsymbol{q}_h^2$ to the whole $\mathbb{R}^2$ space defined in (1.5d). Similarly,

$$u_h^1(\boldsymbol{x}) \approx u_h^1(\bar{\boldsymbol{x}}) + \int_{\sigma(\boldsymbol{x})} \mathbf{K}^{-1} E^{K_1}(\boldsymbol{q}_h^1)\cdot\boldsymbol{m}, \tag{1.14}$$

In this case $E^{K_1}(\boldsymbol{q}_h^1) = \boldsymbol{q}_h^1$.

Combining both equations,

$$u_h^1(\boldsymbol{x}) - u_h^2(\boldsymbol{x}) \approx u_h^1(\bar{\boldsymbol{x}}) - u_h^2(\bar{\boldsymbol{x}}) + \int_{\sigma(\boldsymbol{x})} \mathbf{K}^{-1} E^{K_1}(\boldsymbol{q}_h^1)\cdot\boldsymbol{m} - \int_{\sigma(\boldsymbol{x})} \mathbf{K}^{-1} E^{K_2}(\boldsymbol{q}_h^2)\cdot\boldsymbol{m}.$$

This expression suggest the following approximation

$$s_D^h(\boldsymbol{x}) := s_D(\bar{\boldsymbol{x}}) + \int_{\sigma(\boldsymbol{x})} \mathbf{K}^{-1} E^{K_1}(\boldsymbol{q}_h^1)\cdot\boldsymbol{m} - \int_{\sigma(\boldsymbol{x})} \mathbf{K}^{-1} E^{K_2}(\boldsymbol{q}_h^2)\cdot\boldsymbol{m}. \tag{1.15}$$

1.3.2 Imposition of s_N

For imposing s_N, we use the same idea that we have applied for a Neumann boundary edge. Hence, instead of imposing the normal component of $\boldsymbol{q}_h$ in Σ_h, we will do that on Σ by extrapolating $\boldsymbol{q}_h$. For each interface edge $e \in \Sigma_h$, we consider $\Sigma_e \subset \Sigma$, the part of Σ associated to e. We denote by K_e^1 and K_e^2 the element of Ω_h^1 and Ω_h^2 where e belongs. Then, we impose the following condition at the interface Σ:

$$\langle E^{K_e^1}(\boldsymbol{q}_h)\cdot\boldsymbol{n}^1 + E^{K_e^2}(\boldsymbol{q}_h)\cdot\boldsymbol{n}^2, \mu\rangle_{\Sigma_e} = \langle s_N, \mu\rangle_{\Sigma_e} \quad \forall \mu \in M_{\boldsymbol{\phi}}(\Sigma_e), \tag{1.16}$$

where $M_{\boldsymbol{\phi}}(\Sigma_e)$ is defined similarly as in (1.7).

1.3.3 Numerical results: Interface problem

Finally, in this section we consider three numerical examples showing the performance of our technique in elliptic interface problems. Since the computational domains Ω_h^1 and Ω_h^2 do not exactly fit Ω^1 and Ω^2, we exclude from the computation of the errors the triangles intersecting the interface. Otherwise, quantities computed in one domain would be compared with the exact solution in the other domain. Let $\widetilde{\mathcal{T}}_h$ the set of triangles whose faces are not interface edges. We measure the errors using the following norms $\|\cdot\|_{L^2(\widetilde{\Omega}_h)}$ and

$$\|e_{\hat{u}}\|_{L^2(\widetilde{\mathcal{E}}_h)} := \left(\sum_{K\in\widetilde{\mathcal{T}}_h : K\cap\Sigma_h=\emptyset} h_K \|\mathsf{P}_\partial u - \hat{u}_h\|^2_{L^2(\partial K)}\right)^{1/2}.$$

Example 1.3.1 (Elliptical-shaped domain)**.** We first solve a Poisson equation in a the domain $\Omega = (-1,1)^2$ divided by the elliptical interface Σ described by $(x/0.8)^2 + (y/0.4)^2 = 1$. We take $\mathbf{K} = \mathbf{I}$ and

$$u = \begin{cases} e^x\cos(y) & \text{in } \Omega^1 \\ \sin(\pi x)\sin(\pi y) & \text{in } \Omega^2 \end{cases}.$$

as exact solution. The source term, transmission and Dirichlet boundary conditions are obtained from this exact solution.

In Table 1.7 the history of convergence for this example is displayed. Similarly to the examples involving Neumann boundary data, the order of convergence for u and $\boldsymbol{q}$ are optimal whereas the convergence of the numerical trace is suboptimal, i.e., $O(h^{k+1})$. Moreover, even though superconvergence of the postprocessed solution u_h^* is lost, it provides a more accurate approximation of u. Figure 1.11 shows the approximation u_h obtained with meshsizes of $h = 0.072$ and 0.018; and polynomial degree $k = 0$, 1 and 2.

		$\|e_u\|_{L^2(\widetilde{\mathsf{D}}_h)}$		$\|e_{\boldsymbol{q}}\|_{L^2(\widetilde{\mathsf{D}}_h)}$		$\|e_{\widehat{u}}\|_{L^2(\widetilde{\mathcal{E}}_h)}$		$\|e_{u^*}\|_{L^2(\widetilde{\mathsf{D}}_h)}$	
k	h	error	order	error	order	error	order	error	order
	0.072	2.37e-01	–	3.53e-01	–	3.66e-02	–	4.16e-02	–
	0.035	1.22e-01	0.94	1.92e-01	0.87	2.01e-02	0.85	2.16e-02	0.93
0	0.018	5.97e-02	1.03	9.22e-02	1.04	1.05e-02	0.93	1.09e-02	0.98
	0.009	2.98e-02	1.01	4.66e-02	0.99	5.60e-03	0.92	5.67e-03	0.95
	0.004	1.50e-02	1.00	2.34e-02	1.00	2.84e-03	0.98	2.86e-03	0.99
	0.072	1.98e-02	–	4.20e-02	–	1.75e-03	–	2.24e-03	–
	0.035	4.95e-03	1.97	1.01e-02	2.03	1.63e-04	3.37	2.72e-04	3.00
1	0.018	1.24e-03	1.97	2.36e-03	2.07	2.05e-05	2.96	3.06e-05	3.12
	0.009	3.12e-04	2.01	5.78e-04	2.05	7.79e-06	1.41	8.02e-06	1.95
	0.004	7.85e-05	2.00	1.43e-04	2.02	1.24e-06	2.67	1.22e-06	2.73
	0.072	1.44e-03	–	3.93e-03	–	1.25e-04	–	1.58e-04	–
	0.035	2.00e-04	2.80	5.24e-04	2.86	2.69e-05	2.18	2.78e-05	2.47
2	0.018	2.43e-05	3.01	5.99e-05	3.10	1.89e-06	3.80	1.96e-06	3.79
	0.009	3.07e-06	3.01	7.54e-06	3.01	3.00e-07	2.67	3.03e-07	2.72
	0.004	3.92e-07	2.98	9.54e-07	2.99	3.99e-08	2.92	4.01e-08	2.93
	0.072	1.10e-04	–	3.02e-04	–	7.05e-06	–	8.09e-06	–
	0.035	7.78e-06	3.76	2.16e-05	3.75	1.79e-07	5.21	3.06e-07	4.65
3	0.018	4.49e-07	4.08	1.17e-06	4.16	6.33e-09	4.78	8.78e-09	5.08
	0.009	2.82e-08	4.02	7.17e-08	4.06	4.60e-10	3.81	4.96e-10	4.18
	0.004	1.80e-09	3.98	4.49e-09	4.01	1.93e-11	4.59	2.02e-11	4.63

Table 1.7: History of convergence of the approximation in Example 1.3.1 (elliptical-shaped). (Fuente: Elaboración propia)

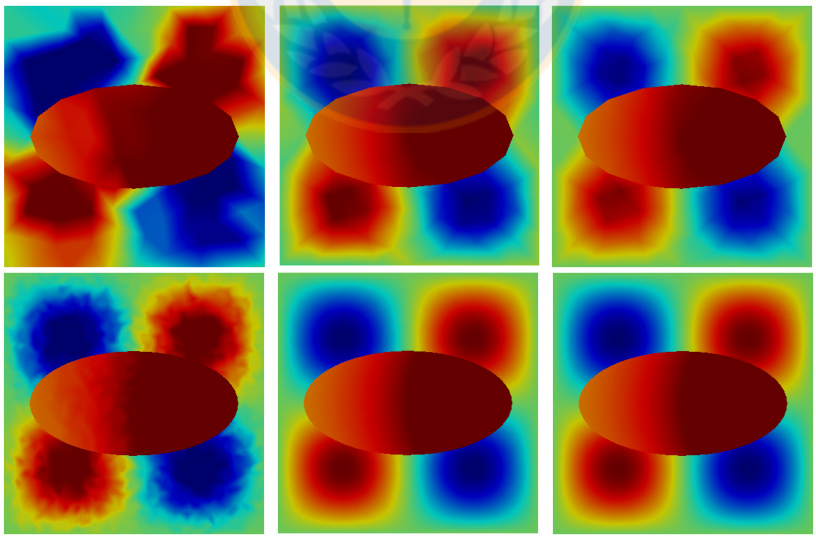

Figure 1.11: Approximation of the scalar variable in Example 1.3.1. Columns: Polynomial of degree $k = 0$, 1 and 2. Rows: meshsize of $h = 0.072$ and 0.018. (Fuente: Elaboración propia)

Example 1.3.2 (Kidney-shaped domain)**.** We now consider the same exact solution as in previous example, but considering a kidney-shaped described by $(2[(x+0.5)^2+y^2]-x-0.5)^2-[(x+0.5)^2+y^2]+0.1=0$. Despite of the changes of convexity of this geometry, Table 1.8 shows similar accuracy

on the approximations as the ones obtained in Example 1.3.1. Figure 1.12 shows the quality of the approximations of the scalar variable u_h and its postprocessing u_h^* obtained with a meshsize of $h = 0.069$ and polynomial degree $k = 0$, 1 and 2. As expected, u_h^* provides a more accurate approximation of u_h without significantly increase the computational cost.

		$\|e_u\|_{L^2(\widetilde{\mathsf{D}}_h)}$		$\|e_{\boldsymbol{q}}\|_{L^2(\widetilde{\mathsf{D}}_h)}$		$\|e_{\widehat{u}}\|_{L^2(\widetilde{\mathcal{E}}_h)}$		$\|e_{u^*}\|_{L^2(\widetilde{\mathsf{D}}_h)}$	
k	h	error	order	error	order	error	order	error	order
	0.069	2.37e-01	–	3.76e-01	–	3.80e-02	–	4.39e-02	–
	0.035	1.23e-01	0.97	2.05e-01	0.90	1.97e-02	0.98	2.12e-02	1.08
0	0.018	6.07e-02	1.03	9.73e-02	1.09	1.09e-02	0.86	1.13e-02	0.92
	0.009	3.01e-02	1.01	4.79e-02	1.02	5.69e-03	0.94	5.77e-03	0.97
	0.004	1.51e-02	1.00	2.41e-02	1.00	2.89e-03	0.99	2.91e-03	1.00
	0.069	2.13e-02	–	4.35e-02	–	1.89e-03	–	2.59e-03	–
	0.035	5.30e-03	2.06	1.08e-02	2.05	4.31e-04	2.19	4.94e-04	2.45
1	0.018	1.33e-03	2.03	2.63e-03	2.07	1.03e-04	2.10	1.08e-04	2.23
	0.009	3.28e-04	2.01	6.24e-04	2.07	2.22e-05	2.20	2.27e-05	2.24
	0.004	8.28e-05	2.00	1.56e-04	2.01	5.74e-06	1.97	5.78e-06	1.99
	0.069	1.56e-03	–	3.72e-03	–	1.39e-04	–	1.74e-04	–
	0.035	2.02e-04	3.02	5.62e-04	2.79	1.78e-05	3.04	1.93e-05	3.25
2	0.018	2.58e-05	3.02	6.53e-05	3.15	2.53e-06	2.86	2.60e-06	2.93
	0.009	3.19e-06	3.01	7.76e-06	3.07	4.17e-07	2.60	4.19e-07	2.63
	0.004	4.04e-07	3.00	9.80e-07	3.01	5.03e-08	3.07	5.04e-08	3.08
	0.069	1.31e-04	–	3.50e-04	–	1.27e-05	–	1.40e-05	–
	0.035	7.96e-06	4.13	2.11e-05	4.15	9.42e-07	3.84	9.68e-07	3.94
3	0.018	4.92e-07	4.08	1.27e-06	4.11	4.03e-08	4.61	4.10e-08	4.63
	0.009	2.92e-08	4.06	7.37e-08	4.10	2.22e-09	4.18	2.23e-09	4.19
	0.004	1.87e-09	3.99	4.71e-09	4.00	1.44e-10	3.98	1.44e-10	3.98

Table 1.8: History of convergence of the approximation in Example 1.3.2 (kidney-shaped). (Fuente: Elaboración propia)

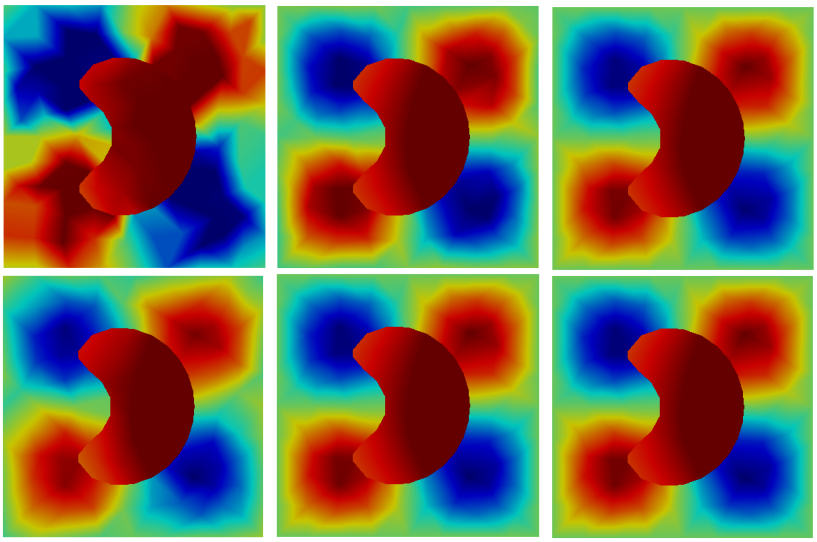

Figure 1.12: Approximations u_h (left) and u_h^* of the scalar variable u of Example 1.3.2. Columns: Polynomial of degree $k = 0$, 1 and 2. Rows: meshsize $h = 0.069$. (Fuente: Elaboración propia)

Example 1.3.3 (Thermal conductivity)**.** Finally, considering the example provided by [75], we simulate the heat distribution u at steady state, due to the heat source f, over the domain $\Omega = (-1,1)^2$ divided by a circular interface of radius $R = 0.5$ centered at the origin. The source term f and the thermal conductivity tensor are given by

$$f(x,y) = -10(x^2+y^2)^{3/2} - 15x^2(x^2+y^2)^{1/2} - 15y^2(x^2+y^2)^{1/2}$$

and $\mathbf{K} = \kappa_j \mathbf{I}$ in Ω^j $(j = 1, 2)$. The exact solution of this problem is

$$u = \begin{cases} \frac{1}{\kappa_1}(x^2+y^2)^{5/2} & \text{in } \Omega^1 \\ \frac{1}{\kappa_2}(x^2+y^2)^{5/2} + \left(\frac{1}{\kappa_1} - \frac{1}{\kappa_2}\right) R^5 & \text{in } \Omega^2 \end{cases},$$

and we consider $\kappa_1 = 1$, $\kappa_2 = 100$. Dirichlet boundary condition on Γ is derived from the previous equation. In this case the jumps s_D and s_N are both equal to zero. Table 1.9 validates the optimal convergence rates of order h^{k+1} for the heat distribution u and the flux $\boldsymbol{q}$. Figure 1.13 shows the approximated heat distribution considering meshes of size $h = 0.072$ and 0.018, and polynomials of degree $k = 0$, 1 and 2.

		$\|e_u\|_{L^2(\widetilde{\mathsf{D}}_h)}$		$\|e_{\boldsymbol{q}}\|_{L^2(\widetilde{\mathsf{D}}_h)}$		$\|e_{\widehat{u}}\|_{L^2(\widetilde{\mathcal{E}}_h)}$		$\|e_{u^*}\|_{L^2(\widetilde{\mathsf{D}}_h)}$	
k	h	error	order	error	order	error	order	error	order
	0.072	9.10e-03	–	5.66e-01	–	1.42e-03	–	1.63e-03	–
	0.035	7.30e-03	0.31	3.09e-01	0.84	7.58e-04	0.88	8.22e-04	0.96
0	0.018	4.56e-03	0.68	1.46e-01	1.08	4.04e-04	0.91	4.21e-04	0.97
	0.009	2.50e-03	0.87	7.32e-02	1.01	2.09e-04	0.96	2.13e-04	0.99
	0.004	1.28e-03	0.96	3.60e-02	1.02	1.06e-04	0.97	1.07e-04	0.99
	0.072	1.39e-03	–	5.99e-02	–	5.95e-05	–	1.55e-04	–
	0.035	4.51e-04	1.57	1.45e-02	1.98	1.23e-05	2.20	1.87e-05	2.95
1	0.018	1.36e-04	1.74	3.36e-03	2.12	2.34e-06	2.39	3.26e-06	2.52
	0.009	3.73e-05	1.88	8.24e-04	2.04	5.18e-07	2.19	6.20e-07	2.41
	0.004	9.42e-06	1.98	2.06e-04	1.99	6.66e-08	2.95	8.03e-08	2.94
	0.072	1.69e-04	–	3.94e-03	–	1.28e-05	–	2.07e-05	–
	0.035	2.33e-05	2.77	4.62e-04	3.00	9.34e-07	3.66	1.19e-06	3.99
2	0.018	3.40e-06	2.78	5.36e-05	3.11	1.05e-07	3.16	1.19e-07	3.32
	0.009	4.73e-07	2.87	6.64e-06	3.04	1.38e-08	2.95	1.45e-08	3.07
	0.004	5.94e-08	2.98	7.84e-07	3.07	1.39e-09	3.30	1.43e-09	3.33
	0.072	1.35e-05	–	1.58e-04	–	8.50e-07	–	1.24e-06	–
	0.035	8.36e-07	3.89	7.36e-06	4.28	1.80e-08	5.39	2.51e-08	5.45
3	0.018	5.64e-08	3.90	4.05e-07	4.19	1.03e-09	4.13	1.23e-09	4.37
	0.009	3.94e-09	3.87	2.43e-08	4.09	6.98e-11	3.92	7.39e-11	4.08
	0.004	2.49e-10	3.97	1.41e-09	4.10	2.02e-12	5.10	2.17e-12	5.08

Table 1.9: History of convergence of the approximation in Example 1.3.3 (thermal conductivity). (Fuente: Elaboración propia)

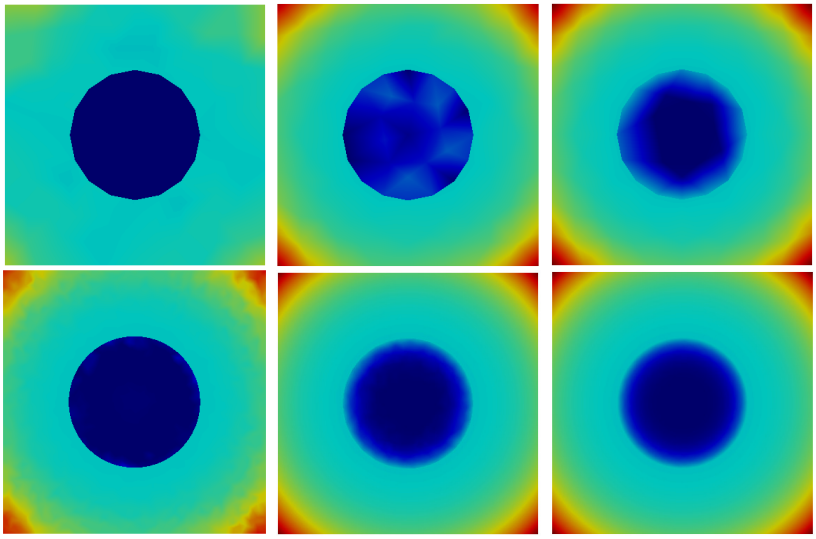

Figure 1.13: Approximation of the scalar variable in Example 1.3.3 (thermal conductivity). Columns: Polynomial of degree $k = 0$, 1 and 2. Rows: meshsize $h = 0.072$ and 0.018. (Fuente: Elaboración propia)

Remark 1.3.1. *If the mesh is fine enough, the errors e_u, $e_{\boldsymbol{q}}$ and e_{u^*} can be computed in the entire computational domain Ω_h since the quadrature points of a triangle $K \subset \Omega_h^j$ will eventually lie in Ω^j. This happens in all previous examples. In fact, we computed the errors $\|e_u\|_{L^2(\Omega_h)}$, $\|e_{\boldsymbol{q}}\|_{L^2(\Omega_h)}$ and $\|e_{u*}\|_{L^2(\Omega_h)}$. Their behavior and magnitude are similar to ones displayed in the convergence tables.*

CHAPTER 2

Analysis of an adaptive HDG method for the Brinkman problem

In this chapter we present an a priori error analysis for an HDG method applied to the Brinkman problem, showing optimal order of convergence of the error. We also introduce an a posteriori error estimator, of the residual type, which helps us to improve the quality of the numerical solution. We establish reliability and local efficiency of our estimator for the L^2-error of the velocity gradient and the pressure and the H^1- error of the velocity, with constants written explicitly in terms of the physical parameters and independent of the meshsize.

2.1 Introduction

We consider the Brinkman equation of an incompressible flow through porous media under the action of an external body force and with prescribed velocity on the boundary of the porous media. The problem can be formulated as follows

$$\mathrm{L} - \nabla \boldsymbol{u} = 0 \qquad \text{in } \Omega, \tag{2.1a}$$

$$-\nabla \cdot (\nu \mathrm{L}) + \nabla p + \alpha \boldsymbol{u} = \boldsymbol{f} \qquad \text{in } \Omega, \tag{2.1b}$$

$$\nabla \cdot \boldsymbol{u} = 0 \qquad \text{in } \Omega, \tag{2.1c}$$

$$\boldsymbol{u} = \boldsymbol{u}_D \qquad \text{on } \Gamma, \tag{2.1d}$$

$$\int_\Omega p = 0, \tag{2.1e}$$

where $\Omega \subset \mathbb{R}^d$ $(d = 2, 3)$ is a polygonal/polyhedral domain with Lipschitz boundary Γ, $\boldsymbol{u}$ is the velocity, p is the pressure, $\nu > 0$ is the effective viscosity of the fluid, $\alpha \geq 0$ is the quotient between the dynamic viscosity and the permeability of the media, $\boldsymbol{f} \in L^2(\Omega)^d$ is the external body force and $\boldsymbol{u}_D \in H^{1/2}(\Gamma)^d$ is the Dirichlet boundary data, assumed to satisfy $\int_\Gamma \boldsymbol{u}_D \cdot \boldsymbol{n} = 0$ for compatibility.

The Brinkman equation constitutes a generalization of the Darcy's equation $\boldsymbol{u} = -\alpha^{-1}\nabla p$ that describes the flow of a fluid through a porous mass with low particle density, i.e. a medium with high permeability [13]. It was motivated by the calculation of the viscous force exerted by a flowing fluid on a dense swarm of particles, where the model includes the viscous effect to state the equilibrium between the forces acting of a volume of fluid, i.e. the pressure gradient and the damping force, $\alpha\boldsymbol{u}$, caused by the porous mass. Applications of the Brinkman equation arise, for instance, from composite

manufacturing [71], heat pipes [80], computational fuel cell dynamics [85] and groundwater/oil reservoir modeling. In the last case, it is of interest to study how the fluid behaves during the transition from slow to fast flow through heterogeneous porous media with different contrasting porosities or with fractures, faults or wells. This phenomenon is described by the incompressible Navier-Stokes equation in the medium with large porosity, whereas Darcy's law could be considered in regions with small porosity. However, Darcy's equation is not enough to determine the transmission conditions across the interface between both media. That is why Brinkman equation is employed instead.

2.1.1 An HDG method for the Brinkman problem

Let us consider the approximation spaces:

$$\mathrm{G}_h := \{\mathrm{G} \in [L^2(\mathcal{T}_h)]^{d\times d} : \mathrm{G}|_K \in [\mathbb{P}_k(K)]^{d\times d} \quad \forall K \in \mathcal{T}_h\}, \tag{2.2a}$$
$$\boldsymbol{V}_h := \{\boldsymbol{v} \in [L^2(\mathcal{T}_h)]^{d} : \boldsymbol{v}|_K \in [\mathbb{P}_k(K)]^{d} \quad \forall K \in \mathcal{T}_h\}, \tag{2.2b}$$
$$P_h := \{w \in L^2(\mathcal{T}_h) : w|_T \in \mathbb{P}_k(K) \quad \forall K \in \mathcal{T}_h\}, \tag{2.2c}$$
$$\boldsymbol{M}_h := \{\boldsymbol{\mu} \in [L^2(\mathcal{E}_h)]^{d} : \boldsymbol{\mu}|_e \in [\mathbb{P}_k(e)]^{d} \quad \forall e \in \mathcal{E}_h\}. \tag{2.2d}$$

Then, based on the method developed in [89] for the Stokes flow, we introduce an HDG formulation for Brinkman problem (2.1) that approximates the exact solution $(\mathrm{L}, \boldsymbol{u}, p, \boldsymbol{u}|_{\mathcal{E}_h})$ by the only solution of the following scheme: *Find* $(\mathrm{L}_h, \boldsymbol{u}_h, p_h, \widehat{\boldsymbol{u}}_h) \in \mathrm{G}_h \times \boldsymbol{V}_h \times P_h \times \boldsymbol{M}_h$ *such that*

$$(\mathrm{L}_h, \mathrm{G})_{\mathcal{T}_h} + (\boldsymbol{u}_h, \nabla\cdot \mathrm{G})_{\mathcal{T}_h} - \langle \widehat{\boldsymbol{u}}_h, \mathrm{G}\boldsymbol{n}\rangle_{\partial\mathcal{T}_h} = 0, \tag{2.3a}$$
$$(\nu\mathrm{L}_h, \nabla\boldsymbol{v})_{\mathcal{T}_h} - (p_h, \nabla\cdot\boldsymbol{v})_{\mathcal{T}_h} + (\alpha\boldsymbol{u}_h, \boldsymbol{v})_{\mathcal{T}_h} - \langle \widehat{\nu\mathrm{L}}_h\boldsymbol{n} - \widehat{p}_h\boldsymbol{n}, \boldsymbol{v}\rangle_{\partial\mathcal{T}_h} = (\boldsymbol{f}, \boldsymbol{v})_{\mathcal{T}_h}, \tag{2.3b}$$
$$-(\boldsymbol{u}_h, \nabla q)_{\mathcal{T}_h} + \langle \widehat{\boldsymbol{u}}_h\cdot\boldsymbol{n}, q\rangle_{\partial\mathcal{T}_h} = 0, \tag{2.3c}$$
$$\langle \widehat{\boldsymbol{u}}_h, \boldsymbol{\mu}\rangle_{\Gamma} = \langle \boldsymbol{u}_D, \boldsymbol{\mu}\rangle_{\Gamma}, \tag{2.3d}$$
$$\langle \widehat{\nu\mathrm{L}}_h\boldsymbol{n} - \widehat{p}_h\boldsymbol{n}, \boldsymbol{\mu}\rangle_{\partial\mathcal{T}_h\setminus\Gamma} = 0, \tag{2.3e}$$
$$(p_h, 1)_{\Omega} = 0, \tag{2.3f}$$

for all $(\mathrm{G}, \boldsymbol{v}, q, \boldsymbol{\mu}) \in \mathrm{G}_h \times \boldsymbol{V}_h \times P_h \times \boldsymbol{M}_h$. Here, $\widehat{\nu\mathrm{L}}_h\boldsymbol{n} - \widehat{p}_h\boldsymbol{n} := \nu\mathrm{L}_h\boldsymbol{n} - p_h\boldsymbol{n} - \nu\tau(\boldsymbol{u}_h - \widehat{\boldsymbol{u}}_h)$ on $\partial\mathcal{T}_h$ and τ is a positive stabilization function on $\partial\mathcal{T}_h$ that we assume, without loss of generality, to be of order one. For other choices of τ we refer to [33].

2.1.2 Local postprocessing of the vector solution

One of the features of HDG method is the construction of a local element-by-element postprocessing $\boldsymbol{u}_h^*$ of $\boldsymbol{u}_h$ that approximates $\boldsymbol{u}$ with enhanced accuracy. In our case, we propose to construct $\boldsymbol{u}_h^*$ suited for the Brinkman problem as follows. We seek $\boldsymbol{u}_h^* \in \boldsymbol{V}_h^* := \{\boldsymbol{w} \in [L^2(\Omega)]^d : \boldsymbol{w}|_K \in [\mathbb{P}_{k+1}(K)]^d \ \forall K \in \mathcal{T}_h\}$ such that, for all $K \in \mathcal{T}_h$, it satisfies

$$\nu(\nabla\boldsymbol{u}_h^*, \nabla\boldsymbol{w})_K + \alpha(\boldsymbol{u}_h^*, \boldsymbol{w})_K = \nu(\mathrm{L}_h, \nabla\boldsymbol{w})_K + \alpha(\boldsymbol{u}_h, \boldsymbol{w})_K \quad \forall \boldsymbol{w} \in [\mathbb{P}_{k+1}(K)]^d \tag{2.4a}$$

and, if $\alpha = 0$, also satisfies the following equation

$$(\boldsymbol{u}_h^*, \boldsymbol{w})_K = (\boldsymbol{u}_h, \boldsymbol{w})_K \qquad \forall \boldsymbol{w} \in [\mathbb{P}_0(K)]^d. \tag{2.4b}$$

It's straightforward to see that $\boldsymbol{u}_h^*$ is well defined. Moreover, this new approximations will play a crucial role in the *a posteriori* error analysis as we will see in Section 2.3.

2.2 A priori error analysis

The *a priori* error estimates are carried out by using the projection-based analysis in [33], which consists of introducing a suitable projection Π_h, defined by (1), that helps us to write the error as the sum of an approximation error, whose estimates are contained in Lemma 0.1, and a projection of the error.

Now, let $\mathsf{P}_M\boldsymbol{u}$ be the L^2-projection of $\boldsymbol{u}$ into $\boldsymbol{M}_h$. Then, the projection of the errors $\Pi_{\mathrm{G}}\mathrm{L} - \mathrm{L}_h$, $\Pi_{\boldsymbol{V}}\boldsymbol{u} - \boldsymbol{u}_h$, $\mathsf{P}_M\boldsymbol{u} - \widehat{\boldsymbol{u}}_h$ and $\Pi_P p - p_h$ satisfy the the following equations

Lemma 2.2.1. *For all* $(\mathrm{G}, \boldsymbol{v}, q, \boldsymbol{\mu}) \in \mathrm{G}_h \times \boldsymbol{V}_h \times P_h \times \boldsymbol{M}_h$ *it holds*

$$
\begin{aligned}
(\Pi_{\mathrm{G}}\mathrm{L} - \mathrm{L}_h, \mathrm{G})_{\mathcal{T}_h} + (\Pi_{\boldsymbol{V}}\boldsymbol{u} - \boldsymbol{u}_h, \nabla\cdot\mathrm{G})_{\mathcal{T}_h} - \langle \mathsf{P}_M\boldsymbol{u} - \widehat{\boldsymbol{u}}_h, \mathrm{G}\boldsymbol{n}\rangle_{\partial\mathcal{T}_h} &= (\Pi_{\mathrm{G}}\mathrm{L} - \mathrm{L}, \mathrm{G})_{\mathcal{T}_h},\\
-(\nabla\cdot(\nu(\Pi_{\mathrm{G}}\mathrm{L} - \mathrm{L}_h)), \boldsymbol{v})_{\mathcal{T}_h} + \alpha(\Pi_{\boldsymbol{V}}\boldsymbol{u} - \boldsymbol{u}_h, \boldsymbol{v})_{\mathcal{T}_h} + (\nabla(\Pi_P p - p_h), \boldsymbol{v})_{\mathcal{T}_h} &\\
+\nu\langle \Pi_{\boldsymbol{V}}\boldsymbol{u} - \boldsymbol{u}_h - \mathsf{P}_M\boldsymbol{u} + \widehat{\boldsymbol{u}}_h, \boldsymbol{v}\rangle_{\partial\mathcal{T}_h} &= 0,\\
-(\Pi_{\boldsymbol{V}}\boldsymbol{u} - \boldsymbol{u}_h, \nabla q)_{\mathcal{T}_h} + \langle \mathsf{P}_M\boldsymbol{u} - \widehat{\boldsymbol{u}}_h, q\boldsymbol{n}\rangle_{\partial\mathcal{T}_h} &= 0,\\
\langle \mathsf{P}_M\boldsymbol{u} - \widehat{\boldsymbol{u}}_h, \boldsymbol{\mu}\rangle_{\Gamma} &= 0,\\
\langle \nu(\Pi_{\mathrm{G}}\mathrm{L} - \mathrm{L}_h)\boldsymbol{n} - (\Pi_P p - p_h)\boldsymbol{n} - (\Pi_{\boldsymbol{V}}\boldsymbol{u} - \boldsymbol{u}_h - \mathsf{P}_M\boldsymbol{u} + \widehat{\boldsymbol{u}}_h), \boldsymbol{\mu}\rangle_{\partial\mathcal{T}_h\setminus\Gamma} &= 0,\\
(\Pi_P p - p_h, 1)_{\Omega} &= (\Pi_P p - p, 1)_{\Omega}.
\end{aligned}
$$

Proof. The result is an extension of Lemma 3.1 in [33] to our HDG method. □

Lemma 2.2.2. *We have*

$$
\nu\|\Pi_{\mathrm{G}}\mathrm{L} - \mathrm{L}_h\|_{0,\mathcal{T}_h}^2 + \alpha\|\Pi_{\boldsymbol{V}}\boldsymbol{u} - \boldsymbol{u}_h\|_{0,\mathcal{T}_h}^2 + \nu\|\Pi_{\boldsymbol{V}}\boldsymbol{u} - \boldsymbol{u}_h - (\mathsf{P}_M\boldsymbol{u} - \widehat{\boldsymbol{u}}_h)\|_{0,\partial\mathcal{T}_h}^2 = \nu(\Pi_{\mathrm{G}}\mathrm{L} - \mathrm{L}, \Pi_{\mathrm{G}}\mathrm{L} - \mathrm{L}_h)_{\mathcal{T}_h}.
$$

Proof. It follows by taking $\mathrm{G} = \nu(\Pi_{\mathrm{G}}\mathrm{L} - \mathrm{L}_h)$, $\boldsymbol{v} = \Pi_{\boldsymbol{V}}\boldsymbol{u} - \boldsymbol{u}_h$, $q = \Pi_P p - p_h$ and $\boldsymbol{\mu} = \mathsf{P}_M\boldsymbol{u} - \widehat{\boldsymbol{u}}_h$ in the first five equations of Lemma 2.2.1 and adding them up. □

Let us emphasize that, if $\alpha \neq 0$, Lemma 2.2.2 provides a bound for the projection of the errors, for the velocity gradient and the velocity, in terms of the approximation error $\|\Pi_{\mathrm{G}}\mathrm{L} - \mathrm{L}_h\|_{0,\mathcal{T}_h}$. As a consequence, if the solution is smooth enough, this lemma guaranties that the L^2-norm of the projection of the error, for the velocity gradient and the velocity, is of order h^{k+1}. On the other hand, by a duality argument, it is possible to show that actually $\|\Pi_{\boldsymbol{V}}\boldsymbol{u} - \boldsymbol{u}_h\|_{0,\mathcal{T}_h}$ is of order h^{k+2} under regularity assumptions. More precisely, given $\boldsymbol{\theta} \in [L^2(\Omega)]^d$, let $(\Phi, \boldsymbol{\phi}, \phi)$ be the solution of:

$$
\begin{aligned}
\Phi + \nabla\boldsymbol{\phi} &= 0 \quad \text{in } \Omega, && \text{(2.5a)}\\
\nabla\cdot(\nu\Phi) - \nabla\phi + \alpha\boldsymbol{\phi} &= \boldsymbol{\theta} \quad \text{in } \Omega, && \text{(2.5b)}\\
-\nabla\cdot\boldsymbol{\phi} &= 0 \quad \text{in } \Omega, && \text{(2.5c)}\\
\boldsymbol{\phi} &= \mathbf{0} \quad \text{on } \partial\Omega. && \text{(2.5d)}
\end{aligned}
$$

Since $\boldsymbol{\theta} - \alpha\boldsymbol{\phi} \in [L^2(\Omega)]^d$, (2.5) has the same regularity as the Stokes problem. Hence, we assume $\Phi \in H^1(\Omega)^{d\times d}$, $\boldsymbol{\phi} \in H^2(\Omega)^d$ and $\phi \in H^1(\Omega)$. This assumption holds, for instance, if Ω is convex [49, 81]. In addition, we assume

$$\nu\|\Phi\|_{1,\Omega} + \alpha\|\boldsymbol{\phi}\|_{2,\Omega} + \|\phi\|_{1,\Omega} \preceq \|\boldsymbol{\theta}\|_{0,\Omega}. \tag{2.6}$$

Lemma 2.2.3. *If the elliptic regularity estimate (2.6) holds, we have*

$$\|\Pi_{\boldsymbol{V}}\boldsymbol{u} - \boldsymbol{u}_h\|_{0,\mathcal{T}_h} \preceq \left(h^{\min\{k,1\}} + \alpha^{1/2}h\right)\|\Pi_{\mathrm{G}}\mathrm{L} - \mathrm{L}\|_{0,\mathcal{T}_h}.$$

Proof. We follow the ideas on [33]. Let $\boldsymbol{\theta} \in [L^2(\Omega)]^d$. Using (1), (2.5) and Lemma 2.2.1 we obtain

$$(\Pi_{\boldsymbol{V}}\boldsymbol{u} - \boldsymbol{u}_h, \boldsymbol{\theta})_{\mathcal{T}_h} = \nu(\Pi_{\mathrm{G}}\mathrm{L} - \mathrm{L}, \Phi - \mathsf{P}_{k-1}\Phi)_{\mathcal{T}_h} + \nu(\mathrm{L}_h - \mathrm{L}, \Pi_{\mathrm{G}}\Phi - \Phi)_{\mathcal{T}_h} + \alpha(\Pi_{\boldsymbol{V}}\boldsymbol{u} - \boldsymbol{u}_h, \boldsymbol{\phi} - \Pi_{\boldsymbol{V}}\boldsymbol{\phi})_{\mathcal{T}_h},$$

where $\mathsf{P}_k\boldsymbol{u}$ is the L^2-projection of $\boldsymbol{u}$ into $[\mathbb{P}_k(K)]^d$.

We notice that $\nu\|\Phi - \mathsf{P}_{k-1}\Phi\|_{0,\mathcal{T}_h} \preceq \nu h^{\min\{k,1\}}\|\Phi\|_{\min\{k,1\},\Omega} \preceq h^{\min\{k,1\}}\|\boldsymbol{\theta}\|_{0,\Omega}$. Moreover, applying the first two estimates of Lemma 0.1 to the solution of (2.5) (with $\ell_\sigma = 0$ and $\ell_{\boldsymbol{u}} = \min\{k,1\}$) and (2.6), we have that $\nu\|\Phi - \Pi_{\mathrm{G}}\Phi\|_{0,K} \preceq h_K^{\min\{k,1\}}\|\boldsymbol{\theta}\|_{0,K}$. From Lemma 2.2.2 we get $\alpha^{1/2}\|\Pi_{\boldsymbol{V}}\boldsymbol{u} - \boldsymbol{u}_h\|_{0,\mathcal{T}_h} \leq \nu^{1/2}\|\Pi_{\mathrm{G}}\mathrm{L} - \mathrm{L}\|_{0,\mathcal{T}_h}$ and, thanks to the first estimate of Lemma 0.1 applied to $\boldsymbol{\phi}$ and by (2.6), we obtain that $\alpha^{1/2}\|\boldsymbol{\phi} - \Pi_{\boldsymbol{V}}\boldsymbol{\phi}\|_{0,\mathcal{T}_h} \preceq \alpha^{1/2}h\|\boldsymbol{\theta}\|_{0,\Omega}$. The result follows by applying the Cauchy-Schwarz inequality to the above identity and taking $\boldsymbol{\theta} = \Pi_{\boldsymbol{V}}\boldsymbol{u} - \boldsymbol{u}_h$. □

Lemma 2.2.4. *We have* $\|\Pi_P p - p_h - \overline{\Pi_P p - p_h}\|_{0,\mathcal{T}_h} \preceq \nu\|\Pi_{\mathrm{G}}\mathrm{L} - \mathrm{L}\|_{0,\mathcal{T}_h}$, *where* $\overline{q}$ *is the average of* q *over* Ω.

Proof. The result follows using Lemma 2.2.1 and proceeding as in Propositions 3.4 and 3.9 in [33]. □

In the next results, we summarize the *a priori* error estimates of our numerical scheme.

Theorem 2.2.1. *Let* $(\mathrm{L}, \boldsymbol{u}, p)$ *and* $(\mathrm{L}_h, \boldsymbol{u}_h, p_h, \widehat{\boldsymbol{u}}_h)$ *be the solution of* (2.1) *and* (2.3), *respectively. The following estimates hold*

$$\|\mathrm{L} - \mathrm{L}_h\|_{0,\mathcal{T}_h} \preceq \|\Pi_{\mathrm{G}}\mathrm{L} - \mathrm{L}_h\|_{0,\mathcal{T}_h}, \tag{2.7a}$$

$$\|p - p_h\|_{0,\mathcal{T}_h} \preceq \|\Pi_P p - p\|_{0,\mathcal{T}_h} + \nu\|\Pi_{\mathrm{G}}\mathrm{L} - \mathrm{L}\|_{0,\mathcal{T}_h}, \tag{2.7b}$$

$$\alpha^{1/2}\|\boldsymbol{u} - \boldsymbol{u}_h\|_{0,\mathcal{T}_h} \preceq \nu^{1/2}\|\Pi_{\mathrm{G}}\mathrm{L} - \mathrm{L}_h\|_{0,\mathcal{T}_h} + \alpha^{1/2}\|\Pi_{\boldsymbol{V}}\boldsymbol{u} - \boldsymbol{u}\|_{0,\mathcal{T}_h}. \tag{2.7c}$$

Moreover, if (2.6) *holds, then*

$$\|\boldsymbol{u} - \boldsymbol{u}_h\|_{0,\mathcal{T}_h} \leq \|\Pi_{\boldsymbol{V}}\boldsymbol{u} - \boldsymbol{u}\|_{0,\mathcal{T}_h} + \left(h^{\min\{k,1\}} + (\alpha/\nu)^{1/2}h\right)\|\Pi_{\mathrm{G}}\mathrm{L} - \mathrm{L}\|_{0,\mathcal{T}_h}, \tag{2.7d}$$

Proof. It is consequence of Lemmas 2.2.3, 2.2.4 and equation (2.2.2), considering that $\|\overline{\Pi_P p - p}\|_{0,\mathcal{T}_h} \leq \|\Pi_P p - p\|_{0,\Omega}$ and the last equation in Lemma 2.2.1. □

Theorem 2.2.2. *Let $\boldsymbol{u}_h^*$ be the approximation defined in (2.4), $l_{\boldsymbol{u}} \in [0,k]$ as in Lemma 0.1 and assume that (2.6) holds. We have the following estimates*

$$\begin{aligned}
\|\boldsymbol{u}-\boldsymbol{u}_h^*\|_{0,\mathcal{T}_h} &\preceq \Big(1+(\alpha/\nu)^{1/2}h\Big)h^{l_{\boldsymbol{u}}+2}|\boldsymbol{u}|_{l_{\boldsymbol{u}}+2,\mathcal{T}_h} + \|\Pi_{\boldsymbol{V}}\boldsymbol{u}-\boldsymbol{u}_h\|_{0,\mathcal{T}_h} + h\|\mathrm{L}-\mathrm{L}_h\|_{0,\mathcal{T}_h} \\
&\quad + (\alpha/\nu)^{1/2}h(\|\boldsymbol{u}-\boldsymbol{u}_h\|_{0,\mathcal{T}_h} + \|\Pi_{\boldsymbol{V}}\boldsymbol{u}-\boldsymbol{u}_h\|_{0,\mathcal{T}_h}), \qquad (2.8a)\\
\nu^{1/2}|\boldsymbol{u}-\boldsymbol{u}_h^*|_{1,\mathcal{T}_h} &\preceq (\nu^{1/2}+\alpha^{1/2}h)h^{l_{\boldsymbol{u}}+1}|\boldsymbol{u}|_{l_{\boldsymbol{u}}+2,\mathcal{T}_h} + \nu^{1/2}\|\mathrm{L}-\mathrm{L}_h\|_{0,\mathcal{T}_h} \\
&\quad + \alpha^{1/2}(\|\boldsymbol{u}-\boldsymbol{u}_h\|_{0,\mathcal{T}_h} + \|\Pi_{\boldsymbol{V}}\boldsymbol{u}-\boldsymbol{u}_h\|_{0,\mathcal{T}_h}), \qquad (2.8b)\\
\sum_{e\in\mathcal{E}_h} h_e^{1/2}\|[\![\boldsymbol{u}_h^*]\!]\|_{0,e} &\preceq \|\boldsymbol{u}-\boldsymbol{u}_h^*\|_{0,\mathcal{T}_h}^{1/2}\left(\|\boldsymbol{u}-\boldsymbol{u}_h^*\|_{0,\mathcal{T}_h}^2 + h^2|\boldsymbol{u}-\boldsymbol{u}_h^*|_{1,\mathcal{T}_h}^2\right)^{1/4}. \qquad (2.8c)
\end{aligned}$$

Proof. Let $\mathsf{P}_{k+1}\boldsymbol{u}$ be the L^2-projection of $\boldsymbol{u}$ into $\boldsymbol{V}_h^*$ and decompose

$$\boldsymbol{u}-\boldsymbol{u}_h^* = (\boldsymbol{u}-\mathsf{P}_{k+1}\boldsymbol{u}) + \boldsymbol{w} + \mathsf{P}_0(\mathsf{P}_{k+1}\boldsymbol{u}-\boldsymbol{u}_h^*), \qquad (2.9)$$

where $\boldsymbol{w} := (\mathsf{I}-\mathsf{P}_0)(\mathsf{P}_{k+1}\boldsymbol{u}-\boldsymbol{u}_h^*)$ and $P_0\boldsymbol{v}$ is the L^2-projection of $\boldsymbol{v}$ into $[\mathbb{P}_0(K)]^d$. Let us first point out two key ingredients in this proof. We observe that the definition of $\boldsymbol{u}_h^*$ implies

$$\mathsf{P}_0\boldsymbol{u}_h = \mathsf{P}_0\boldsymbol{u}_h^*. \qquad (2.10)$$

This is clearly true if $\alpha = 0$ because of (2.4b). If $\alpha \neq 0$, this identity is obtained by taking $\boldsymbol{w} = (1,0)$ and $\boldsymbol{w} = (0,1)$ in (2.4a). In addition, for each $K \in \mathcal{T}_h$ we notice that

$$\|\mathsf{P}_0(\mathsf{P}_{k+1}\boldsymbol{u}-\boldsymbol{u}_h)\|_{0,K} = \|\mathsf{P}_0(\Pi_{\boldsymbol{V}}\boldsymbol{u}-\boldsymbol{u}_h)\|_{0,K} \leq \|\Pi_{\boldsymbol{V}}\boldsymbol{u}-\boldsymbol{u}_h\|_{0,K}. \qquad (2.11)$$

Now, let $K \in \mathcal{T}_h$. We recall the approximation property of the L^2-projection P_{k+1}:

$$\|\boldsymbol{u}-\mathsf{P}_{k+1}\boldsymbol{u}\|_{0,K} \preceq h_K^{l_{\boldsymbol{u}}+2}|\boldsymbol{u}|_{l_{\boldsymbol{u}}+2,K} \qquad (2.12)$$

Then, combining (2.9)-(2.12), and the fact that $\|\boldsymbol{w}\|_{0,K} \preceq h_K|\boldsymbol{w}|_{1,K}$ [9], we get

$$\|\boldsymbol{u}-\boldsymbol{u}_h^*\|_{0,K} \preceq h_K^{l_{\boldsymbol{u}}+2}|\boldsymbol{u}|_{l_{\boldsymbol{u}}+2,K} + \|\Pi_{\boldsymbol{V}}\boldsymbol{u}-\boldsymbol{u}_h\|_{0,K} + h_K|\boldsymbol{w}|_{1,K}. \qquad (2.13a)$$

Moreover

$$\nu^{1/2}|\boldsymbol{u}-\boldsymbol{u}_h^*|_{1,K} \preceq \nu^{1/2}h_K^{l_{\boldsymbol{u}}+1}|\boldsymbol{u}|_{l_{\boldsymbol{u}}+2,K} + \nu^{1/2}|\boldsymbol{w}|_{1,K}. \qquad (2.13b)$$

On the other hand, adding and subtracting $\alpha(\boldsymbol{u},\boldsymbol{w})_K$ to the right hand side of (2.4a), and considering that $\mathrm{L} = \nabla\boldsymbol{u}$, we obtain

$$\nu(\nabla\boldsymbol{u}_h^*,\nabla\boldsymbol{w})_K + \alpha(\boldsymbol{u}_h^*,\boldsymbol{w})_K = \nu(\mathrm{L}_h-\mathrm{L},\nabla\boldsymbol{w})_K + \alpha(\boldsymbol{u}_h-\boldsymbol{u},\boldsymbol{w})_K + \nu(\nabla\boldsymbol{u},\nabla\boldsymbol{w})_K + \alpha(\boldsymbol{u},\boldsymbol{w})_K.$$

This identity, together with (2.10), implies

$$\begin{aligned}
\nu|\boldsymbol{w}|_{1,K}^2 + \alpha\|\boldsymbol{w}\|_{0,K}^2 &= \nu(\mathrm{L}-\mathrm{L}_h,\nabla\boldsymbol{w})_K + \alpha(\boldsymbol{u}-\boldsymbol{u}_h,\boldsymbol{w})_K + \nu(\nabla(\mathsf{P}_{k+1}\boldsymbol{u}-\boldsymbol{u}),\nabla\boldsymbol{w})_K \\
&\quad + \alpha(\mathsf{P}_{k+1}\boldsymbol{u}-\boldsymbol{u},\boldsymbol{w})_K - \alpha(\mathsf{P}_0(\mathsf{P}_{k+1}\boldsymbol{u}-\boldsymbol{u}_h),\boldsymbol{w})_K.
\end{aligned}$$

Then, thanks to the Cauchy-Schwarz inequality, (2.11) and the approximation property (2.12), we get

$$\nu^{1/2}|\boldsymbol{w}|_{1,K}+\alpha^{1/2}\|\boldsymbol{w}\|_{0,K}\preceq \nu^{1/2}\|\mathrm{L}-\mathrm{L}_h\|_{0,K}+\alpha^{1/2}\|\boldsymbol{u}-\boldsymbol{u}_h\|_{0,K} \\ +\nu^{1/2}h_K^{l_{\boldsymbol{u}}+1}|\boldsymbol{u}|_{l_{\boldsymbol{u}}+2,K}+\alpha^{1/2}h_K^{l_{\boldsymbol{u}}+2}|\boldsymbol{u}|_{l_{\boldsymbol{u}}+2,K}+\alpha^{1/2}\|\Pi_{\boldsymbol{V}}\boldsymbol{u}-\boldsymbol{u}_h\|_{0,K}.$$

This inequality allows us to bound $|\boldsymbol{w}|_{1,K}$ in (2.13a) and (2.13b), obtaining (2.8b) and

$$\|\boldsymbol{u}-\boldsymbol{u}_h^*\|_{0,K}\preceq h_K^{l_{\boldsymbol{u}}+2}|\boldsymbol{u}|_{l_{\boldsymbol{u}}+2,K}+\|\Pi_{\boldsymbol{V}}\boldsymbol{u}-\boldsymbol{u}_h\|_{0,K}+h_K\|\mathrm{L}-\mathrm{L}_h\|_{0,K} \\ +(\alpha/\nu)^{1/2}h_K\Big(\|\boldsymbol{u}-\boldsymbol{u}_h\|_{0,K}+\|\Pi_{\boldsymbol{V}}\boldsymbol{u}-\boldsymbol{u}_h\|_{0,K}+h_K^{l_{\boldsymbol{u}}+2}|\boldsymbol{u}|_{l_{\boldsymbol{u}}+2,K}\Big),$$

which implies (2.8a).

Finally, by trace inequality, we have $h_e\|\boldsymbol{v}\|_{0,e}^2\preceq\|\boldsymbol{v}\|_{0,K}\left(\|\boldsymbol{v}\|_{0,K}^2+h_K^2|\boldsymbol{v}|_{1,K}^2\right)^{1/2}\ \forall\boldsymbol{v}\in[H^1(K)]^d$. This implies

$$\sum_{e\in\mathcal{E}_h}h_e\|[\![\boldsymbol{u}_h^*]\!]\|_{0,e}^2\preceq\sum_{e\in\mathcal{E}_h}\sum_{K'\in\omega_e}h_e\|\boldsymbol{u}-\boldsymbol{u}_h^*|_{K'}\|_{0,e}^2 \\ \preceq\sum_{e\in\mathcal{E}_h}\sum_{K'\in\omega_e}\|\boldsymbol{u}-\boldsymbol{u}_h^*\|_{0,K'}\left(\|\boldsymbol{u}-\boldsymbol{u}_h^*\|_{0,K'}^2+h_{K'}^2|\boldsymbol{u}-\boldsymbol{u}_h^*|_{1,K'}^2\right)^{1/2}$$

and (2.8c) follows. □

2.3 A posteriori error analysis

Before we propose our *a posteriori* error estimator, as we said in the preliminary results, we state Lemmas 0.2-0.3 for our case, that is, the Brinkman problem, that will help us, as Lemma 0.1, to prove our main results.

Lemma 2.3.1. *For any $K\in\mathcal{T}_h$, $e\in\mathcal{E}_h^i$ and $0\leq m\leq 1$, the following estimates hold for any $w\in H_0^1(\Omega)$:*

$$\|\mathcal{C}_h w\|_{m,\Omega}\preceq\|w\|_{m,\Omega},\quad \|w-\mathcal{C}_h w\|_{0,K}\preceq\theta_K|\!|\!|\, w\,|\!|\!|_{1,\Delta_K},\quad \|w-\mathcal{C}_h w\|_{0,e}\preceq\nu^{-1/4}\theta_e^{1/2}|\!|\!|\, w\,|\!|\!|_{1,\Delta_e},$$

where $\theta_S:=\min\{h_S\nu^{-1/2},\alpha^{-1/2}\}$, with S an element $K\in\mathcal{T}_h$ or a face $e\in\mathcal{E}_h$, $\Delta_K:=\{K'\in\mathcal{T}_h:\overline{K'}\cap\overline{K}\neq\emptyset\}$ and $\Delta_e:=\{K'\in\mathcal{T}_h:\overline{K'}\cap\overline{e}\neq\emptyset\}$.

Lemma 2.3.2. *The following estimates hold for all $\boldsymbol{v}\in[\mathbb{P}_k(K)]^d$, $K\in\mathcal{T}_h$, $\boldsymbol{\mu}\in[\mathbb{P}_k(e)]^d$, and $e\in\mathcal{E}_h$:*

$$\|\boldsymbol{v}\|_{0,K}^2\preceq(\boldsymbol{v},B_K\boldsymbol{v})_K,\qquad \|B_K\boldsymbol{v}\|_{0,K}\preceq\|\boldsymbol{v}\|_{0,K},\qquad |\!|\!|\, B_K\boldsymbol{v}\,|\!|\!|_{1,K}\preceq\theta_K^{-1}\|\boldsymbol{v}\|_{0,K},$$
$$\|\boldsymbol{\mu}\|_{0,e}^2\preceq(\boldsymbol{\mu},B_e\boldsymbol{\mu})_e,\qquad \|B_e\boldsymbol{\mu}\|_{0,\omega_e}\preceq\nu^{1/4}\theta_e^{1/2}\|\boldsymbol{\mu}\|_{0,e},\qquad |\!|\!|\, B_e\boldsymbol{\mu}\,|\!|\!|_{1,\omega_e}\preceq\nu^{1/4}\theta_e^{-1/2}\|\boldsymbol{\mu}\|_{0,e}.$$

2.3.1 *A posteriori* error estimator

For each $K\in\mathcal{T}_h$, we propose the following local error estimator

$$\eta_K^2:=\theta_K^2\|\boldsymbol{f}+\nabla\cdot(\nu\mathrm{L}_h)-\nabla p_h-\alpha\boldsymbol{u}_h^*\|_{0,K}^2+\nu\|\mathrm{L}_h-\nabla\boldsymbol{u}_h^*\|_{0,K}^2+\nu\|\nabla\cdot\boldsymbol{u}_h^*\|_{0,K}^2 \\ +\frac{1}{2}\sum_{e\in\mathcal{E}_h^i\cap\partial K}\left(\nu^{-1/2}\theta_e\|[\![\nu\mathrm{L}_h-p_h\mathrm{I}]\!]\|_{0,e}^2+\nu h_e^{-1}\|[\![\boldsymbol{u}_h^*]\!]\|_{0,e}^2\right)+\sum_{e\in\mathcal{E}_h^\partial\cap\partial K}\nu h_e^{-1}\|\boldsymbol{u}_D-\boldsymbol{u}_h^*\|_{0,e}^2 \tag{2.14}$$

and its global version $\eta_h := \left(\sum_{K\in\mathcal{T}_h}\eta_K^2\right)^{1/2}$. Here we recall that θ_K and θ_e were defined in Lemma 2.3.1 and $\boldsymbol{u}_h^*$ is the postprocessed solution constructed in (2.4).

Note that the three volumetric terms are the residuals associated to the equilibrium equation, the constitutive equation and the incompressibility condition, respectively. At the same time, the jumps across the faces allude to the continuity of the trace of $\boldsymbol{u}$ and the normal trace of $\nu\mathrm{L}-p\mathrm{I}$, in case of enough regularity of the continuous solution. The last term, which is not usual in *a posteriori* error estimates for Dirichlet problems, is a measure of the quality of the approximation of boundary condition. We will see that our estimator converges to zero with order of $\min\{\ell_{\mathrm{L}},\ell_{\boldsymbol{u}},\ell_\sigma\}+1$ and, if L, $\boldsymbol{u}$ and p have enough regularity, with order $k+1$.

Now, we present intermediate results that will allow us to prove our main theorems. We proceed adapting and extending the techniques introduced in [33], [43] and [44] to the Brinkman problem. We emphasize that we keep track the dependence on ν and α.

We start by showing two lemmas that will allow us to prove the reliability of our estimator.

Lemma 2.3.3. *Let* $(\mathrm{L},\boldsymbol{u},p)$ *and* $(\mathrm{L}_h,\boldsymbol{u}_h,p_h,\widehat{\boldsymbol{u}}_h)$ *be the solution of* (2.1) *and* (2.3)*, respectively. The following estimates hold*

$$\nu^{-1/2}\|p\ -p_h\|_{0,\mathcal{T}_h}\preceq C_{\alpha,\nu}\Big\{\nu^{1/2}\|\mathrm{L}-\mathrm{L}_h\|_{0,\mathcal{T}_h}+\alpha^{1/2}\|\boldsymbol{u}-\widetilde{\boldsymbol{u}}_h^*\|_{0,\mathcal{T}_h}+\alpha^{1/2}\|\boldsymbol{u}_h^*-\widetilde{\boldsymbol{u}}_h^*\|_{0,\mathcal{T}_h}$$
$$+\nu^{1/2}\|\mathrm{L}_h-\nabla\boldsymbol{u}_h^*\|_{0,\mathcal{T}_h}+\sum_{K\in\mathcal{T}_h}\Big(\theta_K\|\boldsymbol{f}+\nabla\cdot(\nu\mathrm{L}_h)-\nabla p_h-\alpha\boldsymbol{u}_h^*\|_{0,K}+\frac{1}{2}\sum_{e\in\mathcal{E}_h^i\cap\partial K}\nu^{-1/4}\theta_e^{1/2}\|\,[\![\nu\mathrm{L}_h-p_h\mathrm{I}]\!]\|_{0,e}\Big)\Big\},$$

where $\widetilde{\boldsymbol{u}}_h^*$ *is the Oswald interpolation of the postprocessed velocity* $\boldsymbol{u}_h^*$ *and* $C_{\alpha,\nu}:=\max\{1,(\alpha/\nu)^{1/2}\}$.

Proof. Note that, for $q\in L_0^2(\Omega)$, we have ([70], Chapter 1, Corollary 2.4)

$$\nu^{-1/2}\|q\|_{0,\mathcal{T}_h}\preceq\sup_{\boldsymbol{w}\in H_0^1(\Omega)^d\setminus\{\boldsymbol{0}\}}\frac{(q,\nabla\cdot\boldsymbol{w})_{\mathcal{T}_h}}{\nu^{1/2}\|\nabla\boldsymbol{w}\|_{0,\mathcal{T}_h}}.$$

We take $q=p-p_h$ which is in $L_0^2(\Omega)$ because of (2.1e) and (2.3f). Then, we use the above inf-sup condition estimate $\nu^{-1/2}\|p-p_h\|_{0,\mathcal{T}_h}$. More precisely, for $\boldsymbol{w}\in H_0^1(\Omega)^d$ we get

$$\begin{aligned}(p-p_h,\nabla\cdot\boldsymbol{w})_{\mathcal{T}_h}=&-\nu(\nabla\cdot(\mathrm{L}-\mathrm{L}_h),\boldsymbol{w})_{\mathcal{T}_h}+\alpha(\boldsymbol{u}-\boldsymbol{u}_h^*,\boldsymbol{w})_{\mathcal{T}_h}-(\boldsymbol{f}+\nabla\cdot(\nu\mathrm{L}_h)-\nabla p_h-\alpha\boldsymbol{u}_h^*,\boldsymbol{w})_{\mathcal{T}_h}\\&+\langle(p-p_h)\boldsymbol{n},\boldsymbol{w}\rangle_{\partial\mathcal{T}_h}\end{aligned}$$

after integrating by parts, by using (2.4a) and rearranging the expression. Then, using integration by parts and breaking the resulting boundary integral into face integrals, we arrive at

$$\begin{aligned}(p-p_h,\nabla\cdot\boldsymbol{w})_{\mathcal{T}_h}=&\,\nu(\mathrm{L}-\mathrm{L}_h,\nabla\boldsymbol{w})_{\mathcal{T}_h}+\alpha(\boldsymbol{u}-\boldsymbol{u}_h^*,\boldsymbol{w})_{\mathcal{T}_h}-(\boldsymbol{f}+\nabla\cdot(\nu\mathrm{L}_h)-\nabla p_h-\alpha\boldsymbol{u}_h^*,(\mathsf{Id}-\mathcal{C}_h)\boldsymbol{w})_{\mathcal{T}_h}\\&+\langle\,[\![\nu\mathrm{L}_h-p_h\mathrm{I}]\!],(\mathsf{Id}-\mathcal{C}_h)\boldsymbol{w}\rangle_{\mathcal{E}_h^i}+R,\end{aligned}$$

where $R:=-(\boldsymbol{f}+\nabla\cdot(\nu\mathrm{L}_h)-\nabla p_h-\alpha\boldsymbol{u}_h^*,\mathcal{C}_h\boldsymbol{w})_{\mathcal{T}_h}+\langle\nu\mathrm{L}_h\boldsymbol{n}-p_h\boldsymbol{n},\mathcal{C}_h\boldsymbol{w}\rangle_{\partial\mathcal{T}_h}$.

On the other hand, after integrating by parts and using (2.4a), (2.3b) reads

$$(\boldsymbol{f}+\nabla\cdot(\nu\mathrm{L}_h)-\nabla p_h-\alpha\boldsymbol{u}_h^*,\boldsymbol{v})_{\mathcal{T}_h}+\nu(\mathrm{L}_h-\nabla\boldsymbol{u}_h^*,\nabla\boldsymbol{v})_{\mathcal{T}_h}=\langle\nu\mathrm{L}_h\boldsymbol{n}-p_h\boldsymbol{n},\boldsymbol{v}\rangle_{\partial\mathcal{T}_h}-\langle\nu\widehat{\mathrm{L}}_h\boldsymbol{n}-\widehat{p}_h\boldsymbol{n},\boldsymbol{v}\rangle_{\partial\mathcal{T}_h}$$

for all $\boldsymbol{v} \in \boldsymbol{V}_h^{1,c} := \{\boldsymbol{v} \in H_0^1(\Omega)^d : \boldsymbol{v}|_K \in [\mathbb{P}_1(K)]^d \ \ \forall K \in \mathcal{T}_h\}$. Then, since $\boldsymbol{v}|_e \in [\mathbb{P}_k(e)]^d$ for all $e \in \mathcal{E}_h$ and using (2.3e), we get

$$(\boldsymbol{f} + \nabla \cdot (\nu \mathrm{L}_h) - \nabla p_h - \alpha \boldsymbol{u}_h^*, \boldsymbol{v})_{\mathcal{T}_h} + \nu(\mathrm{L}_h - \nabla \boldsymbol{u}_h^*, \nabla \boldsymbol{v})_{\mathcal{T}_h} = \langle \nu \mathrm{L}_h \boldsymbol{n} - p_h \boldsymbol{n}, \boldsymbol{v} \rangle_{\partial \mathcal{T}_h \setminus \Gamma} \quad \forall \boldsymbol{v} \in \boldsymbol{V}_h^{1,c}. \tag{2.15}$$

Now, taking $\boldsymbol{v} := \mathcal{C}_h \boldsymbol{w} \in \boldsymbol{V}_h^{1,c}$ and using (2.15), we see that $R = \nu\,(\mathrm{L}_h - \nabla \boldsymbol{u}_h^*, \nabla \mathcal{C}_h \boldsymbol{w})_{\mathcal{T}_h}$. Thus,

$$\begin{aligned}
(p \ - p_h, \nabla \cdot \boldsymbol{w})_{\mathcal{T}_h} &\leq \nu \|\mathrm{L} - \mathrm{L}_h\|_{0,\mathcal{T}_h} \|\nabla \boldsymbol{w}\|_{0,\mathcal{T}_h} + \alpha \|\boldsymbol{u} - \boldsymbol{u}_h^*\|_{0,\mathcal{T}_h} \|\boldsymbol{w}\|_{0,\mathcal{T}_h} + \nu \|\mathrm{L}_h - \nabla \boldsymbol{u}_h^*\|_{0,\mathcal{T}_h} \|\nabla \mathcal{C}_h \boldsymbol{w}\|_{0,\mathcal{T}_h} \\
&\quad + \|\boldsymbol{f} + \nabla \cdot (\nu \mathrm{L}_h) - \nabla p_h - \alpha \boldsymbol{u}_h^*\|_{0,\mathcal{T}_h} \|(\mathsf{Id} - \mathcal{C}_h)\boldsymbol{w}\|_{0,\mathcal{T}_h} + \|\, [\![\nu \mathrm{L}_h - p_h \mathrm{I}]\!]\|_{0,\mathcal{E}_h^i} \|(\mathsf{Id} - \mathcal{C}_h)\boldsymbol{w}\|_{0,\mathcal{E}_h^i} \\
&\preceq C_{\alpha,\nu} \Bigg\{ \nu^{1/2} \|\mathrm{L} - \mathrm{L}_h\|_{0,\mathcal{T}_h} + \alpha^{1/2} \|\boldsymbol{u} - \widetilde{\boldsymbol{u}}_h^*\|_{0,\mathcal{T}_h} + \alpha^{1/2} \|\boldsymbol{u}_h^* - \widetilde{\boldsymbol{u}}_h^*\|_{0,\mathcal{T}_h} + \nu^{1/2} \|\mathrm{L}_h - \nabla \boldsymbol{u}_h^*\|_{0,\mathcal{T}_h} \\
&\quad + \sum_{K \in \mathcal{T}_h} \Bigg(\theta_K \|\boldsymbol{f} + \nabla \cdot (\nu \mathrm{L}_h) - \nabla p_h - \alpha \boldsymbol{u}_h^*\|_{0,K} + \frac{1}{2} \sum_{e \in \mathcal{E}_h^i \cap \partial K} \nu^{-1/4} \theta_e^{1/2} \|\, [\![\nu \mathrm{L}_h - p_h \mathrm{I}]\!]\|_{0,e} \Bigg) \Bigg\} \nu^{1/2} \|\nabla \boldsymbol{w}\|_{0,\Omega},
\end{aligned}$$

where we used the stability property of the Clément interpolator, the Poincaré inequality, Lemma 2.3.1 and the regularity of the mesh. The result follows from dividing the above inequality by $\nu^{1/2}\|\nabla \boldsymbol{w}\|_{0,\Omega}$. ∎

Lemma 2.3.4. *Let $(\mathrm{L}, \boldsymbol{u}, p)$ be the solution of (2.1) and $(\mathrm{L}_h, \boldsymbol{u}_h, p_h, \widehat{\boldsymbol{u}}_h)$ the solution of (2.3). We have the following estimate*

$$\nu \|\mathrm{L} - \mathrm{L}_h\|_{0,\mathcal{T}_h}^2 + \alpha \|\boldsymbol{u} - \widetilde{\boldsymbol{u}}_h^*\|_{0,\mathcal{T}_h}^2 \preceq C_{\alpha,\nu} \left(\eta_h^2 + \nu \|\nabla(\boldsymbol{u}_h^* - \widetilde{\boldsymbol{u}}_h^*)\|_{0,\mathcal{T}_h}^2 \right) + \alpha \|\boldsymbol{u}_h^* - \widetilde{\boldsymbol{u}}_h^*\|_{0,\mathcal{T}_h}^2.$$

Proof. Let $\widetilde{\boldsymbol{u}}_h^* \in [H^1(\Omega)]^d$ be the Oswald interpolation of $\boldsymbol{u}_h^*$. Using equations (2.1) and integrating by parts, we obtain

$$\begin{aligned}
\nu \|\mathrm{L} - \mathrm{L}_h\|_{0,\mathcal{T}_h}^2 + \alpha \|\boldsymbol{u} - \widetilde{\boldsymbol{u}}_h^*\|_{0,\mathcal{T}_h}^2 &= \nu(\mathrm{L} - \mathrm{L}_h, \mathrm{L} - \mathrm{L}_h)_{\mathcal{T}_h} + (\alpha(\boldsymbol{u} - \widetilde{\boldsymbol{u}}_h^*), \boldsymbol{u} - \widetilde{\boldsymbol{u}}_h^*)_{\mathcal{T}_h} \\
&= \nu(\mathrm{L} - \mathrm{L}_h, \mathrm{L} - \mathrm{L}_h)_{\mathcal{T}_h} + (\boldsymbol{f} + \nabla \cdot (\nu \mathrm{L}_h) - \nabla p_h - \alpha \boldsymbol{u}_h^*, \boldsymbol{u} - \widetilde{\boldsymbol{u}}_h^*)_{\mathcal{T}_h} \\
&\quad + (\nabla \cdot \nu(\mathrm{L} - \mathrm{L}_h), \boldsymbol{u} - \widetilde{\boldsymbol{u}}_h^*)_{\mathcal{T}_h} - (\nabla(p - p_h), \boldsymbol{u} - \widetilde{\boldsymbol{u}}_h^*)_{\mathcal{T}_h} \\
&\quad + (\alpha(\boldsymbol{u}_h^* - \widetilde{\boldsymbol{u}}_h^*), \boldsymbol{u} - \widetilde{\boldsymbol{u}}_h^*)_{\mathcal{T}_h}.
\end{aligned}$$

Thus, after integrating by parts the third and fourth terms in previous expression and using the fact that $\mathrm{L} = \nabla \boldsymbol{u}$, we write $\nu \|\mathrm{L} - \mathrm{L}_h\|_{0,\mathcal{T}_h}^2 + \alpha \|\boldsymbol{u} - \widetilde{\boldsymbol{u}}_h^*\|_{0,\mathcal{T}_h}^2 = \sum_{K \in \mathcal{T}_h} T_{1,K} + T_{2,K} + T_{3,K}$, where

$$T_{1,K} := (\boldsymbol{f} + \nabla \cdot (\nu \mathrm{L}_h) - \nabla p_h - \alpha \boldsymbol{u}_h^*, \boldsymbol{u} - \widetilde{\boldsymbol{u}}_h^*)_K + \langle \nu(\mathrm{L} - \mathrm{L}_h)\boldsymbol{n}, \boldsymbol{u} - \widetilde{\boldsymbol{u}}_h^* \rangle_{\partial K \setminus \Gamma} - \langle (p - p_h)\boldsymbol{n}, \boldsymbol{u} - \widetilde{\boldsymbol{u}}_h^* \rangle_{\partial K \setminus \Gamma},$$
$$T_{2,K} := (p - p_h, \nabla \cdot (\boldsymbol{u} - \widetilde{\boldsymbol{u}}_h^*))_K \qquad \text{and} \qquad T_{3,K} := -\nu(\mathrm{L} - \mathrm{L}_h, \mathrm{L}_h - \nabla \widetilde{\boldsymbol{u}}_h^*)_K + \alpha(\boldsymbol{u} - \widetilde{\boldsymbol{u}}_h^*, \boldsymbol{u}_h^* - \widetilde{\boldsymbol{u}}_h^*)_{\mathcal{T}_h}.$$

Since $\boldsymbol{u} - \widetilde{\boldsymbol{u}}_h^* \in H_0^1(\Omega)^d$ (Lemma 0.4 with $\boldsymbol{g} = \boldsymbol{u}_D$), and $\nu\mathrm{L} - p\mathrm{I} \in H(\mathrm{div}, \Omega)^d$, we get

$$\sum_{K \in \mathcal{T}_h} T_{1,K} = (\boldsymbol{f} + \nabla \cdot (\nu \mathrm{L}_h) - \nabla p_h - \alpha \boldsymbol{u}_h^*, (\mathsf{Id} - \mathcal{C}_h)(\boldsymbol{u} - \widetilde{\boldsymbol{u}}_h^*))_{\mathcal{T}_h} - \langle \nu \mathrm{L}_h \boldsymbol{n} - p_h \boldsymbol{n}, (\mathsf{Id} - \mathcal{C}_h)(\boldsymbol{u} - \widetilde{\boldsymbol{u}}_h^*) \rangle_{\partial \mathcal{T}_h \setminus \Gamma} + T,$$

where $T := (\boldsymbol{f} + \nabla \cdot (\nu \mathrm{L}_h) - \nabla p_h - \alpha \boldsymbol{u}_h^*, \mathcal{C}_h(\boldsymbol{u} - \widetilde{\boldsymbol{u}}_h^*))_{\mathcal{T}_h} - \langle \mathrm{L}_h \boldsymbol{n} - p_h \boldsymbol{n}, \mathcal{C}_h(\boldsymbol{u} - \widetilde{\boldsymbol{u}}_h^*) \rangle_{\partial \mathcal{T}_h \setminus \Gamma}$.

Now, taking $w = \mathcal{C}_h(\boldsymbol{u} - \widetilde{\boldsymbol{u}}_h^*)$ in (2.15), we get $T = -\nu(\mathrm{L}_h - \nabla \boldsymbol{u}_h^*, \nabla \mathcal{C}_h(\boldsymbol{u} - \widetilde{\boldsymbol{u}}_h^*))_{\mathcal{T}_h}$. Thus,

$$\sum_{K\in\mathcal{T}_h} T_{1,K} = (\boldsymbol{f} + \nabla\cdot(\nu \mathrm{L}_h) - \nabla p_h - \alpha \boldsymbol{u}_h^*, (\mathsf{Id} - \mathcal{C}_h)(\boldsymbol{u} - \widetilde{\boldsymbol{u}}_h^*))_{\mathcal{T}_h} + \langle [\![\nu \mathrm{L}_h - p_h \mathrm{I}]\!], (\mathsf{Id} - \mathcal{C}_h)(\boldsymbol{u} - \widetilde{\boldsymbol{u}}_h^*)\rangle_{\mathcal{E}_h^i} + T$$

$$\preceq \sum_{K\in\mathcal{T}_h} \theta_K^2 \|\boldsymbol{f} + \nabla\cdot(\nu \mathrm{L}_h) - \nabla p_h - \alpha \boldsymbol{u}_h^*\|_{0,K}^2 + \sum_{e\in\mathcal{E}_h^i} \nu^{-1/2}\theta_e \| [\![\nu \mathrm{L}_h - p_h \mathrm{I}]\!]\|_{0,e}^2 + \nu \|\mathrm{L}_h - \nabla \boldsymbol{u}_h^*\|_{0,\mathcal{T}_h}^2$$

$$+ \frac{1}{24}\left(\sum_{K\in\mathcal{T}_h} \theta_K^{-2} \|(\mathsf{Id} - \mathcal{C}_h)(\boldsymbol{u} - \widetilde{\boldsymbol{u}}_h^*)\|_{0,K}^2 + \sum_{e\in\mathcal{E}_h^i} \nu^{1/2}\theta_e^{-1} \|(\mathsf{Id} - \mathcal{C}_h)(\boldsymbol{u} - \widetilde{\boldsymbol{u}}_h^*)\|_{0,e}^2 + \nu \|\nabla \mathcal{C}_h(\boldsymbol{u} - \widetilde{\boldsymbol{u}}_h^*)\|_{0,\mathcal{T}_h}^2 \right),$$

thanks to Cauchy-Schwarz and Young inequalities. Finally, using Lemma 2.3.1 and the regularity of the mesh, we get

$$\sum_{K\in\mathcal{T}_h} T_{1,K} \preceq \sum_{K\in\mathcal{T}_h} \left(\theta_K^2 \|\boldsymbol{f} + \nabla\cdot(\nu \mathrm{L}_h) - \nabla p_h - \alpha \boldsymbol{u}_h^*\|_{0,K}^2 + \frac{1}{2} \sum_{e\in\mathcal{E}_h^i \cap \partial K} \nu^{-1/2}\theta_e \| [\![\nu \mathrm{L}_h - p_h \mathrm{I}]\!]\|_{0,e}^2 \right.$$

$$\left. + \nu \|\mathrm{L}_h - \nabla \boldsymbol{u}_h^*\|_{0,K}^2 \right) + \frac{1}{8} |\!|\!| \boldsymbol{u} - \widetilde{\boldsymbol{u}}_h^* |\!|\!|_{1,\mathcal{T}_h}^2. \tag{2.16}$$

On the other hand, since $\boldsymbol{u}$ is divergence-free, we obtain

$$\sum_{K\in\mathcal{T}_h} T_{2,K} = -(p - p_h, \nabla\cdot \widetilde{\boldsymbol{u}}_h^*)_{\mathcal{T}_h} \leq \frac{1}{12} C_{\alpha,\nu}^{-2} \nu^{-1} \|p - p_h\|_{0,\mathcal{T}_h}^2 + C_{\alpha,\nu}^2 \nu \|\nabla\cdot \widetilde{\boldsymbol{u}}_h^*\|_{0,\mathcal{T}_h}^2$$

$$\preceq \frac{1}{12} C_{\alpha,\nu}^{-2} \nu^{-1} \|p - p_h\|_{0,\mathcal{T}_h}^2 + C_{\alpha,\nu}^2 \nu \|\nabla(\boldsymbol{u}_h^* - \widetilde{\boldsymbol{u}}_h^*)\|_{0,\mathcal{T}_h}^2 + C_{\alpha,\nu}^2 \nu \|\nabla\cdot \boldsymbol{u}_h^*\|_{0,\mathcal{T}_h}^2. \tag{2.17}$$

For the third term we have

$$\sum_{K\in\mathcal{T}_h} T_{3,K} \leq \frac{1}{12}\nu \|\mathrm{L} - \mathrm{L}_h\|_{0,\mathcal{T}_h}^2 + \nu \|\mathrm{L}_h - \nabla \boldsymbol{u}_h^*\|_{0,\mathcal{T}_h}^2$$

$$+ \nu \|\nabla(\boldsymbol{u}_h^* - \widetilde{\boldsymbol{u}}_h^*)\|_{0,\mathcal{T}_h}^2 + \frac{5}{24}\alpha \|\boldsymbol{u} - \widetilde{\boldsymbol{u}}_h^*\|_{0,\mathcal{T}_h}^2 + \alpha \|\boldsymbol{u}_h^* - \widetilde{\boldsymbol{u}}_h^*\|_{0,\mathcal{T}_h}^2. \tag{2.18}$$

Finally, using estimates (2.16)-(2.18), Lemma 2.3.3, the definitions of $|\!|\!| \cdot |\!|\!|_{1,\mathcal{T}_h}$ and η_h, we get

$$\nu \|\mathrm{L} - \mathrm{L}_h\|_{0,\mathcal{T}_h}^2 + \alpha \|\boldsymbol{u} - \widetilde{\boldsymbol{u}}_h^*\|_{0,\mathcal{T}_h}^2$$

$$\preceq C_{\alpha,\nu}^2 \left(\eta_h^2 + \nu \|\nabla(\boldsymbol{u}_h^* - \widetilde{\boldsymbol{u}}_h^*)\|_{0,\mathcal{T}_h}^2 \right) + \alpha \|\boldsymbol{u}_h^* - \widetilde{\boldsymbol{u}}_h^*\|_{0,\mathcal{T}_h}^2 + \frac{1}{2}\left(\nu \|\mathrm{L} - \mathrm{L}_h\|_{0,\mathcal{T}_h}^2 + \alpha \|\boldsymbol{u} - \widetilde{\boldsymbol{u}}_h^*\|_{0,\mathcal{T}_h}^2 \right)$$

and the result follows. □

The next four lemmas provide us the tools to prove local efficiency of our estimator.

Lemma 2.3.5. *Let $e \in \mathcal{E}_h^i$. The following estimate holds*

$$\nu^{-1/2}\theta_e \| [\![\nu \mathrm{L}_h - p_h \mathrm{I}]\!]\|_{0,e}^2 \preceq \sum_{K\in\omega_e} \left(\nu \|\mathrm{L} - \mathrm{L}_h\|_{0,K}^2 + \nu^{-1} \|p - p_h\|_{0,K}^2 + \alpha \|\boldsymbol{u} - \boldsymbol{u}_h^*\|_{0,K}^2 \right.$$

$$\left. + \theta_K^2 \|\boldsymbol{f} + \nabla\cdot(\nu \mathrm{L}_h) - \nabla p_h - \alpha \boldsymbol{u}_h^*\|_{0,K}^2 \right).$$

Proof. For any $\boldsymbol{v} \in H_0^1(\omega_e)^d$ we have

$$\langle [\![\nu \mathrm{L}_h - p_h \mathrm{I}]\!], \boldsymbol{v}\rangle_e = \sum_{K\in\omega_e} (\langle \nu(\mathrm{L}_h - \mathrm{L})\boldsymbol{n}, \boldsymbol{v}\rangle_{\partial K} + \langle (p-p_h)\boldsymbol{n}, \boldsymbol{v}\rangle_{\partial K})$$

$$= \sum_{K\in\omega_e} ((\nu(\mathrm{L}_h - \mathrm{L}), \nabla \boldsymbol{v})_K + (\nu \nabla\cdot(\mathrm{L}_h - \mathrm{L}), \boldsymbol{v})_K + (\nabla(p-p_h), \boldsymbol{v})_K + (p-p_h, \nabla\cdot\boldsymbol{v})_K)$$

$$= \sum_{K\in\omega_e} ((\nu(\mathrm{L}_h - \mathrm{L}), \nabla \boldsymbol{v})_K + (p-p_h, \nabla\cdot\boldsymbol{v})_K + (\alpha(\boldsymbol{u}-\boldsymbol{u}_h^*), \boldsymbol{v})_K + (\boldsymbol{f} + \nabla\cdot(\nu \mathrm{L}_h) - \nabla p_h - \alpha \boldsymbol{u}_h^*, \boldsymbol{v})_K)$$

$$\leq \sum_{K\in\omega_e} \Big(\nu^{1/2}\|\mathrm{L}-\mathrm{L}_h\|_{0,K} + \nu^{-1/2}\|p-p_h\|_{0,K} + \alpha^{1/2}\|\boldsymbol{u}-\boldsymbol{u}_h^*\|_{0,K} + \theta_K \|\boldsymbol{f} + \nabla\cdot(\nu\mathrm{L}_h) - \nabla p_h - \alpha\boldsymbol{u}_h^*\|_{0,K}\Big)\, T_{\boldsymbol{v}},$$

where $T_{\boldsymbol{v}} := \nu^{1/2}\|\nabla \boldsymbol{v}\|_{0,K} + \nu^{1/2}\|\nabla\cdot\boldsymbol{v}\|_{0,K} + \alpha^{1/2}\|\boldsymbol{v}\|_{0,K} + \theta_K^{-1}\|\boldsymbol{v}\|_{0,K}$.

On the other hand, taking $\boldsymbol{v} := B_e [\![\nu \mathrm{L}_h - p_h \mathrm{I}]\!]$ and applying Lemma 2.3.2, we get

$$T_{\boldsymbol{v}} \preceq |\!|\!| \boldsymbol{v} |\!|\!|_{1,K} + \theta_e^{-1}\|\boldsymbol{v}\|_{0,K} \preceq \nu^{1/4}\theta_e^{-1/2} \| [\![\nu \mathrm{L}_h - p_h \mathrm{I}]\!]\|_{0,e}.$$

Thus, the result follows from Lemma 2.3.2 and the shape-regularity assumption. □

Lemma 2.3.6. *For any element $K \in \mathcal{T}_h$ we have*

$$\theta_K \|\boldsymbol{f} + \nabla\cdot(\nu\mathrm{L}_h) - \nabla p_h - \alpha \boldsymbol{u}_h^*\|_{0,K} \preceq \nu^{1/2}\|\mathrm{L}-\mathrm{L}_h\|_{0,K} + \alpha^{1/2}\|\boldsymbol{u}-\boldsymbol{u}_h^*\|_{0,K} + \nu^{-1/2}\|p-p_h\|_{0,K}.$$

Proof. Let $\boldsymbol{v} = \boldsymbol{f} + \nabla\cdot(\nu\mathrm{L}_h) - \nabla p_h - \alpha\boldsymbol{u}_h^*$ then, using (2.1b), the definition of B_K and integration by parts, we get

$$\begin{aligned}(\boldsymbol{v}, B_K\boldsymbol{v})_K &= -\nu(\nabla\cdot(\mathrm{L}-\mathrm{L}_h), B_K\boldsymbol{v})_K + (\nabla(p-p_h), B_K\boldsymbol{v})_K + \alpha(\boldsymbol{u}-\boldsymbol{u}_h^*, B_K\boldsymbol{v})_K \\ &= \nu(\mathrm{L}-\mathrm{L}_h, \nabla B_K\boldsymbol{v})_K - (p-p_h, \nabla\cdot B_K\boldsymbol{v})_K + \alpha(\boldsymbol{u}-\boldsymbol{u}_h^*, B_K\boldsymbol{v})_K \\ &\preceq (\nu^{1/2}\|\mathrm{L}-\mathrm{L}_h\|_{0,K} + \nu^{-1/2}\|p-p_h\|_{0,K} + \alpha^{1/2}\|\boldsymbol{u}-\boldsymbol{u}_h^*\|_{0,K})\, |\!|\!| B_K\boldsymbol{v} |\!|\!|_{1,K},\end{aligned}$$

Thus, the result follows from Lemma 2.3.2. □

Now, note that to prove an upper bounds for the jump of the postprocessed velocity we will use the decomposition of $\nu h_e^{-1}\| [\![\boldsymbol{u}_h^*]\!]\|_{0,e}^2$ into $\nu h_e^{-1}\|\mathsf{P}_{\mathsf{M}_0} [\![\boldsymbol{u}_h^*]\!]\|_{0,e}^2$ and $\nu h_e^{-1}\|(\mathsf{Id} - \mathsf{P}_{\mathsf{M}_0}) [\![\boldsymbol{u}_h^*]\!]\|_{0,e}^2$, where, $\mathsf{P}_{\mathsf{M}_0}$ is the L^2-orthogonal projection into

$$\mathsf{M}_{0,h} := \{\boldsymbol{\mu} \in [L^2(\mathcal{E}_h)]^d : \boldsymbol{\mu}|_e \in [\mathbb{P}_0(e)]^d \quad \forall e \in \mathcal{E}_h\}.$$

Lemma 2.3.7. *For each face $e \in \mathcal{E}_h$ we have that $h_e^{-1}\|\mathsf{P}_{\mathsf{M}_0} [\![\boldsymbol{u}_h^*]\!]\|_{0,e}^2 \preceq \|\mathrm{L}_h - \nabla\boldsymbol{u}_h^*\|_{0,\omega_e}^2$.*

Proof. Let G be a tensor-valued function with rows in $RT_0(K)$ and set $\boldsymbol{w} := \nabla\cdot\mathrm{G} \in [\mathbb{P}_0(K)]^d$. Then, from (2.4a) (or (2.4b) if $\alpha = 0$) we get that (2.3a) can be written as

$$(\mathrm{L}_h, \mathrm{G})_K + (\boldsymbol{u}_h^*, \nabla\cdot\mathrm{G})_K = \langle \widehat{\boldsymbol{u}}_h, \mathrm{G}\boldsymbol{n}\rangle_{\partial K}.$$

Thus, integrating by parts, we arrive at $(\mathrm{L}_h - \nabla\boldsymbol{u}_h^*, \mathrm{G})_K = \langle \widehat{\boldsymbol{u}}_h - \boldsymbol{u}_h^*, \mathrm{G}\boldsymbol{n}\rangle_{\partial K}$. For the rest of the proof we refer to Lemma 3.4 in [45], adapted to vector-valued functions. □

Now, for the remaining term in the decomposition of $\nu h_e^{-1}\| [\![\boldsymbol{u}_h^*]\!]\|_{0,e}^2$, we have the following estimate.

Lemma 2.3.8. *For each face $e \in \mathcal{E}_h$, $h_e^{-1}\|(\mathsf{Id} - \mathsf{P}_{\mathsf{M}_0}) [\![\boldsymbol{u}_h^*]\!]\|_{0,e}^2 \preceq \|\nabla(\boldsymbol{u}-\boldsymbol{u}_h^*)\|_{0,\omega_e}^2$.*

Proof. See Lemma 3.5 in [45]. □

2.3.2 The main results

For each $K \in \mathcal{T}_h$ we define the local error

$$\mathsf{e}_K^2 := \nu\|\mathrm{L} - \mathrm{L}_h\|_{0,K}^2 + \alpha\|\boldsymbol{u} - \boldsymbol{u}_h^*\|_{0,K}^2 + \nu\|\nabla(\boldsymbol{u} - \boldsymbol{u}_h^*)\|_{0,K}^2 + \nu^{-1}\|p - p_h\|_{0,K}^2, \tag{2.19}$$

and its global version is given by $\mathsf{e}_h := \left(\sum_{K\in\mathcal{T}_h} \mathsf{e}_K^2\right)^{1/2}$.

Now, we can state and prove the reliability and efficiency results for our *a posteriori* error estimator.

Theorem 2.3.1 (Reliability)**.**

$$\mathsf{e}_h \preceq C_{\alpha,\nu}\left(\eta_h + \sum_{e\in\mathcal{E}_h} \nu^{1/2} h_e^{1/2} \|\,[\![\boldsymbol{u}_h^*]\!]\,\|_{0,e}\right).$$

Proof. Thanks to Lemmas 2.3.3, 2.3.4 and the fact that, for each $K \in \mathcal{T}_h$, $\nu^{1/2}\|\nabla(\boldsymbol{u} - \boldsymbol{u}_h^*)\|_{0,K} \preceq \nu^{1/2}\|\mathrm{L} - \mathrm{L}_h\|_{0,K} + \eta_K$, we get

$$\nu\|\mathrm{L} - \mathrm{L}_h\|_{0,\mathcal{T}_h}^2 + |\!|\!|\, \boldsymbol{u} - \boldsymbol{u}_h^* \,|\!|\!|_{1,\mathcal{T}_h}^2 + \nu^{-1}\|p - p_h\|_{0,\mathcal{T}_h}^2 \preceq C_{\alpha,\nu}\left(\eta_h^2 + \nu\|\nabla(\boldsymbol{u}_h^* - \widetilde{\boldsymbol{u}}_h^*)\|_{0,\mathcal{T}_h}^2 + \alpha\|(\boldsymbol{u}_h^* - \widetilde{\boldsymbol{u}}_h^*)\|_{0,\mathcal{T}_h}^2\right).$$

The result follows from Lemma 0.4, taking $\boldsymbol{w}_h = \boldsymbol{u}_h^*$ to bound the second and third terms on the right-hand side and the definition of $C_{\alpha,\nu}$. □

Remark 2.3.1. *Note that if $\alpha = 0$ (Stokes problem), then $C_{\alpha,\nu} = 1$. Thus, to obtain an estimate for the L^2 norm of the error of the velocity, we proceed as follows*

$$\begin{aligned}\nu^{1/2}\|\boldsymbol{u} - \boldsymbol{u}_h^*\|_{0,\mathcal{T}_h} &\leq \nu^{1/2}\|\boldsymbol{u} - \widetilde{\boldsymbol{u}}_h^*\|_{0,\mathcal{T}_h} + \nu^{1/2}\|\boldsymbol{u}_h^* - \widetilde{\boldsymbol{u}}_h^*\|_{0,\mathcal{T}_h} \\ &\preceq \nu^{1/2}\|\nabla(\boldsymbol{u} - \widetilde{\boldsymbol{u}}_h^*)\|_{0,\mathcal{T}_h} + \sum_{e\in\mathcal{E}_h} \nu^{1/2} h_e^{1/2} \|\,[\![\boldsymbol{u}_h^*]\!]\,\|_{0,e} \preceq \eta_h + \sum_{e\in\mathcal{E}_h} \nu^{1/2} h_e^{1/2} \|\,[\![\boldsymbol{u}_h^*]\!]\,\|_{0,e},\end{aligned}$$

thanks to the Poincaré inequality, Lemma 0.4 and the bound for $\nu^{1/2}\|\nabla(\boldsymbol{u} - \widetilde{\boldsymbol{u}}_h^*)\|_{0,\mathcal{T}_h}$ from Theorem 2.3.1.

Theorem 2.3.2 (Efficiency)**.** *Let $K \in \mathcal{T}_h$ and $\omega_K := \{K' \in \mathcal{T}_h : K' \in \omega_e \text{ and } e \in \mathcal{E}_h \cap \partial K\}$. The following inequality holds*

$$\eta_K \preceq \mathsf{e}_{\omega_K}.$$

Proof. By definition of η_K, Lemmas 2.3.5-2.3.8, and the inequalities $\|\mathrm{L}_h - \nabla\boldsymbol{u}_h^*\|_{0,K} \leq \|\mathrm{L} - \mathrm{L}_h\|_{0,K} + \|\nabla(\boldsymbol{u} - \boldsymbol{u}_h^*)\|_{0,K}$ and $\|\nabla\cdot\boldsymbol{u}_h^*\|_{0,K} = \|\nabla\cdot(\boldsymbol{u} - \boldsymbol{u}_h^*)\|_{0,K} \preceq \|\nabla(\boldsymbol{u} - \boldsymbol{u}_h^*)\|_{0,K}$, we have that

$$\begin{aligned}\eta_K^2 \preceq\ & \nu\|\mathrm{L} - \mathrm{L}_h\|_{0,K}^2 + \alpha\|\boldsymbol{u} - \boldsymbol{u}_h^*\|_{0,K}^2 + \nu^{-1}\|p - p_h\|_{0,K}^2 + \nu\|\mathrm{L}_h - \nabla\boldsymbol{u}_h^*\|_{0,K}^2 + \nu\|\nabla\cdot\boldsymbol{u}_h^*\|_{0,K}^2 \\ &+ \nu\|\mathrm{L} - \mathrm{L}_h\|_{0,\omega_K}^2 + \nu^{-1}\|p - p_h\|_{0,\omega_K}^2 \\ &+ \sum_{K'\in\omega_K} \theta_{K'}^2\|\boldsymbol{f} + \nabla\cdot(\nu\mathrm{L}_h) - \nabla p_h - \alpha\boldsymbol{u}_h^*\|_{0,K'}^2 + \nu\|\nabla(\boldsymbol{u} - \boldsymbol{u}_h^*)\|_{0,\omega_K}^2 + \nu\|\mathrm{L}_h - \nabla\boldsymbol{u}_h^*\|_{0,\omega_K}^2 \\ \preceq\ & \nu\|\mathrm{L} - \mathrm{L}_h\|_{0,\omega_K}^2 + |\!|\!|\, \boldsymbol{u} - \boldsymbol{u}_h^* \,|\!|\!|_{1,\omega_K}^2 + \nu^{-1}\|p - p_h\|_{0,\omega_K}^2,\end{aligned}$$

and the result follows. □

Remark 2.3.2. *Using (2.8c), and assuming enough regularity on* L, $\boldsymbol{u}$ *and* p, *we can see that the term* $\sum_{e\in\mathcal{E}_h}\nu^{1/2}h_e^{1/2}\|\,[\![\boldsymbol{u}_h^*]\!]\|_{0,e}$ *is a high order term. Its order of convergence is* $\min\{\ell_{\boldsymbol{u}},\ell_{\mathrm{L}},\ell_\sigma\}+2$ *while the one associated to the estimator and the error is* $\min\{\ell_{\boldsymbol{u}},\ell_{\mathrm{L}},\ell_\sigma\}+1$.

2.4 Numerical experiments

In this section, we provide numerical simulations, for $d=2$, illustrating the performance of the scheme and validating our main results in Theorems 2.3.1 and 2.3.2. In all the examples we consider different values of the polynomial degree ($k=1$, 2 and 3), and set the stabilization parameter τ to be 1 on each edge. The values of the physical parameters α and ν will be specified on each example.

Let us define the errors $\mathsf{e}_{\mathrm{L}}:=\nu^{1/2}\|\mathrm{L}-\mathrm{L}_h\|_{0,\mathcal{T}_h}$, $\mathsf{e}_{\boldsymbol{u}}:=|\!|\!|\,\boldsymbol{u}-\boldsymbol{u}_h^*\,|\!|\!|_{1,\mathcal{T}_h}$, $\mathsf{e}_p:=\nu^{-1/2}\|p-p_h\|_{0,\mathcal{T}_h}$, the estimator terms η_i $(i=1,\ldots,5)$

$$\eta_1^2:=\sum_{K\in\mathcal{T}_h}\theta_K^2\|\boldsymbol{f}+\nabla\cdot(\nu\mathrm{L}_h)-\nabla p_h-\alpha\boldsymbol{u}_h^*\|_{0,K}^2,\qquad \eta_2^2:=\nu\|\mathrm{L}_h-\nabla\boldsymbol{u}_h^*\|_{0,\mathcal{T}_h}^2,\qquad \eta_3^2:=\nu\|\nabla\cdot\boldsymbol{u}_h^*\|_{0,\mathcal{T}_h}^2$$

$$\eta_4^2:=\nu^{-1/2}\sum_{e\in\mathcal{E}_h}\theta_e\|\,[\![\nu\mathrm{L}_h-p_h\mathrm{I}]\!]\|_{0,e}^2\qquad\text{and}\qquad \eta_5^2:=\nu\sum_{e\in\mathcal{E}_h}h_e^{-1}\|\,[\![\boldsymbol{u}_h^*]\!]\|_{0,e}^2,$$

and the effectivity index $\mathsf{eff}:=\eta_h/\mathsf{e}_h$. In some tables, we include a column *h.o.t.*, showing that the term defined in Remark 2.3.2 is in fact a high order term, and thus it is not necessary to include it in the definition of our error estimator. The orders of convergence will be computed in terms of the number of elements N and we will use the fact that $h\simeq N^{-1/2}$.

For the tests that include adaptivity, we use the strategy given by:

(i) Start with a coarse mesh $\mathcal{T}_h$.

(ii) Solve the discrete problem on the current mesh $\mathcal{T}_h$.

(iii) Compute η_K for each $K\in\mathcal{T}_h$.

(iv) Use *red-blue-green* (for details, see [104]) procedure to refine each $K'\in\mathcal{T}_h$ such that $\eta_{K'}\geq\theta\max_{K\in\mathcal{T}_h}\eta_K$, with $\theta\in[0,1]$.

(v) Consider this new mesh as $\mathcal{T}_h$ and, unless a prescribed stopping criteria is satisfied, go to (ii).

2.4.1 A polynomial solution

For this test case, we choose $\alpha=1$ and $\Omega=(0,1)^2$. The source term $\boldsymbol{f}$ and the boundary data $\boldsymbol{u}_D$ are chosen such that the exact solution of the problem is given by $\boldsymbol{u}:=(u_1,u_2)$, where $u_1(x_1,x_2):=x_1(1-x_1)x_2(1-x_2)$ and $u_2(x_1,x_2):=(2x_1-1)x_2^2\left(\frac{1}{2}-\frac{x_2}{3}\right)$, and $p(x_1,x_2):=x_1^2x_2^2-\frac{1}{9}$. We note that $\boldsymbol{f}$ and $\boldsymbol{u}_D$ are such that this numerical test satisfies *Assumption H* when $k\geq 3$.

k	N	e_{L}	order	$\mathsf{e}_{\boldsymbol{u}}$	order	e_p	order
	16	9.13e-03	–	1.09e-02	–	7.29e-03	–
	64	2.41e-03	1.92	2.84e-03	1.94	1.75e-03	2.05
1	256	6.22e-04	1.96	7.29e-04	1.96	4.19e-04	2.06
	1024	1.58e-04	1.98	1.85e-04	1.98	1.02e-04	2.04
	4096	3.99e-05	1.99	4.66e-05	1.99	2.52e-05	2.02
	16384	1.00e-05	1.99	1.17e-05	1.99	6.27e-06	2.01
	16	9.40e-04	–	9.80e-04	–	5.10e-04	–
	64	1.14e-04	3.04	1.19e-04	3.04	6.09e-05	3.06
2	256	1.40e-05	3.02	1.46e-05	3.02	7.46e-06	3.03
	1024	1.74e-06	3.01	1.81e-06	3.01	9.21e-07	3.02
	4096	2.17e-07	3.01	2.26e-07	3.01	1.14e-07	3.01
	16384	2.70e-08	3.00	2.81e-08	3.00	1.42e-08	3.00
	16	1.63e-05	–	1.61e-05	–	1.69e-05	–
	64	1.05e-06	3.95	1.03e-06	3.97	1.03e-06	4.04
3	256	6.65e-08	3.98	6.50e-08	3.99	6.33e-08	4.02
	1024	4.18e-09	3.99	4.08e-09	3.99	3.93e-09	4.01
	4096	2.62e-10	4.00	2.55e-10	4.00	2.45e-10	4.00
	16384	1.64e-11	4.00	1.60e-11	4.00	1.53e-11	4.00

Table 2.1: History of convergence of the error terms for the Example 2.4.1 ($\nu = 1$). (Fuente: Elaboración propia)

k	N	η_1	order	η_2	order	η_3	order	η_4	order	η_5	order	$h.o.t.$	order	eff
	16	1.49e-01	–	8.82e-03	–	6.16e-03	–	4.17e-02	–	7.26e-03	–	3.06e-03	–	9.734
	64	3.66e-02	2.03	2.30e-03	1.94	1.58e-03	1.96	1.06e-02	1.97	1.93e-03	1.92	4.14e-04	2.88	9.293
1	256	9.11e-03	2.01	5.76e-04	2.00	3.95e-04	2.00	2.73e-03	1.96	5.03e-04	1.94	5.51e-05	2.91	9.128
	1024	2.27e-03	2.00	1.43e-04	2.01	9.80e-05	2.01	6.96e-04	1.97	1.29e-04	1.96	7.13e-06	2.95	9.048
	4096	5.68e-04	2.00	3.56e-05	2.01	2.44e-05	2.01	1.76e-04	1.98	3.27e-05	1.98	9.08e-07	2.97	9.007
	16384	1.42e-04	2.00	8.88e-06	2.00	6.08e-06	2.00	4.42e-05	1.99	8.23e-06	1.99	1.15e-07	2.99	8.986
	16	1.86e-02	–	8.61e-04	–	6.78e-04	–	4.31e-03	–	3.97e-04	–	1.77e-04	–	13.214
	64	2.32e-03	3.01	1.08e-04	3.00	8.65e-05	2.97	5.76e-04	2.91	5.26e-05	2.91	1.18e-05	3.91	13.612
2	256	2.89e-04	3.00	1.34e-05	3.00	1.09e-05	2.99	7.44e-05	2.95	6.76e-06	2.96	7.58e-07	3.96	13.847
	1024	3.61e-05	3.00	1.68e-06	3.00	1.36e-06	3.00	9.47e-06	2.98	8.55e-07	2.98	4.80e-08	3.98	13.977
	4096	4.51e-06	3.00	2.10e-07	3.00	1.71e-07	3.00	1.19e-06	2.99	1.08e-07	2.99	3.02e-09	3.99	14.046
	16384	5.64e-07	3.00	2.62e-08	3.00	2.14e-08	3.00	1.50e-07	2.99	1.35e-08	3.00	1.89e-10	4.00	14.081
	16	6.54e-04	–	1.41e-05	–	7.02e-06	–	1.27e-04	–	2.97e-06	–	1.24e-06	–	23.429
	64	4.11e-05	3.99	8.80e-07	4.00	4.36e-07	4.01	8.51e-06	3.90	1.85e-07	4.01	3.80e-08	5.03	23.437
3	256	2.58e-06	4.00	5.51e-08	4.00	2.72e-08	4.00	5.49e-07	3.96	1.15e-08	4.01	1.17e-09	5.02	23.458
	1024	1.62e-07	4.00	3.45e-09	4.00	1.70e-09	4.00	3.48e-08	3.98	7.18e-10	4.00	3.62e-11	5.01	23.473
	4096	1.01e-08	4.00	2.16e-10	4.00	1.07e-10	4.00	2.19e-09	3.99	4.48e-11	4.00	1.12e-12	5.01	23.482
	16384	6.32e-10	4.00	1.35e-11	4.00	6.68e-12	4.00	1.37e-10	3.99	2.80e-12	4.00	3.50e-14	5.01	23.466

Table 2.2: History of convergence of the terms composing the error estimator for the Example 2.4.1 ($\nu = 1$). (Fuente: Elaboración propia)

Table 2.1 shows the history of convergence of the error of each variable when the number of elements N quadruplicates, i.e., the mesh size h decreases by a factor two. We see that all the error terms converge with optimal order of $k + 1$, exactly as the error estimates in Section 2.2 predicted. In addition, we see in Table 2.2 that each term of the error estimator converges with the optimal order

$k+1$ and the high order term with order $k+2$.

We repeat the experiment considering now $\nu = 10^{-2}$. As Tables 2.3-2.4 show, similar conclusions can be drawn regarding the optimal order of convergence of the error and the estimator. The last column of Tables 2.2 and 2.4 displays the effectivity index. It remains bounded for each polynomial degree k, however it increases with k. This is natural to expect since some of the constants on the estimates depend on k.

On the other hand, we observe in all the cases that the first term of the estimator (η_1) is larger than the other terms. This behavior, together with the fact that the effectivity index is larger than one, might suggest that the estimator is locating regions where the divergence of $\nu(\mathrm{L} - \mathrm{L}_h) + (p - p_h)\mathrm{I}$ is large. Motivated by this issue, if we assume that the solution of the Brinkman problem is such that $\mathrm{L} \in H(\mathrm{div}, \Omega)^d$ and $p \in H^1(\Omega)$, we can add the term $\theta_K \|\nabla \cdot (\nu \mathrm{L} - p\mathrm{I}) - \nabla \cdot (\nu \mathrm{L}_h - p_h \mathrm{I})\|_{0,K}$ to error e_K defined (3.19), since

$$\begin{aligned}\theta_K \|\nabla \cdot (\nu \mathrm{L} - p\mathrm{I}) - \nabla \cdot (\nu \mathrm{L}_h - p_h \mathrm{I})\|_{0,K} &\leq \theta_K \|\boldsymbol{f} + \nabla \cdot (\nu \mathrm{L}_h) - \nabla p_h - \alpha \boldsymbol{u}_h^*\|_{0,K} + \theta_K \alpha \|\boldsymbol{u} - \boldsymbol{u}_h^*\|_{0,K} \\ &\preceq \eta_K + \alpha^{1/2} \|\boldsymbol{u} - \boldsymbol{u}_h^*\|_{0,K},\end{aligned}$$

thanks to (2.1b), the definition θ_K and (2.14).

Table 2.5 shows the behavior of the global estimator and the global error that includes the aforementioned term. In this case, we observe that effectivity index is close to 1.

In summary, this example shows that, even though $\boldsymbol{u}_D \notin \boldsymbol{V}_h^*$, as in the case of $k = 1$ and 2, Tables 2.1-2.5 verify that our error estimate is reliable and locally efficient as stated in Theorems 2.3.1 and 2.3.2. Moreover, the estimator is robust in the sense that the upper and lower bounds of error are uniformly bounded with respect to the physical parameters α and ν.

k	N	e_{L}	order	$\mathsf{e}_{\boldsymbol{u}}$	order	e_p	order
	16	2.89e-02	–	9.35e-02	–	6.55e-02	–
	64	1.09e-02	1.41	2.43e-02	1.94	1.47e-02	2.16
1	256	3.09e-03	1.82	5.12e-03	2.25	3.35e-03	2.13
	1024	8.22e-04	1.91	1.05e-03	2.29	7.43e-04	2.17
	4096	2.14e-04	1.94	2.32e-04	2.17	1.68e-04	2.15
	16384	5.51e-05	1.96	5.56e-05	2.06	3.93e-05	2.09
	16	2.06e-03	–	4.70e-03	–	5.73e-03	–
	64	3.16e-04	2.71	4.96e-04	3.25	6.46e-04	3.15
2	256	4.07e-05	2.96	4.89e-05	3.34	6.95e-05	3.22
	1024	5.01e-06	3.02	5.12e-06	3.26	7.61e-06	3.19
	4096	6.21e-07	3.01	5.86e-07	3.13	8.66e-07	3.14
	16384	7.76e-08	3.00	7.10e-08	3.05	1.02e-07	3.08
	16	7.83e-05	–	1.06e-04	–	1.83e-04	–
	64	5.14e-06	3.93	5.64e-06	4.23	9.97e-06	4.19
3	256	3.22e-07	4.00	3.01e-07	4.23	5.60e-07	4.16
	1024	2.03e-08	3.99	1.70e-08	4.14	3.25e-08	4.11
	4096	1.29e-09	3.98	1.01e-09	4.07	1.94e-09	4.07
	16384	8.12e-11	3.99	6.22e-11	4.03	1.18e-10	4.04

Table 2.3: History of convergence of the error terms for the Example 2.4.1 ($\nu = 10^{-2}$). (Fuente: Elaboración propia)

k	N	η_1	order	η_2	order	η_3	order	η_4	order	η_5	order	$h.o.t.$	order	eff
	16	1.29e-01	–	7.20e-02	–	5.26e-02	–	3.96e-02	–	5.90e-02	–	2.47e-02	–	1.463
	64	8.55e-02	0.60	2.26e-02	1.67	1.67e-02	1.65	2.22e-02	0.84	1.78e-02	1.73	3.61e-03	2.77	3.106
1	256	4.64e-02	0.88	4.96e-03	2.19	3.72e-03	2.17	1.01e-02	1.14	3.68e-03	2.28	3.68e-04	3.29	7.011
	1024	1.48e-02	1.65	9.76e-04	2.35	7.22e-04	2.37	3.28e-03	1.62	6.95e-04	2.40	3.56e-05	3.37	9.971
	4096	3.70e-03	2.00	2.05e-04	2.25	1.42e-04	2.35	9.30e-04	1.82	1.47e-04	2.25	3.87e-06	3.20	10.706
	16384	9.26e-04	2.00	4.77e-05	2.10	3.03e-05	2.23	2.50e-04	1.90	3.50e-05	2.07	4.69e-07	3.05	10.971
	16	1.74e-02	–	5.02e-03	–	3.31e-03	–	4.02e-03	–	2.62e-03	–	1.13e-03	–	2.471
	64	4.70e-03	1.89	5.89e-04	3.09	3.91e-04	3.08	9.63e-04	2.06	3.02e-04	3.12	6.42e-05	4.13	5.567
2	256	1.20e-03	1.97	6.30e-05	3.22	4.20e-05	3.22	1.99e-04	2.28	2.95e-05	3.35	3.13e-06	4.36	12.947
	1024	1.89e-04	2.67	7.07e-06	3.16	4.54e-06	3.21	2.94e-05	2.76	2.95e-06	3.32	1.56e-07	4.33	18.355
	4096	2.38e-05	2.99	8.49e-07	3.06	5.16e-07	3.14	4.00e-06	2.88	3.28e-07	3.17	8.63e-09	4.17	19.841
	16384	2.98e-06	3.00	1.06e-07	3.01	6.12e-08	3.08	5.23e-07	2.93	3.95e-08	3.06	5.17e-10	4.06	20.642
	16	7.99e-04	–	1.34e-04	–	7.70e-05	–	1.41e-04	–	4.40e-05	–	1.87e-05	–	3.673
	64	1.04e-04	2.95	7.49e-06	4.16	3.55e-06	4.44	1.63e-05	3.11	2.25e-06	4.29	4.70e-07	5.31	8.375
3	256	1.32e-05	2.97	4.31e-07	4.12	1.46e-07	4.60	1.66e-06	3.30	1.14e-07	4.30	1.13e-08	5.37	18.684
	1024	1.05e-06	3.66	2.64e-08	4.03	6.26e-09	4.54	1.21e-07	3.77	6.25e-09	4.19	2.95e-10	5.27	25.119
	4096	6.59e-08	3.99	1.66e-09	3.99	3.31e-10	4.24	8.09e-09	3.90	3.71e-10	4.08	8.47e-12	5.12	26.171
	16384	4.14e-09	3.99	1.05e-10	3.98	2.04e-11	4.02	5.24e-10	3.95	2.28e-11	4.02	2.58e-13	5.04	26.719

Table 2.4: History of convergence of the terms composing the error estimator for the Example 2.4.1 ($\nu = 10^{-2}$). (Fuente: Elaboración propia)

k	N	e_h	order	η_h	order	eff
	16	1.60e-02	–	1.56e-01	–	1.036
	64	4.12e-03	1.96	3.83e-02	2.02	1.039
1	256	1.05e-03	1.98	9.55e-03	2.00	1.041
	1024	2.64e-04	1.99	2.39e-03	2.00	1.043
	4096	6.63e-05	1.99	5.97e-04	2.00	1.044
	16384	1.66e-05	2.00	1.49e-04	2.00	1.044
	16	1.45e-03	–	1.92e-02	–	1.026
	64	1.76e-04	3.05	2.39e-03	3.00	1.030
2	256	2.16e-05	3.02	2.99e-04	3.00	1.032
	1024	2.68e-06	3.01	3.74e-05	3.00	1.033
	4096	3.33e-07	3.01	4.68e-06	3.00	1.034
	16384	4.15e-08	3.00	5.85e-07	3.00	1.034
	16	2.84e-05	–	6.66e-04	–	1.018
	64	1.79e-06	3.99	4.20e-05	3.99	1.021
3	256	1.12e-07	3.99	2.64e-06	3.99	1.022
	1024	7.04e-09	4.00	1.65e-07	4.00	1.022
	4096	4.40e-10	4.00	1.03e-08	4.00	1.023
	16384	2.76e-11	4.00	6.47e-10	4.00	1.023

k	N	e_h	order	η_h	order	eff
	16	1.18e-01	–	3.01e-01	–	0.759
	64	3.04e-02	1.96	1.01e-01	1.57	0.944
1	256	6.85e-03	2.15	4.82e-02	1.07	1.003
	1024	1.52e-03	2.17	1.52e-02	1.67	1.020
	4096	3.57e-04	2.09	3.83e-03	1.99	1.029
	16384	8.76e-05	2.03	9.61e-04	1.99	1.034
	16	7.70e-03	–	2.21e-02	–	0.913
	64	8.73e-04	3.14	4.90e-03	2.17	0.996
2	256	9.42e-05	3.21	1.22e-03	2.01	1.009
	1024	1.04e-05	3.17	1.92e-04	2.67	1.011
	4096	1.22e-06	3.10	2.41e-05	2.99	1.014
	16384	1.47e-07	3.05	3.03e-06	2.99	1.015
	16	2.25e-04	–	8.48e-04	–	0.971
	64	1.26e-05	4.16	1.05e-04	3.01	1.004
3	256	7.12e-07	4.14	1.33e-05	2.98	1.006
	1024	4.19e-08	4.09	1.05e-06	3.66	1.006
	4096	2.54e-09	4.05	6.64e-08	3.99	1.007
	16384	1.56e-10	4.02	4.17e-09	3.99	1.008

Table 2.5: History of convergence of the modified global error and estimator for the Example 2.4.1 with $\nu = 1$ (left) and $\nu = 10^{-2}$ (right). (Fuente: Elaboración propia)

2.4.2 The Kovasznay flow

We set $\Omega = (0,2) \times (-0.5, 1.5)$ and consider the Stokes problem ($\alpha = 0$) whose exact solution coincides with the analytical solution of the two-dimensional incompressible Navier-Stokes equations presented in [82]: $\boldsymbol{u} := (u_1, u_2)$, where $u_1(x_1, x_2) = 1 - \exp(\lambda x_1)\cos(2\pi x_2)$ and $u_2(x_1, x_2) = \frac{\lambda}{2\pi}\exp(\lambda x_1)\sin(2\pi x_2)$, and $p(x_1, x_2) = \frac{1}{2}\exp(2\lambda x_1) - \frac{\exp(4\lambda)-1}{8\lambda}$. Here $\lambda = \frac{\mathsf{Re}}{2} - \sqrt{\frac{\mathsf{Re}^2}{4} + 4\pi^2}$ and $\mathsf{Re} = \frac{1}{\nu}$. This is also a solution of our problem with $\boldsymbol{f} = -(\boldsymbol{u}\cdot\nabla)\boldsymbol{u}$ and $\boldsymbol{u}_D = \boldsymbol{u}|_\Gamma$.

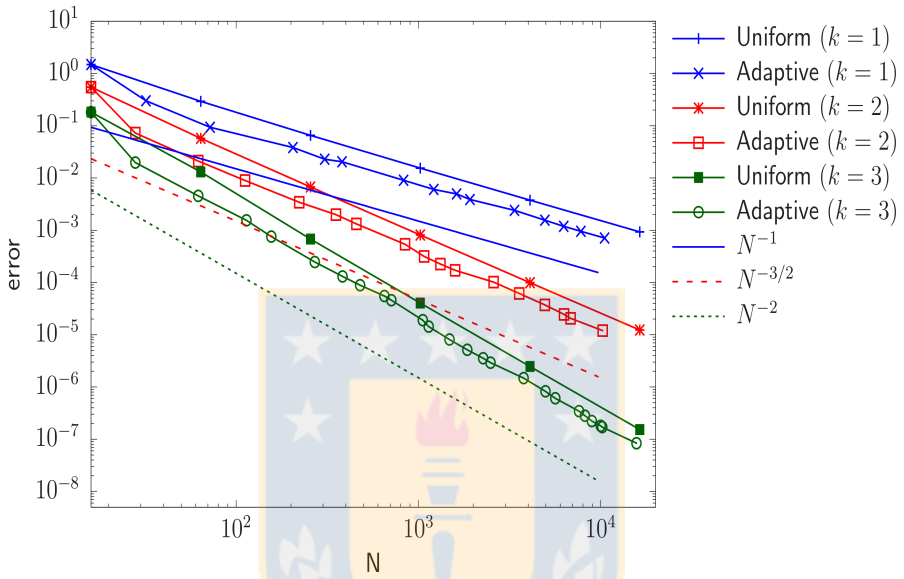

Figure 2.1: History of convergence ($k = 1, 2, 3$) for e_h with uniform and adaptive ($\theta = 0.25$) refinements, for the Kovasznay flow ($\nu = 1$). (Fuente: Elaboración propia)

Figure 2.1 depicts the error e_h (defined in (3.19)) versus the number of elements N, using uniform and adaptive ($\theta = 0.25$) refinements. Since the solution is smooth, we can see that the curves associated to uniform and adaptive refinements display the same order of convergence predicted by the theory, i.e, order $N^{-(k+1)/2}$. In addition, we observe that the adaptive strategy is able to provide errors with the same magnitude as the uniform refinement, but with fewer elements.

2.4.3 A singularly perturbed problem

We set $\nu = 0.01$ and $\alpha = 1$. The domain is the unit square $\Omega = (0,1)^2$, and $\boldsymbol{f}$, $\boldsymbol{u}_D$ are such that the exact solution is $\boldsymbol{u} := (u_1, u_2)$, where $u_1(x_1, x_2) = x_2 - \frac{1-\exp(x_2/\nu)}{1-\exp(1/\nu)}$ and $u_2(x_1, x_2) = x_1 - \frac{1-\exp(x_1/\nu)}{1-\exp(1/\nu)}$, and $p(x_1, x_2) = x_1 - x_2$. This solution has boundary layers at $x_1 = 1$ and $x_2 = 1$. In Figure 2.2, we present the orders of convergence for e_h using uniform and adaptive refinements, for $k = 1, 2, 3$. We recover the predicted rates of convergence, up to an expected loss of convergence on very coarse meshes due to the unresolved boundary layers. Figure 2.3 shows the initial mesh and the final mesh obtained with the adaptive scheme. We observe here how the estimator is properly localizing the boundary layers.

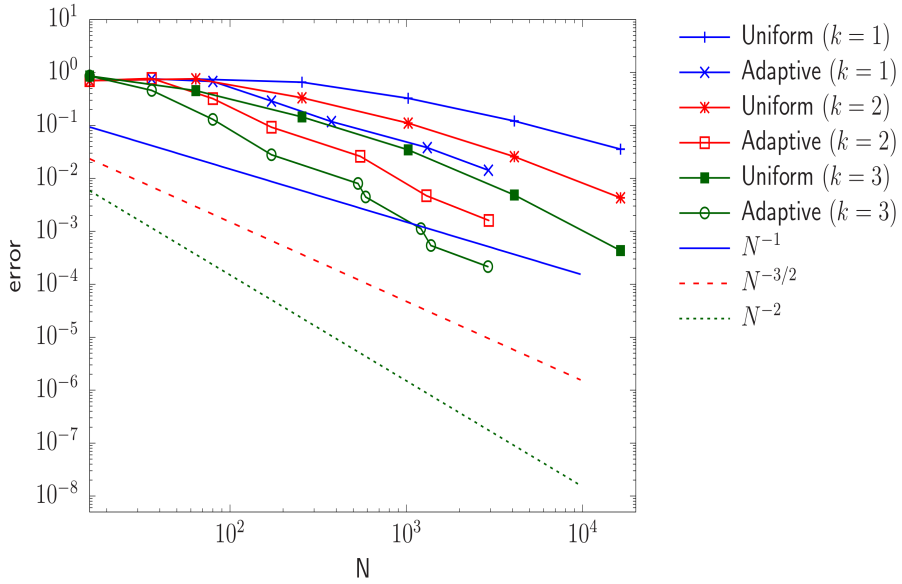

Figure 2.2: History of convergence for e_h with uniform and adaptive ($\theta = 0.25$) refinement ($k = 1, 2, 3$), singularly perturbed problem. (Fuente: Elaboración propia)

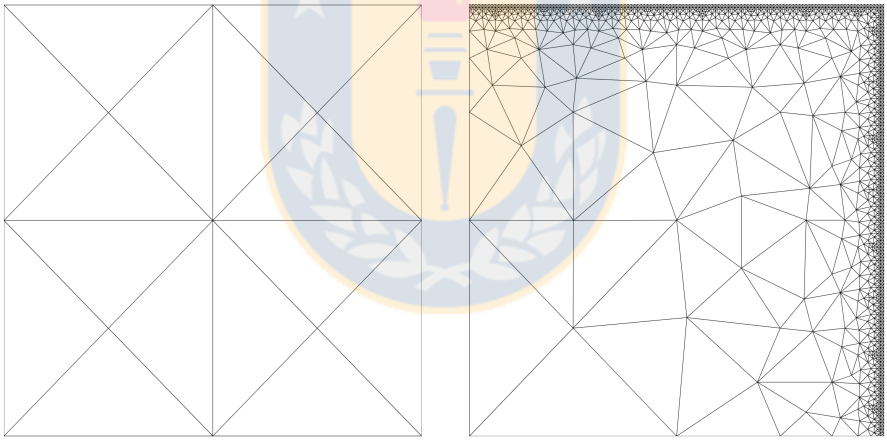

Figure 2.3: Initial (left, 16 elements) and final adapted (right, 2920 elements) meshes for the the singularly perturbed problem ($k = 1$). (Fuente: Elaboración propia)

2.4.4 The lid-driven cavity problem

For this test, we use the same domain as in the previous experiment and $\tau = 10^{-2}, 1, 10^2$. We set $\nu = 1$, $\alpha = 0$, $\boldsymbol{f} = \mathbf{0}$ and $\boldsymbol{u}_D = (1, 0)$, on $x_2 = 1$, and $\mathbf{0}$ on the rest of the boundary of Ω. Note that two singularities arise at the top corners of the domain, due to the discontinuities on the boundary condition. This fact is captured by our estimator by refining mainly in those corners as can be seen in Figure 2.4, where the initial and adapted ($\theta = 0.1$) meshes are displayed. We also note that the number of element of the adapted meshes do not change significantly even when we use different values of τ.

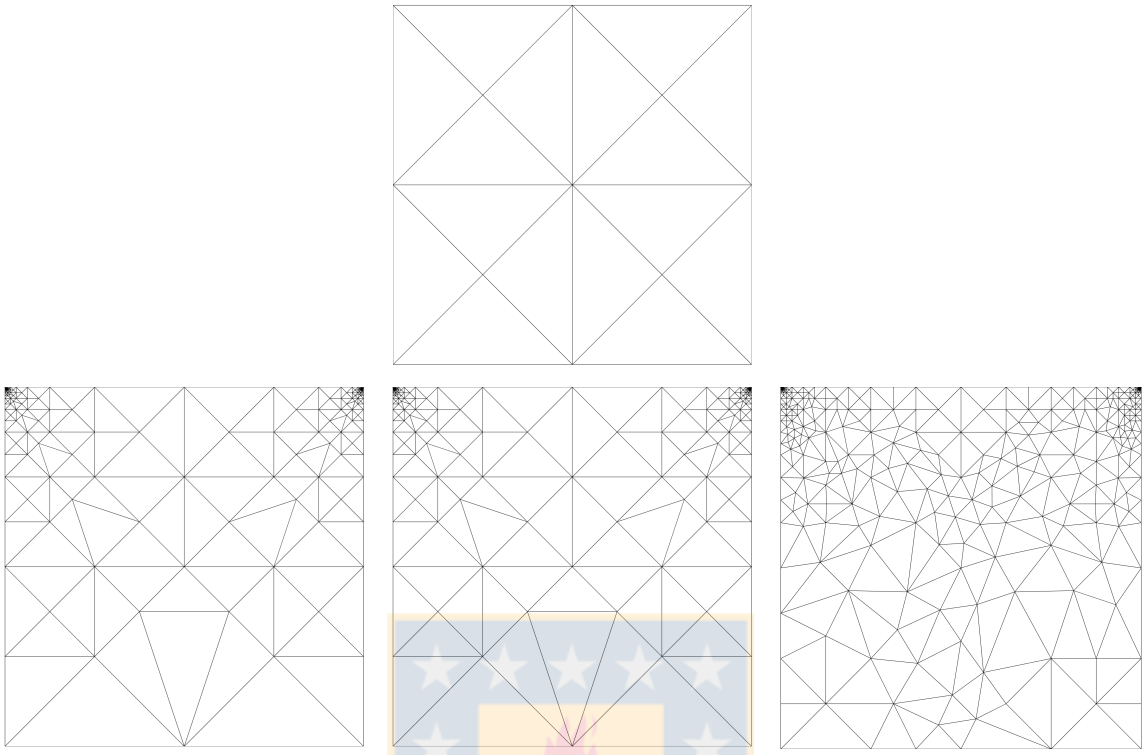

Figure 2.4: Initial (top, 16 elements) and adapted (bottom) meshes for the cavity problem ($k = 1$) for $\tau = 10^{-2}$, 1 and 10^2 (left, center and right, respectively). Adapted meshes with 942 (first two) and 1200 elements (last one). (Fuente: Elaboración propia)

CHAPTER 3

A posteriori error analysis of an HDG method for the Oseen problem

In this chapter we propose a residual-type a posteriori error estimator for an HDG method applied to the Oseen problem. We present reliability and local efficiency results with respect to an error measured in the natural norms, with constants depending explicitly on the physical parameters. Additionally we will use a weighted function technique to control the L^2-error of the velocity.

3.1 Introduction

We consider the Oseen equations of a viscous and incompressible fluid at small Reynolds numbers under the action of an external body force and with prescribed velocity on the boundary of the volume containing it. The problem that we solve can be expressed as follows

$$\mathrm{L} - \nabla \boldsymbol{u} = 0 \qquad \text{in } \Omega, \tag{3.1a}$$

$$-\nabla \cdot (\nu \mathrm{L}) + \nabla p + (\boldsymbol{\beta} \cdot \nabla)\boldsymbol{u} = \boldsymbol{f} \qquad \text{in } \Omega, \tag{3.1b}$$

$$\nabla \cdot \boldsymbol{u} = 0 \qquad \text{in } \Omega, \tag{3.1c}$$

$$\boldsymbol{u} = \boldsymbol{u}_D \qquad \text{on } \Gamma, \tag{3.1d}$$

$$\int_\Omega p = 0, \tag{3.1e}$$

where $\Omega \subset \mathbb{R}^d$ $(d = 2, 3)$ is a polygonal/polyhedral domain with Lipschitz boundary Γ, $\boldsymbol{u}$ is the velocity field, p the pressure, $\nu > 0$ the effective viscosity of the fluid, $\boldsymbol{\beta} \in W^{1,\infty}(\Omega)^d$ the convective velocity of the fluid, $\boldsymbol{f} \in L^2(\Omega)^d$ an external body force and $\boldsymbol{u}_D \in H^{1/2}(\Gamma)^d$ a Dirichlet boundary data, assumed to satisfy $\int_\Gamma \boldsymbol{u}_D \cdot \boldsymbol{n} = 0$ for compatibility. We assume $\nabla \cdot \boldsymbol{\beta} = 0$ motivated by the application to the incompressible Navier–Stokes equations. In fact, one of the most common approaches to approximate the solution of the incompressible Navier–Stokes equations is to consider Picard's iteration, which consists in solving Oseen equations at every step, where the convective velocity, which is divergence free, is nothing but the velocity of the previous iteration. Now, since $\boldsymbol{\beta}$ is divergence free, it is not possible to use the standard energy argument to bound the L^2-norm of the error of $\boldsymbol{u}$ and that is why a duality argument is employed [51]. Another alternative to control this error is based on the idea of [6] (see also [62]) and assume that there is a function $\psi \in W^{1,\infty}(\Omega)$ such that $\boldsymbol{\beta} \cdot \nabla \psi \geq \frac{\|\boldsymbol{\beta}\|_{\infty,\Omega}}{\mathsf{diam}(\Omega)}$. This is satisfied, according to [6], if $\boldsymbol{\beta}$ has no closed curves and $|\boldsymbol{\beta}(\boldsymbol{x})| \neq 0$ for all $\boldsymbol{x} \in \Omega$. In this work we

consider the later approach which will help us to obtain an *a posteriori* estimates for an error that includes the L^2-error of the velocity.

The Oseen equations constitute an improved description of viscous and incompressible fluids at small Reynolds numbers, as compared to Stokes equations, with the partial inclusion of convective acceleration [91]. As an application of Oseen equations we can consider slow motion of small particles in a fluid, that is common in bio-mechanics [64].

3.1.1 An HDG method for the Oseen problem

Let us consider the finite element spaces

$$\mathrm{G}_h := \{\mathrm{G} \in [L^2(\mathcal{T}_h)]^{d\times d} : \mathrm{G}|_K \in [\mathbb{P}_k(K)]^{d\times d} \quad \forall K \in \mathcal{T}_h\}, \tag{3.2a}$$
$$\boldsymbol{V}_h := \{\boldsymbol{v} \in [L^2(\mathcal{T}_h)]^{d} : \boldsymbol{v}|_K \in [\mathbb{P}_k(K)]^{d} \quad \forall K \in \mathcal{T}_h\}, \tag{3.2b}$$
$$P_h := \{w \in L^2(\mathcal{T}_h) : w|_T \in \mathbb{P}_k(K) \quad \forall K \in \mathcal{T}_h\}, \tag{3.2c}$$
$$\boldsymbol{M}_h := \{\boldsymbol{\mu} \in [L^2(\mathcal{E}_h)]^{d} : \boldsymbol{\mu}|_e \in [\mathbb{P}_k(e)]^{d} \quad \forall e \in \mathcal{E}_h\} \tag{3.2d}$$

and the HDG formulation, introduced in [21], for the Oseen problem (3.1): *Find* $(\mathrm{L}_h, \boldsymbol{u}_h, p_h, \widehat{\boldsymbol{u}}_h) \in \mathrm{G}_h \times \boldsymbol{V}_h \times P_h \times \boldsymbol{M}_h$ *such that*

$$(\mathrm{L}_h, \mathrm{G})_{\mathcal{T}_h} + (\boldsymbol{u}_h, \nabla\cdot \mathrm{G})_{\mathcal{T}_h} - \langle \widehat{\boldsymbol{u}}_h, \mathrm{G}\boldsymbol{n}\rangle_{\partial\mathcal{T}_h} = 0, \tag{3.3a}$$
$$(\nu\mathrm{L}_h, \nabla\boldsymbol{v})_{\mathcal{T}_h} - (\boldsymbol{u}_h\otimes\boldsymbol{\beta}, \nabla\boldsymbol{v})_{\mathcal{T}_h} - (p_h, \nabla\cdot\boldsymbol{v})_{\mathcal{T}_h} - \langle \widehat{\nu\mathrm{L}_h\boldsymbol{n} - (\boldsymbol{u}_h\otimes\boldsymbol{\beta})\boldsymbol{n}} - \widehat{p}_h\boldsymbol{n}, \boldsymbol{v}\rangle_{\partial\mathcal{T}_h} = (\boldsymbol{f}, \boldsymbol{v})_{\mathcal{T}_h}, \tag{3.3b}$$
$$-(\boldsymbol{u}_h, \nabla q)_{\mathcal{T}_h} + \langle \widehat{\boldsymbol{u}}_h\cdot\boldsymbol{n}, q\rangle_{\partial\mathcal{T}_h} = 0, \tag{3.3c}$$
$$\langle \widehat{\boldsymbol{u}}_h, \boldsymbol{\mu}\rangle_{\Gamma} = \langle \boldsymbol{u}_D, \boldsymbol{\mu}\rangle_{\Gamma}, \tag{3.3d}$$
$$\langle \widehat{\nu\mathrm{L}_h\boldsymbol{n} - (\boldsymbol{u}_h\otimes\boldsymbol{\beta})\boldsymbol{n}} - \widehat{p}_h\boldsymbol{n}, \boldsymbol{\mu}\rangle_{\partial\mathcal{T}_h\setminus\Gamma} = 0, \tag{3.3e}$$
$$(p_h, 1)_{\Omega} = 0, \tag{3.3f}$$

for all $(\mathrm{G}, \boldsymbol{v}, q, \boldsymbol{\mu}) \in \mathrm{G}_h \times \boldsymbol{V}_h \times P_h \times \boldsymbol{M}_h$. To complete the definition of the scheme, we specify the numerical trace $\widehat{\nu\mathrm{L}_h\boldsymbol{n} - (\boldsymbol{u}_h\otimes\boldsymbol{\beta})\boldsymbol{n}} - \widehat{p}_h\boldsymbol{n} := \nu\mathrm{L}_h\boldsymbol{n} - (\widehat{\boldsymbol{u}}_h\otimes\boldsymbol{\beta})\boldsymbol{n} - p_h\boldsymbol{n} - \nu\tau(\boldsymbol{u}_h - \widehat{\boldsymbol{u}}_h)$ on $\partial\mathcal{T}_h$, where τ is a positive stabilization function on $\partial\mathcal{T}_h$ that satisfies

$$\min_{\boldsymbol{x}\in\partial K}\left(\nu\tau - \frac{1}{2}\boldsymbol{\beta}\cdot\boldsymbol{n}\right) > 0 \quad \forall K \in \mathcal{T}_h. \tag{3.4}$$

As it is shown in [21], this scheme is well-posed and, if L, $\boldsymbol{u}$ and p have enough regularity, the approximate solution satisfies

$$\|\mathrm{L} - \mathrm{L}_h\|_{0,\mathcal{T}_h} + \|\boldsymbol{u} - \boldsymbol{u}_h\|_{0,\mathcal{T}_h} + \|p - p_h\|_{0,\mathcal{T}_h} \le c_{\nu,\boldsymbol{\beta}} \sum_{K\in\mathcal{T}_h} h_K^{k+1}\Theta_K, \tag{3.5a}$$

where $c_{\nu,\boldsymbol{\beta}} > 0$ is a constant depending on ν and $\boldsymbol{\beta}$ and $\Theta_K := |\mathrm{L}|_{k+1} + |\boldsymbol{u}|_{k+1} + |\nabla\cdot(\nu\mathrm{L} - p\mathrm{I})|_{k,K} + |p|_{k+1,K}$.

3.1.2 Local postprocessing of the velocity

Our a posteriori error estimator will be defined in terms of a local postprocessing $\boldsymbol{u}_h^*$ of $\boldsymbol{u}_h$ that approximates $\boldsymbol{u}$ with enhanced accuracy. In our case, we construct $\boldsymbol{u}_h^*$ as follows. We seek $\boldsymbol{u}_h^* \in \boldsymbol{V}_h^* := \{\boldsymbol{w} \in [L^2(\Omega)]^d : \boldsymbol{w}|_K \in [\mathbb{P}_{k+1}(K)]^d \ \forall K \in \mathcal{T}_h\}$ such that, for all $K \in \mathcal{T}_h$, it satisfies

$$(\nabla \boldsymbol{u}_h^*, \nabla \boldsymbol{w})_K = (\mathrm{L}_h, \nabla \boldsymbol{w})_K \quad \forall \boldsymbol{w} \in [\mathbb{P}_{k+1}(K)]^d \tag{3.6a}$$

$$(\boldsymbol{u}_h^*, \boldsymbol{w})_K = (\boldsymbol{u}_h, \boldsymbol{w})_K \qquad \forall \boldsymbol{w} \in [\mathbb{P}_0(K)]^d. \tag{3.6b}$$

It's straightforward to see that $\boldsymbol{u}_h^*$ is well defined. Moreover, this new approximation has superconvergence properties (see [102]).

3.2 A posteriori error analysis

To start, we provide auxiliary results needed to prove the reliability and efficiency of the error estimator. They were announced in the preliminary results section, but have been included here in order to make more clear its statements in term of the physical parameters. We will also use the approximation property of the Oswald interpolation operator stated in Lemma 0.4.

Lemma 3.2.1. *For any $K \in \mathcal{T}_h$, $e \in \mathcal{E}_h^i$, $0 \le m \le 1$ and $w \in H_0^1(\Omega)$, there hold:*

$$\|\mathcal{C}_h w\|_{m,\Omega} \preceq \|w\|_{m,\Omega}, \quad \|w - \mathcal{C}_h w\|_{0,K} \preceq \theta_K |\!|\!| w |\!|\!|_{1,\Delta_K} \quad \text{and} \quad \|w - \mathcal{C}_h w\|_{0,e} \preceq \nu^{-1/4}\theta_e^{1/2} |\!|\!| w |\!|\!|_{1,\Delta_e},$$

where $\theta_S := \min\{h_S\nu^{-1/2}, \mathsf{diam}(\Omega)^{1/2}\|\boldsymbol{\beta}\|_{\infty,\Omega}^{-1/2}\}$, with S an element $K \in \mathcal{T}_h$ or a face $e \in \mathcal{E}_h$, $\Delta_K := \{K' \in \mathcal{T}_h : \overline{K'} \cap \overline{K} \neq \emptyset\}$ and $\Delta_e := \{K' \in \mathcal{T}_h : \overline{K'} \cap \overline{e} \neq \emptyset\}$.

Lemma 3.2.2. *The following estimates hold for all $\boldsymbol{v} \in [\mathbb{P}_k(K)]^d$, $K \in \mathcal{T}_h$, $\boldsymbol{\mu} \in [\mathbb{P}_k(e)]^d$, and $e \in \mathcal{E}_h$:*

$$\|\boldsymbol{v}\|_{0,K}^2 \preceq (\boldsymbol{v}, B_K\boldsymbol{v})_K, \qquad \|B_K\boldsymbol{v}\|_{0,K} \preceq \|\boldsymbol{v}\|_{0,K}, \qquad |\!|\!| B_K\boldsymbol{v} |\!|\!|_{1,K} \preceq \theta_K^{-1}\|\boldsymbol{v}\|_{0,K},$$

$$\|\boldsymbol{\mu}\|_{0,e}^2 \preceq (\boldsymbol{\mu}, B_e\boldsymbol{\mu})_e, \qquad \|B_e\boldsymbol{\mu}\|_{0,\omega_e} \preceq \nu^{1/4}\theta_e^{1/2}\|\boldsymbol{\mu}\|_{0,e}, \qquad |\!|\!| B_e\boldsymbol{\mu} |\!|\!|_{1,\omega_e} \preceq \nu^{1/4}\theta_e^{-1/2}\|\boldsymbol{\mu}\|_{0,e}.$$

3.2.1 *A posteriori* error estimator

For each $K \in \mathcal{T}_h$, we propose the following local error estimator

$$\eta_K^2 := \theta_K^2\|\boldsymbol{f} + \nabla\cdot(\nu\mathrm{L}_h) - \nabla\cdot(\boldsymbol{u}_h^*\otimes\boldsymbol{\beta}) - \nabla p_h\|_{0,K}^2 + \nu\|\mathrm{L}_h - \nabla\boldsymbol{u}_h^*\|_{0,K}^2 + \nu\|\nabla\cdot\boldsymbol{u}_h^*\|_{0,K}^2 \tag{3.7}$$
$$+ \frac{1}{2}\sum_{e\in\mathcal{E}_h^i\cap\partial K}\left(\nu^{-1/2}\theta_e\|\,[\![\nu\mathrm{L}_h - (\boldsymbol{u}_h^*\otimes\boldsymbol{\beta}) - p_h\mathrm{I}]\!]\|_{0,e}^2 + \nu h_e^{-1}\|\,[\![\boldsymbol{u}_h^*]\!]\|_{0,e}^2\right) + \sum_{e\in\mathcal{E}_h^\partial\cap\partial K}\nu h_e^{-1}\|\boldsymbol{g}_D - \boldsymbol{u}_h^*\|_{0,e}^2$$

and its global version given by $\eta_h := \left(\sum_{K\in\mathcal{T}_h}\eta_K^2\right)^{1/2}$. Here we recall that θ_K and θ_e were defined in Lemma 3.2.1.

The first three terms are the residuals associated to the equilibrium equation, the constitutive equation and the incompressibility condition, respectively, while the jumps across the faces refer to the

continuity of the trace of $\boldsymbol{u}$ and the normal trace of $\nu \mathrm{L} - (\boldsymbol{u} \otimes \boldsymbol{\beta}) - p\mathrm{I}$, if the solution of the continuous problem had enough regularity.

To prove our main result, we combine two techniques. One of them consists of adapting, to our setting, the procedure followed in [4] for the Brinkman problem. However, in contrast to Brinkman equations, in our case the L^2-error of the scalar variable cannot be obtained directly from the formulation. That is why we employ the weighted function technique used by [23] in the context of the convection-diffusion equations. We emphasize that we keep track the dependence on ν and $\boldsymbol{\beta}$.

We start by introducing three lemmas that will allow us to prove the reliability of the error estimator.

Lemma 3.2.3. *Let* $(\mathrm{L}, \boldsymbol{u}, p)$ *and* $(\mathrm{L}_h, \boldsymbol{u}_h, p_h \widehat{\boldsymbol{u}}_h)$ *the solutions of* (3.1) *and* (3.3)*, respectively, and* $\boldsymbol{u}_h^*$ *the postprocessed velocity defined by* (3.6)*. The following estimate holds*

$$\nu^{-1/2}\|p - p_h\|_{0,\mathcal{T}_h} \preceq \max\{1, C_{\nu,\boldsymbol{\beta}}\} \left[\nu^{1/2}\|\mathrm{L} - \mathrm{L}_h\|_{0,\mathcal{T}_h} + \frac{\|\boldsymbol{\beta}\|_{\infty,\Omega}^{1/2}}{\mathsf{diam}(\Omega)^{1/2}} \|\boldsymbol{u} - \boldsymbol{u}_h^*\|_{0,\mathcal{T}_h} \right.$$
$$+ \sum_{K \in \mathcal{T}_h} \left(\theta_K \|\boldsymbol{f} + \nabla \cdot (\nu \mathrm{L}_h) - \nabla \cdot (\boldsymbol{u}_h^* \otimes \boldsymbol{\beta}) - \nabla p_h\|_{0,K} + \frac{1}{2} \sum_{e \in \mathcal{E}_h^i \cap \partial K} \nu^{-1/4} \theta_e^{1/2} \| [\![\nu \mathrm{L}_h - (\boldsymbol{u}_h^* \otimes \boldsymbol{\beta}) - p_h \mathrm{I}]\!] \|_{0,e} \right)$$
$$\left. + \frac{\|\boldsymbol{\beta}\|_{\boldsymbol{W}^{1,\infty}(\Omega)}}{\nu^{1/2}} \sum_{K \in \mathcal{T}_h} h_K \|\boldsymbol{u}_h - \boldsymbol{u}_h^*\|_{0,K} \right],$$

where $C_{\nu,\boldsymbol{\beta}} := \dfrac{\|\boldsymbol{\beta}\|_{\infty,\Omega}^{1/2} \mathsf{diam}(\Omega)^{1/2}}{\nu^{1/2}}$.

Proof. For $q \in L_0^2(\Omega)$ we know that ([70], Chapter 1, Corollary 2.4)

$$\nu^{-1/2}\|q\|_{0,\mathcal{T}_h} \preceq \sup_{\boldsymbol{w} \in H_0^1(\Omega)^d \setminus \{\boldsymbol{0}\}} \frac{(q, \nabla \cdot \boldsymbol{w})_{\mathcal{T}_h}}{\nu^{1/2}\|\nabla \boldsymbol{w}\|_{0,\mathcal{T}_h}}.$$

Since $p - p_h \in L_0^2(\Omega)$ (cf. (3.1e) and (3.3f)) we can use the above inf-sup condition, with $q = p - p_h$, to get an estimate for $\nu^{-1/2}\|p - p_h\|_{0,\mathcal{T}_h}$. In fact, let $\boldsymbol{w} \in H_0^1(\Omega)^d$. Then, integrating by parts, considering (3.1b), reordering terms and integrating by parts again , we obtain

$$\begin{aligned}
(p - p_h, \nabla \cdot \boldsymbol{w})_{\mathcal{T}_h} &= -\nu(\nabla \cdot (\mathrm{L} - \mathrm{L}_h), \boldsymbol{w})_{\mathcal{T}_h} + (\nabla \cdot ((\boldsymbol{u} - \boldsymbol{u}_h^*) \otimes \boldsymbol{\beta}), \boldsymbol{w})_{\mathcal{T}_h} \\
&\quad - (\boldsymbol{f} + \nabla \cdot (\nu \mathrm{L}_h) - \nabla \cdot (\boldsymbol{u}_h^* \otimes \boldsymbol{\beta}) - \nabla p_h, \boldsymbol{w})_{\mathcal{T}_h} + \langle (p - p_h)\boldsymbol{n}, \boldsymbol{w} \rangle_{\partial \mathcal{T}_h} \\
&= \nu(\mathrm{L} - \mathrm{L}_h, \nabla \boldsymbol{w})_{\mathcal{T}_h} - ((\boldsymbol{u} - \boldsymbol{u}_h^*) \otimes \boldsymbol{\beta}, \nabla \boldsymbol{w})_{\mathcal{T}_h} \\
&\quad - (\boldsymbol{f} + \nabla \cdot (\nu \mathrm{L}_h) - \nabla \cdot (\boldsymbol{u}_h^* \otimes \boldsymbol{\beta}) - \nabla p_h, \boldsymbol{w})_{\mathcal{T}_h} \\
&\quad + \langle [\![\nu \mathrm{L}_h - \boldsymbol{u}_h^* \otimes \boldsymbol{\beta} - p_h \mathrm{I}]\!], \boldsymbol{w} \rangle_{\mathcal{E}_h^i}.
\end{aligned} \tag{3.8}$$

On the other hand, integrating by parts in (3.3b) and considering (3.3e), we have

$$(\boldsymbol{f} + \nabla \cdot (\nu \mathrm{L}_h) - \nabla \cdot (\boldsymbol{u}_h \otimes \boldsymbol{\beta}) - \nabla p_h\, \boldsymbol{v})_{\mathcal{T}_h} = \langle \nu \mathrm{L}_h \boldsymbol{n} - (\boldsymbol{u}_h \otimes \boldsymbol{\beta})\boldsymbol{n} - p_h \boldsymbol{n}, \boldsymbol{v} \rangle_{\partial \mathcal{T}_h \setminus \Gamma} \quad \forall \boldsymbol{v} \in \boldsymbol{V}_h^{1,c}, \tag{3.9}$$

where $\boldsymbol{V}_h^{1,c} := \{\boldsymbol{v} \in H_0^1(\Omega)^d : \boldsymbol{v}|_K \in [\mathbb{P}_1(K)]^d \ \ \forall K \in \mathcal{T}_h\}$. Moreover, for $\boldsymbol{v} \in \boldsymbol{V}_h^{1,c}$ and $K \in \mathcal{T}_h$, we have that

$$\begin{aligned}
-(\nabla\cdot(\boldsymbol{u}_h\otimes\boldsymbol{\beta}),\boldsymbol{v})_K &= (\boldsymbol{u}_h\otimes\boldsymbol{\beta},\nabla\boldsymbol{v})_K - \langle(\boldsymbol{u}_h\otimes\boldsymbol{\beta})\boldsymbol{n},\boldsymbol{v}\rangle_{\partial K\setminus\Gamma}\\
&= (\boldsymbol{u}_h\otimes\mathsf{P}_0\boldsymbol{\beta},\nabla\boldsymbol{v})_K + (\boldsymbol{u}_h\otimes(\mathsf{I}-\mathsf{P}_0)\boldsymbol{\beta},\nabla\boldsymbol{v})_K - \langle(\boldsymbol{u}_h\otimes\boldsymbol{\beta})\boldsymbol{n},\boldsymbol{v}\rangle_{\partial K\setminus\Gamma}\\
&= (\boldsymbol{u}_h^*\otimes\mathsf{P}_0\boldsymbol{\beta},\nabla\boldsymbol{v})_K + (\boldsymbol{u}_h\otimes(\mathsf{I}-\mathsf{P}_0)\boldsymbol{\beta},\nabla\boldsymbol{v})_K - \langle(\boldsymbol{u}_h\otimes\boldsymbol{\beta})\boldsymbol{n},\boldsymbol{v}\rangle_{\partial K\setminus\Gamma}\\
&= (\boldsymbol{u}_h^*\otimes\boldsymbol{\beta},\nabla\boldsymbol{v})_K + ((\boldsymbol{u}_h-\boldsymbol{u}_h^*)\otimes(\mathsf{I}-\mathsf{P}_0)\boldsymbol{\beta},\nabla\boldsymbol{v})_K - \langle(\boldsymbol{u}_h\otimes\boldsymbol{\beta})\boldsymbol{n},\boldsymbol{v}\rangle_{\partial K\setminus\Gamma}\\
&= -(\nabla\cdot(\boldsymbol{u}_h^*\otimes\boldsymbol{\beta}),\boldsymbol{v})_K + ((\boldsymbol{u}_h-\boldsymbol{u}_h^*)\otimes(\mathsf{I}-\mathsf{P}_0)\boldsymbol{\beta},\nabla\boldsymbol{v})_K\\
&\quad - \langle(\boldsymbol{u}_h\otimes\boldsymbol{\beta})\boldsymbol{n},\boldsymbol{v}\rangle_{\partial K\setminus\Gamma} + \langle(\boldsymbol{u}_h^*\otimes\boldsymbol{\beta})\boldsymbol{n},\boldsymbol{v}\rangle_{\partial K\setminus\Gamma},
\end{aligned}$$

that combined with (3.9) result in

$$\begin{aligned}
&(\boldsymbol{f}+\nabla\cdot(\nu\mathrm{L}_h)-\nabla\cdot(\boldsymbol{u}_h^*\otimes\boldsymbol{\beta})-\nabla p_h\,\boldsymbol{v})_{\mathcal{T}_h} \qquad (3.10)\\
&\qquad = \langle[\![\nu\mathrm{L}_h-\boldsymbol{u}_h^*\otimes\boldsymbol{\beta}-p_h\mathrm{I}]\!],\boldsymbol{v}\rangle_{\mathcal{E}_h^i} - ((\boldsymbol{u}_h-\boldsymbol{u}_h^*)\otimes(\mathsf{I}-\mathsf{P}_0)\boldsymbol{\beta},\nabla\boldsymbol{v})_{\mathcal{T}_h} \quad \forall\boldsymbol{v}\in\boldsymbol{V}_h^{1,c},
\end{aligned}$$

where P_0 is the L^2-projection onto $[\mathbb{P}_0(K)]^d$.

Then, combining (3.8) and (3.10) with $\boldsymbol{v} = \mathcal{C}_h\boldsymbol{w}$, we obtain

$$\begin{aligned}
(p-p_h,\nabla\cdot\boldsymbol{w})_{\mathcal{T}_h} &= \nu(\mathrm{L}-\mathrm{L}_h,\nabla\boldsymbol{w})_{\mathcal{T}_h} - ((\boldsymbol{u}-\boldsymbol{u}_h^*)\otimes\boldsymbol{\beta},\nabla\boldsymbol{w})_{\mathcal{T}_h}\\
&\quad - (\boldsymbol{f}+\nabla\cdot(\nu\mathrm{L}_h)-\nabla\cdot(\boldsymbol{u}_h^*\otimes\boldsymbol{\beta})-\nabla p_h,(\mathcal{I}-\mathcal{C}_h)\boldsymbol{w})_{\mathcal{T}_h}\\
&\quad + \langle[\![\nu\mathrm{L}_h-\boldsymbol{u}_h^*\otimes\boldsymbol{\beta}-p_h\mathrm{I}]\!],(\mathcal{I}-\mathcal{C}_h)\boldsymbol{w}\rangle_{\mathcal{E}_h^i} + ((\boldsymbol{u}_h-\boldsymbol{u}_h^*)\otimes(\mathsf{I}-\mathsf{P}_0)\boldsymbol{\beta},\nabla\mathcal{C}_h\boldsymbol{w})_{\mathcal{T}_h}.
\end{aligned}$$

The properties of the Clément interpolant in Lemma 3.2.1 and the regularity of the mesh imply

$$\begin{aligned}
&(p-p_h,\nabla\cdot\boldsymbol{w})_{\mathcal{T}_h}\\
&\le \sum_{K\in\mathcal{T}_h}\nu\|\mathrm{L}-\mathrm{L}_h\|_{0,K}\|\nabla\boldsymbol{w}\|_{0,K} + \sum_{K\in\mathcal{T}_h}\|(\boldsymbol{u}-\boldsymbol{u}_h^*)\otimes\boldsymbol{\beta}\|_{0,K}\|\nabla\boldsymbol{w}\|_{0,K}\\
&\quad + \sum_{K\in\mathcal{T}_h}\|\boldsymbol{f}+\nabla\cdot(\nu\mathrm{L}_h)-\nabla\cdot(\boldsymbol{u}_h^*\otimes\boldsymbol{\beta})-\nabla p_h\|_{0,K}\|(\mathcal{I}-\mathcal{C}_h)\boldsymbol{w}\|_{0,K}\\
&\quad + \sum_{e\in\mathcal{E}_h^i}\|[\![\nu\mathrm{L}_h-(\boldsymbol{u}_h^*\otimes\boldsymbol{\beta})-p_h\mathrm{I}]\!]\|_{0,e}\|(\mathcal{I}-\mathcal{C}_h)\boldsymbol{w}\|_{0,e} + \sum_{K\in\mathcal{T}_h}\|\boldsymbol{u}_h-\boldsymbol{u}_h^*\|_{0,K}\|(\mathsf{I}-\mathsf{P}_0)\boldsymbol{\beta}\|_{\infty,K}\|\nabla\mathcal{C}_h\boldsymbol{w}\|_{0,K}\\
&\le \left(\nu^{1/2}\|\mathrm{L}-\mathrm{L}_h\|_{0,\mathcal{T}_h} + C_{\nu,\boldsymbol{\beta}}\frac{\|\boldsymbol{\beta}\|_{\infty,\Omega}^{1/2}}{\mathsf{diam}(\Omega)^{1/2}}\|\boldsymbol{u}-\boldsymbol{u}_h^*\|_{0,\mathcal{T}_h}\right)\nu^{1/2}\|\nabla\boldsymbol{w}\|_{0,\mathcal{T}_h}\\
&\quad + \left[\sum_{K\in\mathcal{T}_h}\left(\theta_K\|\boldsymbol{f}+\nabla\cdot(\nu\mathrm{L}_h)-\nabla\cdot(\boldsymbol{u}_h^*\otimes\boldsymbol{\beta})-\nabla p_h\|_{0,K} + \frac{1}{2}\sum_{e\in\mathcal{E}_h^i\cap\partial K}\nu^{-1/4}\theta_e^{1/2}\|[\![\nu\mathrm{L}_h-(\boldsymbol{u}_h^*\otimes\boldsymbol{\beta})-p_h\mathrm{I}]\!]\|_{0,e}\right)\right.\\
&\qquad \left. + C_0\frac{\|\boldsymbol{\beta}\|_{\boldsymbol{W}^{1,\infty}(\Omega)}}{\nu^{1/2}}\sum_{K\in\mathcal{T}_h}h_K\|\boldsymbol{u}_h-\boldsymbol{u}_h^*\|_{0,K}\right]|\!|\!|\,\boldsymbol{w}\,|\!|\!|_{1,\Omega}
\end{aligned}$$

$$\leq \max\{1, C_{\nu,\boldsymbol{\beta}}\}\left(\nu^{1/2}\|\mathrm{L}-\mathrm{L}_h\|_{0,\mathcal{T}_h}+\frac{\|\boldsymbol{\beta}\|_{\infty,\Omega}^{1/2}}{\mathsf{diam}(\Omega)^{1/2}}\|\boldsymbol{u}-\boldsymbol{u}_h^*\|_{0,\mathcal{T}_h}\right)\nu^{1/2}\|\nabla\boldsymbol{w}\|_{0,\mathcal{T}_h}$$
$$+\left[\sum_{K\in\mathcal{T}_h}\left(\theta_K\|\boldsymbol{f}+\nabla\cdot(\nu\mathrm{L}_h)-\nabla\cdot(\boldsymbol{u}_h^*\otimes\boldsymbol{\beta})-\nabla p_h\|_{0,K}+\frac{1}{2}\sum_{e\in\mathcal{E}_h^i\cap\partial K}\nu^{-1/4}\theta_e^{1/2}\|[\![\nu\mathrm{L}_h-(\boldsymbol{u}_h^*\otimes\boldsymbol{\beta})-p_h\mathrm{I}]\!]\|_{0,e}\right)\right.$$
$$\left.+C_0\frac{\|\boldsymbol{\beta}\|_{\boldsymbol{W}^{1,\infty}(\Omega)}}{\nu^{1/2}}\sum_{K\in\mathcal{T}_h}h_K\|\boldsymbol{u}_h-\boldsymbol{u}_h^*\|_{0,K}\right]\max\{1,C_PC_{\nu,\boldsymbol{\beta}}\}\,\nu^{1/2}\|\nabla\boldsymbol{w}\|_{0,\mathcal{T}_h},$$

where C_P is the Poincaré constant associated to Ω and C_0 joints the constants associated to P_0. □

Now, to derive an estimate for the L^2-error of the velocity, we proceed as in [18, 23, 50, 51] defining the auxiliary weighted function

$$\varphi := e^{-\psi}+\chi, \tag{3.11}$$

where χ is a positive constant to be determined below. Then, we have the following result.

Lemma 3.2.4. *Let* $(\mathrm{L},\boldsymbol{u},p)$ *and* $(\mathrm{L}_h,\boldsymbol{u}_h,p_h,\widehat{\boldsymbol{u}}_h)$*be the solutions of* (3.1) *and* (3.3)*, respectively, and* $\boldsymbol{u}_h^*$ *the postprocessed velocity defined by* (3.6)*. If we set*

$$\chi := \frac{2\nu\ \mathsf{diam}(\Omega)\|\nabla\psi\|_{\infty,\Omega}^2\|e^{-\psi}\|_{\infty,\Omega}^2}{\|\boldsymbol{\beta}\|_{\infty,\Omega}\min\limits_{\boldsymbol{x}\in\Omega}e^{-\psi(\boldsymbol{x})}}+\frac{64\|\nabla\psi\|_{\infty,\Omega}^2}{\min\limits_{\boldsymbol{x}\in\Omega}e^{-\psi(\boldsymbol{x})}}C_P^2\left(\max\{1,C_{\nu,\boldsymbol{\beta}}\}\right)^2+\frac{3}{4}\min_{\boldsymbol{x}\in\Omega}e^{-\psi(\boldsymbol{x})}+1, \tag{3.12}$$

where $C_P>0$ *is the Poincaré inequality constant associated to* Ω*, then*

$$\nu\|\mathrm{L}-\mathrm{L}_h\|_{0,\mathcal{T}_h}^2+\frac{\|\boldsymbol{\beta}\|_{\infty,\Omega}}{\mathsf{diam}(\Omega)}\|\boldsymbol{u}-\boldsymbol{u}_h^*\|_{0,\mathcal{T}_h}^2\preceq\max\{1,\|\varphi\|_{\infty,\Omega}^2\}\left(\max\{1,C_{\nu,\boldsymbol{\beta}}\}\right)^2\left(\eta_h^2\right.$$
$$\left.+\frac{\|\boldsymbol{\beta}\|_{\boldsymbol{W}^{1,\infty}(\Omega)}^2}{\nu}\sum_{K\in\mathcal{T}_h}h_K^2\|\boldsymbol{u}_h-\boldsymbol{u}_h^*\|_{0,K}^2+\max\left\{\frac{\nu}{\mathsf{diam}(\Omega)^2},\frac{\|\boldsymbol{\beta}\|_{\infty,\Omega}}{\mathsf{diam}(\Omega)},\frac{\|\boldsymbol{\beta}\|_{\infty,\Omega}^2}{\nu}\right\}\|\boldsymbol{u}_h-\widetilde{\boldsymbol{u}}_h\|_{0,\mathcal{T}_h}^2\right),$$

where $\widetilde{\boldsymbol{u}}_h^*$ *is the Oswald interpolant of* $\boldsymbol{u}_h^*$ *provided by Lemma 0.4.*

To prove this estimate, we need the following auxiliary result, adapted from Lemma 4.1 in [23]. The definition of χ will be used as an intermediate step in the proof of Lemma 3.2.4.

Lemma 3.2.5. *Let* $e_{\mathrm{L}}:=\mathrm{L}-\mathrm{L}_h$ *and* $e_{\boldsymbol{u}}:=\boldsymbol{u}-\boldsymbol{u}_h^*$*. The following inequality holds*

$$\left(\chi\nu-\frac{\nu^2\mathsf{diam}(\Omega)\|\nabla\psi\|_{\infty,\Omega}^2\|e^{-\psi}\|_{\infty,\Omega}^2}{\|\boldsymbol{\beta}\|_{\infty,\Omega}\min_{\boldsymbol{x}\in\Omega}e^{-\psi(\boldsymbol{x})}}\right)\|e_{\mathrm{L}}\|_{0,\mathcal{T}_h}^2+\frac{1}{2}\min_{\boldsymbol{x}\in\Omega}e^{-\psi(\boldsymbol{x})}\frac{\|\boldsymbol{\beta}\|_{\infty,\Omega}}{\mathsf{diam}(\Omega)}\|e_{\boldsymbol{u}}\|_{0,\mathcal{T}_h}^2$$
$$\leq\nu(e_{\mathrm{L}},\varphi e_{\mathrm{L}})_{\mathcal{T}_h}+\nu(e_{\mathrm{L}}\nabla\varphi,e_{\boldsymbol{u}})_{\mathcal{T}_h}-\frac{1}{2}((\boldsymbol{\beta}\cdot\nabla\varphi)e_{\boldsymbol{u}},e_{\boldsymbol{u}})_{\mathcal{T}_h}.$$

Proof.

From the definition of φ and the fact that $\boldsymbol{\beta}\cdot\nabla\psi\geq\frac{\|\boldsymbol{\beta}\|_{\infty,\Omega}}{\mathsf{diam}(\Omega)}$, we obtain

$$\nu(e_{\mathrm{L}},\varphi e_{\mathrm{L}})_{\mathcal{T}_h}-\nu(e^{-\psi}e_{\mathrm{L}}\nabla\psi,e_{\boldsymbol{u}})_{\mathcal{T}_h}+\frac{1}{2}((\boldsymbol{\beta}\cdot\nabla\psi)e^{-\psi}e_{\boldsymbol{u}},e_{\boldsymbol{u}})_{\mathcal{T}_h}$$
$$\geq\chi\nu\|e_{\mathrm{L}}\|_{0,\mathcal{T}_h}^2-\nu(e^{-\psi}e_{\mathrm{L}}\nabla\psi,e_{\boldsymbol{u}})_{\mathcal{T}_h}+\frac{\|\boldsymbol{\beta}\|_{\infty,\Omega}}{2\mathsf{diam}(\Omega)}(e^{-\psi}e_{\boldsymbol{u}},e_{\boldsymbol{u}})_{\mathcal{T}_h}.$$

To bound the second term on the right hand side, we use Cauchy-Schwarz and Young's inequalities to obtain, for any $\delta > 0$, that

$$|(e^{-\psi}e_{\mathrm{L}}\nabla\psi, e_{\boldsymbol{u}})_{\mathcal{T}_h}| \leq \frac{1}{2}(\delta^{-1}\|\nabla\psi\|^2_{\infty,\Omega}\|e^{-\psi}\|_{\infty,\Omega}\|e_{\mathrm{L}}\|^2_{0,\mathcal{T}_h} + \delta\|e^{-\psi}\|_{\infty,\Omega}\|e_{\boldsymbol{u}}\|^2_{0,\mathcal{T}_h}).$$

Then, the results follows from taking $\delta = \dfrac{\|\boldsymbol{\beta}\|_{\infty,\Omega}\min_{\boldsymbol{x}\in\Omega} e^{-\psi(\boldsymbol{x})}}{2\nu\mathsf{diam}(\Omega)\|e^{-\psi}\|_{\infty,\Omega}}$, combining both inequalities and noticing that $\nabla\varphi = -\nabla\psi e^{-\psi}$. □

Now, we proceed to prove Lemma 3.2.4.

Proof. Let $\widetilde{\boldsymbol{u}}^*_h \in [H^1(\Omega)]^d$ the Oswald interpolation of $\boldsymbol{u}^*_h$, $e_{\mathrm{L}} = \mathrm{L} - \mathrm{L}_h$ and $e_{\boldsymbol{u}} = \boldsymbol{u} - \boldsymbol{u}^*_h$. Adding and subtracting $\varphi\nabla\widetilde{\boldsymbol{u}}^*_h$, and integrating by parts we obtain

$$\begin{aligned}
\nu(e_{\mathrm{L}}, \varphi e_{\mathrm{L}})_{\mathcal{T}_h} &= \nu(\mathrm{L} - \mathrm{L}_h, \varphi\nabla(\boldsymbol{u} - \widetilde{\boldsymbol{u}}^*_h))_{\mathcal{T}_h} + \nu(\mathrm{L} - \mathrm{L}_h, \varphi(\nabla\widetilde{\boldsymbol{u}}^*_h - \mathrm{L}_h))_{\mathcal{T}_h}\\
&= -\nu((\mathrm{L} - \mathrm{L}_h)(\nabla\varphi), \boldsymbol{u} - \widetilde{\boldsymbol{u}}^*_h)_{\mathcal{T}_h} - \nu(\varphi\ \nabla\cdot(\mathrm{L} - \mathrm{L}_h), \boldsymbol{u} - \widetilde{\boldsymbol{u}}^*_h)_{\mathcal{T}_h}\\
&\quad + \nu\langle(\mathrm{L} - \mathrm{L}_h)\boldsymbol{n}, \varphi(\boldsymbol{u} - \widetilde{\boldsymbol{u}}^*_h)\rangle_{\partial\mathcal{T}_h} + \nu(\mathrm{L} - \mathrm{L}_h, \varphi(\nabla\widetilde{\boldsymbol{u}}^*_h - \mathrm{L}_h))_{\mathcal{T}_h}.
\end{aligned}$$

Using equations (3.1), adding and subtracting terms and integrating by parts, we arrive at

$$\begin{aligned}
\nu(e_{\mathrm{L}}, \varphi e_{\mathrm{L}})_{\mathcal{T}_h} = &-\nu(e_{\mathrm{L}}\nabla\varphi, e_{\boldsymbol{u}})_{\mathcal{T}_h} - \nu((\mathrm{L} - \mathrm{L}_h)(\nabla\varphi), \boldsymbol{u}^*_h - \widetilde{\boldsymbol{u}}^*_h)_{\mathcal{T}_h}\\
&+ (\boldsymbol{f} + \nabla\cdot(\nu\mathrm{L}_h) - \nabla\cdot(\boldsymbol{u}^*_h\otimes\boldsymbol{\beta}) - \nabla p_h, \varphi(\boldsymbol{u} - \widetilde{\boldsymbol{u}}^*_h))_{\mathcal{T}_h}\\
&+ \langle(\nu\mathrm{L} - (\boldsymbol{u}\otimes\boldsymbol{\beta}) - p\mathrm{I})\boldsymbol{n}, \varphi(\boldsymbol{u} - \widetilde{\boldsymbol{u}}^*_h)\rangle_{\partial\mathcal{T}_h\setminus\Gamma} - \langle(\nu\mathrm{L}_h - (\boldsymbol{u}^*_h\otimes\boldsymbol{\beta}) - p_h\mathrm{I})\boldsymbol{n}, \varphi(\boldsymbol{u} - \widetilde{\boldsymbol{u}}^*_h)\rangle_{\partial\mathcal{T}_h\setminus\Gamma}\\
&+ ((\boldsymbol{u} - \boldsymbol{u}^*_h)\otimes\boldsymbol{\beta}, \nabla(\varphi(\boldsymbol{u} - \widetilde{\boldsymbol{u}}^*_h)))_{\mathcal{T}_h} + ((p - p_h)\mathrm{I}, \nabla(\varphi(\boldsymbol{u} - \widetilde{\boldsymbol{u}}^*_h)))_{\mathcal{T}_h}\\
&+ \nu(\mathrm{L} - \mathrm{L}_h, \varphi(\nabla\widetilde{\boldsymbol{u}}^*_h - \mathrm{L}_h))_{\mathcal{T}_h}.
\end{aligned}$$

Since $\boldsymbol{u} - \widetilde{\boldsymbol{u}}^*_h \in H^1_0(\Omega)^d$ (Lemma **??** with $\boldsymbol{g} = \boldsymbol{u}_D$) and $\nu\mathrm{L} - (\boldsymbol{u}\otimes\boldsymbol{\beta}) - p\mathrm{I} \in H(\mathrm{div}, \Omega)^d$, we have that

$$\begin{aligned}
\nu(e_{\mathrm{L}}, \varphi e_{\mathrm{L}})_{\mathcal{T}_h} = &-\nu(e_{\mathrm{L}}\nabla\varphi, e_{\boldsymbol{u}})_{\mathcal{T}_h} - \nu((\mathrm{L} - \mathrm{L}_h)(\nabla\varphi), \boldsymbol{u}^*_h - \widetilde{\boldsymbol{u}}^*_h)_{\mathcal{T}_h} + \nu(\mathrm{L} - \mathrm{L}_h, \varphi(\nabla\widetilde{\boldsymbol{u}}^*_h - \mathrm{L}_h))_{\mathcal{T}_h}\\
&+ (\boldsymbol{f} + \nabla\cdot(\nu\mathrm{L}_h) - \nabla\cdot(\boldsymbol{u}^*_h\otimes\boldsymbol{\beta}) - \nabla p_h, \varphi(\boldsymbol{u} - \widetilde{\boldsymbol{u}}^*_h))_{\mathcal{T}_h}\\
&- \langle(\nu\mathrm{L}_h - (\boldsymbol{u}^*_h\otimes\boldsymbol{\beta}) - p_h\mathrm{I})\boldsymbol{n}, \varphi(\boldsymbol{u} - \widetilde{\boldsymbol{u}}^*_h)\rangle_{\partial\mathcal{T}_h\setminus\Gamma}\\
&+ ((\boldsymbol{u} - \boldsymbol{u}^*_h)\otimes\boldsymbol{\beta}, \nabla(\varphi(\boldsymbol{u} - \widetilde{\boldsymbol{u}}^*_h)))_{\mathcal{T}_h} + (p - p_h, \nabla\cdot(\varphi(\boldsymbol{u} - \widetilde{\boldsymbol{u}}^*_h)))_{\mathcal{T}_h}.
\end{aligned}$$

Then, from Lemma 3.2.5 and (3.10), we obtain that

$$\left(\chi\nu - \frac{\nu^2\mathsf{diam}(\Omega)\|\nabla\psi\|^2_{\infty,\Omega}\|e^{-\psi}\|^2_{\infty,\Omega}}{\|\boldsymbol{\beta}\|_{\infty,\Omega}\min_{\boldsymbol{x}\in\Omega} e^{-\psi(\boldsymbol{x})}}\right)\|e_{\mathrm{L}}\|^2_{0,\mathcal{T}_h} + \frac{1}{2}\min_{\boldsymbol{x}\in\Omega} e^{-\psi(\boldsymbol{x})}\frac{\|\boldsymbol{\beta}\|_{\infty,\Omega}}{\mathsf{diam}(\Omega)}\|e_{\boldsymbol{u}}\|^2_{0,\mathcal{T}_h} \leq T_1 + T_2 + T_3, \tag{3.13}$$

where

$$\begin{aligned}
T_1 := &-\nu((\mathrm{L} - \mathrm{L}_h)(\nabla\varphi), \boldsymbol{u}^*_h - \widetilde{\boldsymbol{u}}^*_h)_{\mathcal{T}_h} + \nu(\mathrm{L} - \mathrm{L}_h, \varphi(\nabla\widetilde{\boldsymbol{u}}^*_h - \mathrm{L}_h))_{\mathcal{T}_h}\\
&+ (\boldsymbol{f} + \nabla\cdot(\nu\mathrm{L}_h) - \nabla\cdot(\boldsymbol{u}^*_h\otimes\boldsymbol{\beta}) - \nabla p_h, (\mathcal{I} - \mathcal{C}_h)(\varphi(\boldsymbol{u} - \widetilde{\boldsymbol{u}}^*_h)))_{\mathcal{T}_h}\\
&- \langle(\nu\mathrm{L}_h - (\boldsymbol{u}^*_h\otimes\boldsymbol{\beta}) - p_h\mathrm{I})\boldsymbol{n}, (\mathcal{I} - \mathcal{C}_h)(\varphi(\boldsymbol{u} - \widetilde{\boldsymbol{u}}^*_h))\rangle_{\partial\mathcal{T}_h\setminus\Gamma}\\
&- ((\boldsymbol{u}_h - \boldsymbol{u}^*_h)\otimes(\mathsf{I} - \mathsf{P}_0)\boldsymbol{\beta}, \nabla\mathcal{C}_h(\varphi(\boldsymbol{u} - \widetilde{\boldsymbol{u}}^*_h)))_{\mathcal{T}_h}\\
T_2 := &((\boldsymbol{u} - \boldsymbol{u}^*_h)\otimes\boldsymbol{\beta}, \nabla(\varphi(\boldsymbol{u} - \widetilde{\boldsymbol{u}}^*_h)))_{\mathcal{T}_h} - \frac{1}{2}((\boldsymbol{\beta}\cdot\nabla\varphi)e_{\boldsymbol{u}}, e_{\boldsymbol{u}})_{\mathcal{T}_h}\\
T_3 := &((p - p_h)\mathrm{I}, \nabla(\varphi(\boldsymbol{u} - \widetilde{\boldsymbol{u}}^*_h)))_{\mathcal{T}_h}.
\end{aligned}$$

First, we set $\mu = (1/32)\min_{\boldsymbol{x}\in\Omega} e^{-\psi(\boldsymbol{x})}$. Thanks to Cauchy-Schwarz and Young's inequalities, the stability and approximation properties of the Clément interpolant, the approximation property of P_0 and the regularity of the family of meshes, we get that

$$
\begin{aligned}
T_1 \leq\ & \frac{1}{4}\nu\|e_{\mathrm{L}}\|^2_{0,\mathcal{T}_h} + \|\nabla\varphi\|^2_{\infty,\Omega}\nu\|\boldsymbol{u}_h^* - \widetilde{\boldsymbol{u}}_h^*\|^2_{0,\mathcal{T}_h} + \frac{1}{4}\nu\|e_{\mathrm{L}}\|^2_{0,\mathcal{T}_h} + 2\|\varphi\|^2_{\infty,\Omega}\nu\|\mathrm{L}_h - \nabla\boldsymbol{u}_h^*\|^2_{0,\mathcal{T}_h} \\
& + 2\|\varphi\|^2_{\infty,\Omega}\nu\|\nabla(\boldsymbol{u}_h^* - \widetilde{\boldsymbol{u}}_h^*)\|^2_{0,\mathcal{T}_h} + 6\mu|\!|\!| e_{\boldsymbol{u}} |\!|\!|^2_{1,\mathcal{T}_h} + 6\mu|\!|\!| \boldsymbol{u}_h^* - \widetilde{\boldsymbol{u}}_h^* |\!|\!|^2_{1,\mathcal{T}_h} \\
& + \frac{1}{4\mu}\|\varphi\|^2_{\infty,\Omega}\sum_{K\in\mathcal{T}_h}\theta_K^2\|\boldsymbol{f} + \nabla\cdot(\nu\mathrm{L}_h) - \nabla\cdot(\boldsymbol{u}_h^*\otimes\boldsymbol{\beta}) - \nabla p_h\|^2_{0,K} \\
& + \frac{1}{4\mu}\|\varphi\|^2_{\infty,\Omega}\sum_{K\in\mathcal{T}_h}\frac{1}{2}\sum_{e\in\mathcal{E}_h^i\cap\partial K}\nu^{-1/2}\theta_e\|\,[\![\nu\mathrm{L}_h - (\boldsymbol{u}_h^*\otimes\boldsymbol{\beta}) - p_h\mathrm{I}]\!]\|^2_{0,e} \\
& + \frac{1}{4\mu}C_0\frac{\|\boldsymbol{\beta}\|^2_{\boldsymbol{W}^{1,\infty}(\Omega)}}{\nu}\sum_{K\in\mathcal{T}_h}h_K^2\|\boldsymbol{u}_h - \boldsymbol{u}_h^*\|^2_{0,K}.
\end{aligned}
\tag{3.14}
$$

On the other hand, for $\boldsymbol{w}\in H^1_0(\Omega)^d$, we have

$$
\begin{aligned}
\frac{1}{2}(\nabla\cdot\boldsymbol{\beta},\varphi|\boldsymbol{w}|^2)_{\mathcal{T}_h} &= -\frac{1}{2}(\boldsymbol{\beta},\nabla(\varphi|\boldsymbol{w}|^2))_{\mathcal{T}_h} = -\frac{1}{2}(\boldsymbol{\beta},\varphi\nabla|\boldsymbol{w}|^2)_{\mathcal{T}_h} - \frac{1}{2}(\boldsymbol{\beta},|\boldsymbol{w}|^2\nabla\varphi)_{\mathcal{T}_h} \\
&= -(\boldsymbol{\beta},\varphi(\nabla\boldsymbol{w})^t\boldsymbol{w})_{\mathcal{T}_h} - \frac{1}{2}(\boldsymbol{\beta}\cdot\nabla\varphi,|\boldsymbol{w}|^2)_{\mathcal{T}_h} = -((\boldsymbol{\beta}\cdot\nabla)\boldsymbol{w},\varphi\boldsymbol{w})_{\mathcal{T}_h} - \frac{1}{2}((\boldsymbol{\beta}\cdot\nabla\varphi)\boldsymbol{w},\boldsymbol{w})_{\mathcal{T}_h}
\end{aligned}
$$

and since $\nabla\cdot\boldsymbol{\beta} = 0$, we obtain that $((\boldsymbol{\beta}\cdot\nabla)\boldsymbol{w},\varphi\boldsymbol{w})_{\mathcal{T}_h} = -\frac{1}{2}((\boldsymbol{\beta}\cdot\nabla\varphi)\boldsymbol{w},\boldsymbol{w})_{\mathcal{T}_h}$.

Then, using again the fact that $\boldsymbol{u} - \widetilde{\boldsymbol{u}}_h \in H^1_0(\Omega)^d$, we can write

$$
\begin{aligned}
((\boldsymbol{u} - \boldsymbol{u}_h^*)\otimes\boldsymbol{\beta},\nabla(\varphi(\boldsymbol{u} - \widetilde{\boldsymbol{u}}_h^*)))_{\mathcal{T}_h} &= -(\nabla\cdot((\boldsymbol{u} - \widetilde{\boldsymbol{u}}_h^*)\otimes\boldsymbol{\beta}),\varphi(\boldsymbol{u} - \widetilde{\boldsymbol{u}}_h^*))_{\mathcal{T}_h} + ((\widetilde{\boldsymbol{u}}_h^* - \boldsymbol{u}_h^*)\otimes\boldsymbol{\beta},\nabla(\varphi(\boldsymbol{u} - \widetilde{\boldsymbol{u}}_h^*)))_{\mathcal{T}_h} \\
&= -((\boldsymbol{\beta}\cdot\nabla)(\boldsymbol{u} - \widetilde{\boldsymbol{u}}_h^*),\varphi(\boldsymbol{u} - \widetilde{\boldsymbol{u}}_h^*))_{\mathcal{T}_h} + ((\widetilde{\boldsymbol{u}}_h^* - \boldsymbol{u}_h^*)\otimes\boldsymbol{\beta},\nabla(\varphi(\boldsymbol{u} - \widetilde{\boldsymbol{u}}_h^*)))_{\mathcal{T}_h} \\
&= \frac{1}{2}((\boldsymbol{\beta}\cdot\nabla\varphi)(\boldsymbol{u} - \widetilde{\boldsymbol{u}}_h^*),\boldsymbol{u} - \widetilde{\boldsymbol{u}}_h^*)_{\mathcal{T}_h} + ((\widetilde{\boldsymbol{u}}_h^* - \boldsymbol{u}_h^*)\otimes\boldsymbol{\beta},(\boldsymbol{u} - \widetilde{\boldsymbol{u}}_h^*)\otimes\nabla\varphi)_{\mathcal{T}_h} \\
&\quad + ((\widetilde{\boldsymbol{u}}_h^* - \boldsymbol{u}_h^*)\otimes\boldsymbol{\beta},\varphi\nabla(\boldsymbol{u} - \widetilde{\boldsymbol{u}}_h^*))_{\mathcal{T}_h},
\end{aligned}
$$

and then

$$
\begin{aligned}
T_2 &= -(\nabla e_{\boldsymbol{u}},\varphi(\boldsymbol{u}_h^* - \widetilde{\boldsymbol{u}}_h^*)\otimes\boldsymbol{\beta})_{\mathcal{T}_h} - (\nabla(\boldsymbol{u}_h^* - \widetilde{\boldsymbol{u}}_h^*),\varphi(\boldsymbol{u}_h^* - \widetilde{\boldsymbol{u}}_h^*)\otimes\boldsymbol{\beta})_{\mathcal{T}_h} - \frac{1}{2}((\boldsymbol{\beta}\cdot\nabla\varphi)(\boldsymbol{u}_h^* - \widetilde{\boldsymbol{u}}_h^*),\boldsymbol{u}_h^* - \widetilde{\boldsymbol{u}}_h^*)_{\mathcal{T}_h} \\
&\leq \frac{1}{8}\nu\|\nabla e_{\boldsymbol{u}}\|^2_{0,\mathcal{T}_h} + 2\frac{\|\boldsymbol{\beta}\|^2_{\infty,\Omega}}{\nu}\|\varphi\|^2_{\infty,\Omega}\|\boldsymbol{u}_h^* - \widetilde{\boldsymbol{u}}_h^*\|^2_{0,\mathcal{T}_h} + \frac{1}{2}\nu\|\nabla(\boldsymbol{u}_h^* - \widetilde{\boldsymbol{u}}_h^*)\|^2_{0,\mathcal{T}_h} + \frac{1}{2}\frac{\|\boldsymbol{\beta}\|^2_{\infty,\Omega}}{\nu}\|\boldsymbol{u}_h^* - \widetilde{\boldsymbol{u}}_h^*\|^2_{0,\mathcal{T}_h} \\
&\quad + \|\boldsymbol{\beta}\|_{\infty,\Omega}\|\nabla\varphi\|_{\infty,\Omega}\|\boldsymbol{u}_h^* - \widetilde{\boldsymbol{u}}_h^*\|^2_{0,\mathcal{T}_h},
\end{aligned}
\tag{3.15}
$$

by using Cauchy-Schwarz and Young's inequalities.

Then, after integrating by part, we write

$$
\begin{aligned}
T_3 &= ((p - p_h)\nabla\varphi,\boldsymbol{u} - \widetilde{\boldsymbol{u}}_h^*)_{\mathcal{T}_h} + (p - p_h,\varphi\,\nabla\cdot(\boldsymbol{u} - \widetilde{\boldsymbol{u}}_h^*))_{\mathcal{T}_h} \\
&= ((p - p_h)\nabla\varphi,e_{\boldsymbol{u}})_{\mathcal{T}_h} + ((p - p_h)\nabla\varphi,\boldsymbol{u}_h^* - \widetilde{\boldsymbol{u}}_h^*)_{\mathcal{T}_h} - (p - p_h,\varphi\,\nabla\cdot\boldsymbol{u}_h^*)_{\mathcal{T}_h} + (p - p_h,\varphi\,\nabla\cdot(\boldsymbol{u}_h^* - \widetilde{\boldsymbol{u}}_h^*))_{\mathcal{T}_h} \\
&\leq 2\mu\left(\max\{1,C_{\nu,\boldsymbol{\beta}}\}\right)^{-2}\nu^{-1}\|p - p_h\|^2_{0,\mathcal{T}_h} \\
&\quad + \frac{1}{2\mu}\|\nabla\varphi\|^2_{\infty,\Omega}C_P^2\left(\max\{1,C_{\nu,\boldsymbol{\beta}}\}\right)^2\nu\|\nabla e_{\boldsymbol{u}}\|^2_{0,\mathcal{T}_h} + \frac{1}{2\mu}\|\nabla\varphi\|^2_{\infty,\Omega}\left(\max\{1,C_{\nu,\boldsymbol{\beta}}\}\right)^2\nu\|\boldsymbol{u}_h^* - \widetilde{\boldsymbol{u}}_h^*\|^2_{0,\mathcal{T}_h} \\
&\quad + \frac{1}{2\mu}\|\varphi\|^2_{\infty,\Omega}\left(\max\{1,C_{\nu,\boldsymbol{\beta}}\}\right)^2\nu\|\nabla\cdot\boldsymbol{u}_h^*\|^2_{0,\mathcal{T}_h} + \frac{1}{2\mu}d\|\varphi\|^2_{\infty,\Omega}\left(\max\{1,C_{\nu,\boldsymbol{\beta}}\}\right)^2\nu\|\nabla(\boldsymbol{u}_h^* - \widetilde{\boldsymbol{u}}_h^*)\|^2_{0,\mathcal{T}_h}.
\end{aligned}
\tag{3.16}
$$

Finally, after inserting (3.14), (3.15) and (3.16) in (3.13), Lemma 3.2.3, the definition of $\|\!|\cdot|\!\|_{\mathcal{T}_h}$, the facts that $\|\nabla e_{\boldsymbol{u}}\|_{0,\mathcal{T}_h} \preceq \|e_{\mathrm{L}}\|_{0,\mathcal{T}_h} + \|\mathrm{L}_h - \nabla \boldsymbol{u}_h^*\|_{0,\mathcal{T}_h}$ and $\nabla\varphi = -\nabla\psi e^{-\psi}$, we obtain

$$\begin{aligned}
&\left(\chi\nu - \frac{\nu^2 \mathsf{diam}(\Omega)\|\nabla\psi\|^2_{\infty,\Omega}\|e^{-\psi}\|^2_{\infty,\Omega}}{\|\boldsymbol{\beta}\|_{\infty,\Omega}\min_{\boldsymbol{x}\in\Omega} e^{-\psi(\boldsymbol{x})}} - \frac{32}{\min_{\boldsymbol{x}\in\Omega} e^{-\psi(\boldsymbol{x})}}\|\nabla\psi\|^2_{\infty,\Omega}C_P^2\left(\max\{1, C_{\nu,\boldsymbol{\beta}}\}\right)^2\nu\right.\\
&\quad\left. - \frac{3}{8}\nu\min_{\boldsymbol{x}\in\Omega} e^{-\psi(\boldsymbol{x})} - \frac{1}{2}\nu\right)\|e_{\mathrm{L}}\|^2_{0,\mathcal{T}_h} + \frac{1}{4}\min_{\boldsymbol{x}\in\Omega} e^{-\psi(\boldsymbol{x})}\frac{\|\boldsymbol{\beta}\|_{\infty,\Omega}}{\mathsf{diam}(\Omega)}\|e_{\boldsymbol{u}}\|^2_{0,\mathcal{T}_h}\\
&\leq C_{\psi,\Omega}\max\{1, \|\varphi\|^2_{\infty,\Omega}\}\left(\max\{1, C_{\nu,\boldsymbol{\beta}}\}\right)^2\left(\eta_h^2 + C_0\frac{\|\boldsymbol{\beta}\|^2_{\boldsymbol{W}^{1,\infty}(\Omega)}}{\nu}\sum_{K\in\mathcal{T}_h} h_K^2\|\boldsymbol{u}_h - \boldsymbol{u}_h^*\|^2_{0,K}\right.\\
&\qquad\left. + \max\left\{\frac{\nu}{\mathsf{diam}(\Omega)^2}, \frac{\|\boldsymbol{\beta}\|_{\infty,\Omega}}{\mathsf{diam}(\Omega)}, \frac{\|\boldsymbol{\beta}\|^2_{\infty,\Omega}}{\nu}\right\}\|\boldsymbol{u}_h^* - \widetilde{\boldsymbol{u}}_h^*\|^2_{0,\mathcal{T}_h}\right),
\end{aligned}$$

where $C_{\psi,\Omega} > 0$ is a constant depending only on ψ and Ω.

Thus, by the choice of χ in (3.12), last expression becomes

$$\begin{aligned}
&\frac{\chi\nu}{2}\|e_{\mathrm{L}}\|^2_{0,\mathcal{T}_h} + \frac{1}{4}\min_{\boldsymbol{x}\in\Omega} e^{-\psi(\boldsymbol{x})}\frac{\|\boldsymbol{\beta}\|_{\infty,\Omega}}{\mathsf{diam}(\Omega)}\|e_{\boldsymbol{u}}\|^2_{0,\mathcal{T}_h}\\
&\quad\leq C_{\psi,\Omega}\max\{1, \|\varphi\|^2_{\infty,\Omega}\}\left(\max\{1, C_{\nu,\boldsymbol{\beta}}\}\right)^2\left(\eta_h^2 + C_0\frac{\|\boldsymbol{\beta}\|_{\boldsymbol{W}^{1,\infty}(\Omega)}}{\nu^{1/2}}\sum_{K\in\mathcal{T}_h} h_K\|\boldsymbol{u}_h - \boldsymbol{u}_h^*\|_{0,K}\right.\\
&\qquad\left. + \max\left\{\nu, \frac{\|\boldsymbol{\beta}\|_{\infty,\Omega}}{\mathsf{diam}(\Omega)}, \frac{\|\boldsymbol{\beta}\|^2_{\infty,\Omega}}{\nu}\right\}\|\boldsymbol{u}_h^* - \widetilde{\boldsymbol{u}}_h^*\|^2_{0,\mathcal{T}_h}\right).
\end{aligned}$$

Thus, the result follows noticing that $\chi > 1$. □

The next lemmas provide us tools to prove local efficiency of the error estimator.

Lemma 3.2.6. *Let $e \in \mathcal{E}_h^i$. We have the following estimate*

$$\begin{aligned}
\nu^{-1/2}\theta_e\|\,[\![\nu\mathrm{L}_h - (\boldsymbol{u}_h^*\otimes\boldsymbol{\beta}) - p_h\mathrm{I}]\!]\|^2_{0,e} \preceq \left(\max\{1, C_{\nu,\boldsymbol{\beta}}\}\right)^2\left(\nu\|\mathrm{L} - \mathrm{L}_h\|^2_{0,\omega_e} + \frac{\|\boldsymbol{\beta}\|_{\infty,\Omega}}{\mathsf{diam}(\Omega)}\|\boldsymbol{u} - \boldsymbol{u}_h^*\|^2_{0,\omega_e}\right.\\
\left. + \nu^{-1}\|p - p_h\|^2_{0,\omega_e}\right) + \sum_{K\in\omega_e}\theta_K^2\|\boldsymbol{f} + \nabla\cdot(\nu\mathrm{L}_h) - \nabla\cdot(\boldsymbol{u}_h^*\otimes\boldsymbol{\beta}) - \nabla p_h\|^2_{0,K}.
\end{aligned}$$

Proof. For any $\boldsymbol{v} \in H_0^1(\omega_e)^d$ we have

$$\begin{aligned}
\langle\,[\![\nu\mathrm{L}_h - (\boldsymbol{u}_h^*\otimes\boldsymbol{\beta}) - p_h\mathrm{I}]\!], \boldsymbol{v}\rangle_e &= \sum_{K\in\omega_e}\left(\langle\nu(\mathrm{L}_h - \mathrm{L})\boldsymbol{n}, \boldsymbol{v}\rangle_{\partial K} + \langle((\boldsymbol{u} - \boldsymbol{u}_h^*)\otimes\boldsymbol{\beta})\boldsymbol{n}, \boldsymbol{v}\rangle_{\partial K} + \langle(p - p_h)\boldsymbol{n}, \boldsymbol{v}\rangle_{\partial K}\right)\\
&= \sum_{K\in\omega_e}\left((\nu(\mathrm{L}_h - \mathrm{L}), \nabla\boldsymbol{v})_K + (\nu\nabla\cdot(\mathrm{L}_h - \mathrm{L}), \boldsymbol{v})_K + (((\boldsymbol{u} - \boldsymbol{u}_h^*)\otimes\boldsymbol{\beta}), \nabla\boldsymbol{v}\rangle_{\partial K} + (\nabla\cdot((\boldsymbol{u} - \boldsymbol{u}_h^*)\otimes\boldsymbol{\beta}), \boldsymbol{v}\rangle_{\partial K}\right.\\
&\qquad\left. + (\nabla(p - p_h), \boldsymbol{v})_K + (p - p_h, \nabla\cdot\boldsymbol{v})_K\right)\\
&= \sum_{K\in\omega_e}\left((\nu(\mathrm{L}_h - \mathrm{L}), \nabla\boldsymbol{v})_K + ((\boldsymbol{u} - \boldsymbol{u}_h^*)\otimes\boldsymbol{\beta}, \nabla\boldsymbol{v})_K + (p - p_h, \nabla\cdot\boldsymbol{v})_K\right.\\
&\qquad\left. + (\boldsymbol{f} + \nabla\cdot(\nu\mathrm{L}_h) - \nabla\cdot(\boldsymbol{u}_h^*\otimes\boldsymbol{\beta}) - \nabla p_h, \boldsymbol{v})_K\right)
\end{aligned}$$

$$\leq \sum_{K\in\omega_e}\Big(\nu^{1/2}\|\mathrm{L}-\mathrm{L}_h\|_{0,K}+\mathsf{diam}(\Omega)\frac{\|\boldsymbol{\beta}\|^{1/2}_{\infty,\Omega}}{\nu^{1/2}\mathsf{diam}(\Omega)^{1/2}}\frac{\|\boldsymbol{\beta}\|^{1/2}_{\infty,\Omega}}{\mathsf{diam}(\Omega)^{1/2}}\|\boldsymbol{u}-\boldsymbol{u}_h^*\|_{0,K}+\nu^{-1/2}\|p-p_h\|_{0,K}$$
$$+\theta_K\|\boldsymbol{f}+\nabla\cdot(\nu\mathrm{L}_h)-\nabla\cdot(\boldsymbol{u}_h^*\otimes\boldsymbol{\beta})-\nabla p_h\|_{0,K}\Big)T_{\boldsymbol{v}},$$

where $T_{\boldsymbol{v}}:=2\nu^{1/2}\|\nabla\boldsymbol{v}\|_{0,K}+\nu^{1/2}\|\nabla\cdot\boldsymbol{v}\|_{0,K}+\theta_K^{-1}\|\boldsymbol{v}\|_{0,K}$.

Then, taking $\boldsymbol{v}:=B_e\,[\![\nu\mathrm{L}_h-(\boldsymbol{u}_h^*\otimes\boldsymbol{\beta})-p_h\mathrm{I}]\!]$ and applying Lemma 3.2.2, we get

$$T_{\boldsymbol{v}}\preceq|\!|\!|\,\boldsymbol{v}\,|\!|\!|_{1,K}+\theta_e^{-1}\|\boldsymbol{v}\|_{0,K}\preceq\nu^{1/4}\theta_e^{-1/2}\|\,[\![\nu\mathrm{L}_h-(\boldsymbol{u}_h^*\otimes\boldsymbol{\beta})-p_h\mathrm{I}]\!]\|_{0,e}.$$

The result follows from Lemma 3.2.2 and the shape-regularity assumption. □

Lemma 3.2.7. *For any element $K\in\mathcal{T}_h$ we have*

$$\theta_K\|\boldsymbol{f}+\nabla\cdot(\nu\mathrm{L}_h)-(\boldsymbol{u}_h^*\otimes\boldsymbol{\beta})-\nabla p_h\|_{0,K}$$
$$\preceq\max\{1,C_{\nu,\boldsymbol{\beta}}\}\left(\nu^{1/2}\|\mathrm{L}-\mathrm{L}_h\|_{0,K}+\frac{\|\boldsymbol{\beta}\|^{1/2}_{\infty,\Omega}}{\mathsf{diam}(\Omega)^{1/2}}\|\boldsymbol{u}-\boldsymbol{u}_h^*\|_{0,K}+\nu^{-1/2}\|p-p_h\|_{0,K}\right).$$

Proof. Let $\boldsymbol{v}=\boldsymbol{f}+\nabla\cdot(\nu\mathrm{L}_h)-(\boldsymbol{u}_h^*\otimes\boldsymbol{\beta})-\nabla p_h$ then

$$(\boldsymbol{v},B_K\boldsymbol{v})_K=-\nu(\nabla\cdot(\mathrm{L}-\mathrm{L}_h),B_K\boldsymbol{v})_K+(\nabla\cdot((\boldsymbol{u}-\boldsymbol{u}_h^*)\otimes\boldsymbol{\beta}),B_K\boldsymbol{v})_K+(\nabla(p-p_h),B_K\boldsymbol{v})_K$$
$$=\nu(\mathrm{L}-\mathrm{L}_h,\nabla B_K\boldsymbol{v})_K-((\boldsymbol{u}-\boldsymbol{u}_h^*)\otimes\boldsymbol{\beta},\nabla B_K\boldsymbol{v})_K-(p-p_h,\nabla\cdot B_K\boldsymbol{v})_K$$
$$\preceq(\nu^{1/2}\|\mathrm{L}-\mathrm{L}_h\|_{0,K}+\mathsf{diam}(\Omega)C_{\nu,\boldsymbol{\beta}}\frac{\|\boldsymbol{\beta}\|^{1/2}_{\infty,\Omega}}{\mathsf{diam}(\Omega)^{1/2}}\|\boldsymbol{u}-\boldsymbol{u}_h^*\|_{0,K}+\nu^{-1/2}\|p-p_h\|_{0,K})|\!|\!|\,B_K\boldsymbol{v}\,|\!|\!|_{1,K}.$$

The result follows from Lemma 3.2.2. □

Now, to derive upper bounds for the jump of the velocity we will decompose $\nu h_e^{-1}\|\,[\![\boldsymbol{u}_h^*]\!]\|^2_{0,e}$ into $\nu h_e^{-1}\|\mathsf{P}_{\mathsf{M}_0}\,[\![\boldsymbol{u}_h^*]\!]\|^2_{0,e}$ and $\nu h_e^{-1}\|(\mathsf{Id}-\mathsf{P}_{\mathsf{M}_0})\,[\![\boldsymbol{u}_h^*]\!]\|^2_{0,e}$, where, $\mathsf{P}_{\mathsf{M}_0}$ is the L^2-orthogonal projection into

$$\mathsf{M}_{0,h}:=\{\boldsymbol{\mu}\in[L^2(\mathcal{E}_h)]^d:\boldsymbol{\mu}|_e\in[\mathbb{P}_0(e)]^d\quad\forall e\in\mathcal{E}_h\}.$$

Then, Lemmas 3.4 and 3.5 in [45], adapted to vector-valued functions and considering the approximate velocity instead of its postprocessing, imply

$$h_e^{-1}\|\mathsf{P}_{\mathsf{M}_0}\,[\![\boldsymbol{u}_h^*]\!]\|^2_{0,e}\preceq\|\mathrm{L}_h-\nabla\boldsymbol{u}_h^*\|^2_{0,\omega_e}\quad\text{for } k\geq1,\tag{3.17}$$

and

$$h_e^{-1}\|(\mathsf{Id}-\mathsf{P}_{\mathsf{M}_0})\,[\![\boldsymbol{u}_h^*]\!]\|^2_{0,e}\preceq\|\nabla(\boldsymbol{u}-\boldsymbol{u}_h^*)\|^2_{0,\omega_e},\tag{3.18}$$

for each face $e\in\mathcal{E}_h$.

3.2.2 The main results

We define, on each $K \in \mathcal{T}_h$, the local error

$$\mathsf{e}_K^2 := \nu\|\mathrm{L} - \mathrm{L}_h\|_{0,K}^2 + \frac{\|\boldsymbol{\beta}\|_{\infty,\Omega}}{\mathsf{diam}(\Omega)}\|\boldsymbol{u} - \boldsymbol{u}_h^*\|_{0,K}^2 + \nu\|\nabla(\boldsymbol{u} - \boldsymbol{u}_h^*)\|_{0,K}^2 + \nu^{-1}\|p - p_h\|_{0,K}^2, \tag{3.19}$$

and its global version given by $\mathsf{e}_h := \left(\sum_{K\in\mathcal{T}_h} \mathsf{e}_K^2\right)^{1/2}$.

Now, we state and prove reliability and local efficiency results of our *a posteriori* error estimator (3.7).

Theorem 3.2.1 (Reliability)**.** *Let φ as in (3.11). The following estimate holds*

$$\mathsf{e}_h \preceq \max\{1, \|\varphi\|_{\infty,\Omega}\} \max\{1, C_{\nu,\boldsymbol{\beta}}\}\Bigg(\eta_h + \frac{\|\boldsymbol{\beta}\|_{\boldsymbol{W}^{1,\infty}(\Omega)}}{\nu^{1/2}} \sum_{K\in\mathcal{T}_h} h_K\|\boldsymbol{u}_h - \boldsymbol{u}_h^*\|_{0,K} + \max\left\{\frac{\nu}{\mathsf{diam}(\Omega)^2}, \frac{\|\boldsymbol{\beta}\|_{\infty,\Omega}}{\mathsf{diam}(\Omega)}, \frac{\|\boldsymbol{\beta}\|_{\infty,\Omega}^2}{\nu}\right\}^{1/2} \sum_{e\in\mathcal{E}_h} h_e^{1/2}\|[\![\boldsymbol{u}_h^*]\!]\|_{0,e}\Bigg).$$

Proof. Thanks to Lemmas 3.2.3, 3.2.4, the definition of $C_{\nu,\boldsymbol{\beta}}$ and the fact that, for each $K \in \mathcal{T}_h$, $\nu^{1/2}\|\nabla(\boldsymbol{u} - \boldsymbol{u}_h^*)\|_{0,K} \preceq \nu^{1/2}\|\mathrm{L} - \mathrm{L}_h\|_{0,K} + \eta_K$, we get

$$\begin{aligned}\nu\|\mathrm{L} - \mathrm{L}_h\|_{0,\mathcal{T}_h}^2 + |\!|\!|\, \boldsymbol{u} - \boldsymbol{u}_h \,|\!|\!|_{1,\mathcal{T}_h}^2 + \nu^{-1}\|p - p_h\|_{0,\mathcal{T}_h}^2 \\ \preceq \max\{1, \|\varphi\|_{\infty,\Omega}^2\} \left(\max\{1, C_{\nu,\boldsymbol{\beta}}\}\right)^2 \Bigg(\eta_h^2 + \frac{\|\boldsymbol{\beta}\|_{\boldsymbol{W}^{1,\infty}(\Omega)}^2}{\nu} \sum_{K\in\mathcal{T}_h} h_K^2\|\boldsymbol{u}_h - \boldsymbol{u}_h^*\|_{0,K}^2 \\ + \max\left\{\frac{\nu}{\mathsf{diam}(\Omega)^2}, \frac{\|\boldsymbol{\beta}\|_{\infty,\Omega}}{\mathsf{diam}(\Omega)}, \frac{\|\boldsymbol{\beta}\|_{\infty,\Omega}^2}{\nu}\right\} |\!|\!|\, \boldsymbol{u}_h^* - \widetilde{\boldsymbol{u}}_h^* \,|\!|\!|_{0,\mathcal{T}_h}^2\Bigg).\end{aligned}$$

The result follows from taking $\boldsymbol{w}_h = \boldsymbol{u}_h^*$ in Lemma 0.4 to bound the last term on the right-hand side. ∎

Remark 3.2.1. *In Theorem 3.2.1 we have tracked the dependence on φ, because depends on χ, on ν and $\boldsymbol{\beta}$. In fact, recalling (3.11), we get that*

$$\|\varphi\|_{\infty,\Omega} \leq C_{\psi,\Omega} \max\left\{1, \|\chi\|_{\infty,\Omega}\right\} \leq C_{\psi,\Omega}\left(\max\{1, C_{\nu,\boldsymbol{\beta}}^{-1}, C_{\nu,\boldsymbol{\beta}}\}\right)^2.$$

Theorem 3.2.2 (Efficiency)**.** *Let $K \in \mathcal{T}_h$, $\mathsf{e}_{\omega_K} := \left(\sum_{K'\in\omega_K} \mathsf{e}_{\omega_K}^2\right)^{1/2}$ and $\omega_K := \{K' \in \mathcal{T}_h : K' \in \omega_e$ and $e \in \mathcal{E}_h \cap \partial K\}$. For $k \geq 1$ We have the following estimate*

$$\eta_K \preceq \max\{1, C_{\nu,\boldsymbol{\beta}}\}\, \mathsf{e}_{\omega_K}.$$

Proof. By definition of η_K, lemmas 3.2.6–3.2.7, equations (3.17)-(3.18) and inequalities $\|\mathrm{L}_h - \nabla \boldsymbol{u}_h^*\|_{0,K} \leq \|\mathrm{L} - \mathrm{L}_h\|_{0,K} + \|\nabla(\boldsymbol{u} - \boldsymbol{u}_h^*)\|_{0,K}$ and $\|\nabla \cdot \boldsymbol{u}_h^*\|_{0,K} = \|\nabla \cdot (\boldsymbol{u} - \boldsymbol{u}_h^*)\|_{0,K} \preceq \|\nabla(\boldsymbol{u} - \boldsymbol{u}_h^*)\|_{0,K}$, we have that

$$\begin{aligned}
\eta_K^2 &\preceq (\max\{1, C_{\nu,\boldsymbol{\beta}}\})^2 \left(\nu \|\mathrm{L} - \mathrm{L}_h\|_{0,K}^2 + \frac{\|\boldsymbol{\beta}\|_{\infty,\Omega}}{\mathsf{diam}(\Omega)} \|\boldsymbol{u} - \boldsymbol{u}_h^*\|_{0,K}^2 + \nu^{-1} \|p - p_h\|_{0,K}^2 \right) + \nu \|\mathrm{L}_h - \nabla \boldsymbol{u}_h^*\|_{0,K}^2 \\
&\quad + \nu \|\nabla \cdot \boldsymbol{u}_h^*\|_{0,K}^2 + (\max\{1, C_{\nu,\boldsymbol{\beta}}\})^2 \left(\nu \|\mathrm{L} - \mathrm{L}_h\|_{0,\omega_K}^2 + \frac{\|\boldsymbol{\beta}\|_{\infty,\Omega}}{\mathsf{diam}(\Omega)} \|\boldsymbol{u} - \boldsymbol{u}_h^*\|_{0,\omega_K}^2 + \nu^{-1} \|p - p_h\|_{0,\omega_K}^2 \right) \\
&\quad + \sum_{K' \in \omega_K} \theta_{K'}^2 \|\boldsymbol{f} + \nabla \cdot (\nu \mathrm{L}_h) - (\boldsymbol{u}_h^* \otimes \boldsymbol{\beta}) - \nabla p_h\|_{0,K'}^2 + \nu \|\mathrm{L}_h - \nabla \boldsymbol{u}_h^*\|_{0,\omega_K}^2 + \nu \|\nabla(\boldsymbol{u} - \boldsymbol{u}_h^*)\|_{0,\omega_K}^2 \\
&\preceq (\max\{1, C_{\nu,\boldsymbol{\beta}}\})^2 \left(\nu \|\mathrm{L} - \mathrm{L}_h\|_{0,\omega_K}^2 + |\!|\!| \boldsymbol{u} - \boldsymbol{u}_h^* |\!|\!|_{1,\omega_K}^2 + \nu^{-1} \|p - p_h\|_{0,\omega_K}^2 \right),
\end{aligned}$$

and the result follows. □

3.3 Numerical experiments

In this section, we carry out numerical simulations, for $d = 3$, to verify our main results in Theorems 3.2.1 and 3.2.2. To satisfy condition we consider,as in [21], the stabilization parameter τ given by

$$\tau = \frac{1}{2\nu} \max_{\boldsymbol{x} \in \mathcal{T}_h} \boldsymbol{\beta}(\boldsymbol{x}) \cdot \boldsymbol{n} + 1.$$

The values of the polynomial degree and physical parameters $\boldsymbol{\beta}$ and ν will be specified on each example.

Let us define the errors $\mathsf{e}_{\mathrm{L}} := \nu^{1/2} \|\mathrm{L} - \mathrm{L}_h\|_{0,\mathcal{T}_h}$, $\mathsf{e}_{\boldsymbol{u}} := |\!|\!| \boldsymbol{u} - \boldsymbol{u}_h^* |\!|\!|_{1,\mathcal{T}_h}$, $\mathsf{e}_p := \nu^{-1/2} \|p - p_h\|_{0,\mathcal{T}_h}$, the estimator terms η_i $(i = 1, \ldots, 5)$

$$\eta_1^2 := \sum_{K \in \mathcal{T}_h} \theta_K^2 \|\boldsymbol{f} + \nabla \cdot (\nu \mathrm{L}_h) - \nabla \cdot (\boldsymbol{u}_h^* \otimes \boldsymbol{\beta}) - \nabla p_h\|_{0,K}^2, \quad \eta_2^2 := \nu \|\mathrm{L}_h - \nabla \boldsymbol{u}_h^*\|_{0,\mathcal{T}_h}^2,$$

$$\eta_3^2 := \nu \|\nabla \cdot \boldsymbol{u}_h^*\|_{0,\mathcal{T}_h}^2, \quad \eta_4^2 := \nu^{-1/2} \sum_{e \in \mathcal{E}_h} \theta_e \| [\![\nu \mathrm{L}_h - (\boldsymbol{u}_h^* \otimes \boldsymbol{\beta}) - p_h \mathrm{I}]\!] \|_{0,e}^2 \quad \text{and} \quad \eta_5^2 := \nu \sum_{e \in \mathcal{E}_h} h_e^{-1} \| [\![\boldsymbol{u}_h^*]\!] \|_{0,e}^2,$$

and the effectivity index $\mathsf{eff} := \eta_h / \mathsf{e}_h$. The experimental orders of convergence will be computed in terms of the number of elements N and we will use the fact that $h \simeq N^{-1/3}$. We also include, on each table, a column with the size of the linear system that we solve, N_{sist}, to quantify the computational effort in each case. The implementation of the HDG method was based on [63], an efficient vectorized implementation of the HDG method for linear variable coefficient reaction-diffusion problems in polyhedral domains.

For the tests that include adaptivity, we use the strategy:

(i) Start with a coarse mesh $\mathcal{T}_h$.
(ii) Solve the discrete problem on the current mesh $\mathcal{T}_h$.
(iii) Compute η_K for each $K \in \mathcal{T}_h$.
(iv) Mark each $K' \in \mathcal{T}_h$ such that $\eta_{K'} \geq \theta \max_{K \in \mathcal{T}_h} \eta_K$, with $\theta \in [0, 1]$ and refine it using `Tetgen` (see [101]).
(v) Consider this new mesh as $\mathcal{T}_h$ and, unless a prescribed stopping criteria is satisfied, go to (ii).

3.3.1 A smooth solution

For this test case, we choose $\nu = 1$, $\boldsymbol{\beta} = (x, y, -2z)$ and $\Omega = (0,1)^3$. The source term $\boldsymbol{f}$ and the boundary data $\boldsymbol{u}_D$ are chosen such that the exact solution of the problem is given by $\boldsymbol{u} := (u_1, u_2, u_3)$, where $u_1(x_1, x_2, x_3) := 2x_1^2 x_2 x_3$, $u_2(x_1, x_2, x_3) := -x_1 x_2^2 x_3$, $u_3(x_1, x_2, x_3) := -x_1 x_2 x_3^2$, and $p(x_1, x_2.x_3) := x_1 - 1/2$.

k	N	N_{sist}	e_{L}	order	$\mathsf{e}_{\boldsymbol{u}}$	order	e_p	order
	6	168	5.79e-01	–	2.26e-01	–	1.27e-01	–
	48	1,128	1.71e-01	1.76	6.28e-02	1.84	2.76e-02	2.20
1	384	8,160	4.52e-02	1.92	1.62e-02	1.95	6.24e-03	2.15
	3,072	61,824	1.15e-02	1.97	4.11e-03	1.98	1.45e-03	2.11
	24,576	480,786	2.91e-03	1.99	1.03e-03	1.99	3.42e-04	2.09
	6	330	1.28e-01	–	5.36e-02	–	3.87e-02	–
	48	2,208	1.78e-02	2.85	6.99e-03	2.94	3.69e-03	3.39
2	384	15,936	2.32e-03	2.94	8.91e-04	2.97	3.96e-04	3.22
	3,072	120,576	2.96e-04	2.97	1.12e-04	2.99	4.59e-05	3.11
	24,576	936,960	3.74e-05	2.98	1.41e-05	2.99	5.43e-06	3.08
	6	546	9.77e-03	–	3.20e-03	–	5.94e-03	–
	48	3,648	7.80e-04	3.65	2.47e-04	3.69	2.52e-04	4.56
3	384	26,304	5.35e-05	3.87	1.69e-05	3.87	1.29e-05	4.29
	3,072	198,912	3.49e-06	3.94	1.10e-06	3.94	7.23e-07	4.15
	24,576	1,545,216	2.23e-07	3.97	7.05e-08	3.97	4.27e-08	4.08

Table 3.1: History of convergence of the error terms for the Example 3.3.1 ($\nu = 1$). (Fuente: Elaboración propia)

k	N	η_1	order	η_2	order	η_3	order	η_4	order	η_5	order	eff
	6	3.76e-01	–	1.09e-01	–	3.94e-02	–	7.42e-01	–	1.38e-01	–	1.342
	48	1.09e-01	1.79	3.82e-02	1.52	1.45e-02	1.44	2.39e-01	1.64	4.17e-02	1.72	1.455
1	384	2.84e-02	1.93	1.06e-02	1.85	3.96e-03	1.87	6.66e-02	1.84	1.11e-02	1.90	1.530
	3,072	7.24e-03	1.97	2.75e-03	1.95	1.02e-03	1.97	1.75e-02	1.93	2.86e-03	1.96	1.572
	24,576	1.82e-03	1.99	6.97e-04	1.98	2.60e-04	1.96	4.49e-03	1.97	7.22e-04	1.99	1.591
	6	1.82e-01	–	3.55e-02	–	1.59e-02	–	1.74e-01	–	2.67e-02	–	1.775
	48	2.41e-02	2.91	5.03e-03	2.82	2.26e-03	2.81	2.84e-02	2.61	3.61e-03	2.89	1.948
2	384	3.11e-03	2.96	6.61e-04	2.93	2.95e-04	2.94	3.92e-03	2.86	4.65e-04	2.96	2.019
	3,072	3.94e-04	2.98	8.45e-05	2.97	3.75e-05	2.98	5.12e-04	2.94	5.90e-05	2.98	2.052
	24,576	4.97e-05	2.99	1.07e-05	2.99	4.76e-06	2.98	6.56e-05	2.97	7.42e-06	2.99	2.068
	6	3.56e-02	–	1.39e-03	–	4.60e-04	–	1.56e-02	–	6.32e-04	–	3.273
	48	2.27e-03	3.97	1.09e-04	3.68	3.86e-05	3.58	1.41e-03	3.47	5.40e-05	3.55	3.124
3	384	1.45e-04	3.97	7.35e-06	3.89	2.60e-06	3.89	9.97e-05	3.82	3.68e-06	3.88	3.061
	3,072	9.19e-06	3.98	4.75e-07	3.95	1.67e-07	3.96	6.59e-06	3.92	2.38e-07	3.95	3.034
	24,576	5.79e-07	3.99	3.02e-08	3.98	1.07e-08	3.96	4.23e-07	3.96	1.51e-08	3.98	3.021

Table 3.2: History of convergence of the terms composing the error estimator for the Example 3.3.1 ($\nu = 1$). (Fuente: Elaboración propia)

Table 3.1 shows the history of convergence of the error of each variable when the number of elements

N increases by a factor of 8. We see that all the error terms converge with optimal order of $k+1$, exactly as the error estimates in [21] predicted. In addition, we see in Table 3.2 that each term of the error estimator converge with order $k+1$. Moreover, the effectivity index remains bounded.

We repeat the experiment considering now $\nu = 10^{-1}$ and $\nu = 10^{-2}$. As Tables 3.3–3.6 show, similar conclusions can be drawn regarding the optimal order of convergence of the error and the estimator. The last column of Tables 3.4 and 3.6 displays the effectivity index. It remains bounded for each polynomial degree k.

k	N	N_{dof}	e_{L}	order	$\mathsf{e}_{\boldsymbol{u}}$	order	e_p	order
	6	168	2.12e-01	–	8.99e-02	–	1.13e-01	–
	48	1,128	7.63e-02	1.47	2.86e-02	1.65	2.74e-02	2.05
1	384	8,160	2.24e-02	1.77	7.96e-03	1.84	6.00e-03	2.19
	3,072	61,824	6.07e-03	1.88	2.14e-03	1.89	1.31e-03	2.20
	24,576	480,786	1.59e-03	1.94	5.60e-04	1.93	2.96e-04	2.14
	6	330	6.40e-02	–	2.82e-02	–	4.62e-02	–
	48	2,208	1.09e-02	2.55	4.01e-03	2.82	4.24e-03	3.45
2	384	15,936	1.58e-03	2.79	5.46e-04	2.88	4.40e-04	3.27
	3,072	120,576	2.15e-04	2.88	7.27e-05	2.91	4.98e-05	3.14
	24,576	936,960	2.84e-05	2.92	9.48e-06	2.94	5.85e-06	3.09
	6	546	1.07e-02	–	4.02e-03	–	7.93e-03	–
	48	3,648	8.67e-04	3.63	2.90e-04	3.80	3.16e-04	4.65
3	384	26,304	6.26e-05	3.79	2.01e-05	3.85	1.60e-05	4.30
	3,072	198,912	4.24e-06	3.89	1.35e-06	3.90	9.03e-07	4.15
	24,576	1,545,216	2.70e-07	3.97	8.52e-08	3.98	5.58e-08	4.02

Table 3.3: History of convergence of the error terms for the Example 3.3.1 ($\nu = 10^{-1}$).

k	N	η_1	order	η_2	order	η_3	order	η_4	order	η_5	order	eff
	6	1.06e-02	–	1.09e-01	–	4.27e-02	–	7.47e-02	–	4.26e-02	–	0.569
	48	2.63e-03	2.00	4.22e-02	1.37	1.71e-02	1.32	2.23e-02	1.75	1.44e-02	1.56	0.614
1	384	6.63e-04	1.99	1.19e-02	1.83	4.59e-03	1.89	6.08e-03	1.87	3.91e-03	1.89	0.600
	3072	1.73e-04	1.94	3.10e-03	1.94	1.14e-03	2.01	1.64e-03	1.89	1.00e-03	1.96	0.582
	24576	4.47e-05	1.95	7.85e-04	1.98	2.81e-04	2.02	4.30e-04	1.93	2.55e-04	1.98	0.569
	6	6.18e-03	–	3.78e-02	–	1.69e-02	–	2.28e-02	–	9.25e-03	–	0.579
	48	7.68e-04	3.01	6.43e-03	2.55	2.86e-03	2.56	3.46e-03	2.72	1.42e-03	2.70	0.648
2	384	1.01e-04	2.92	9.29e-04	2.79	4.05e-04	2.82	4.84e-04	2.84	1.96e-04	2.86	0.662
	3072	1.33e-05	2.93	1.26e-04	2.88	5.43e-05	2.90	6.54e-05	2.89	2.60e-05	2.92	0.665
	24576	1.71e-06	2.96	1.62e-05	2.96	8.40e-06	2.69	8.74e-06	2.90	3.31e-06	2.97	0.675
	6	1.31e-03	–	4.50e-03	–	1.71e-03	–	3.59e-03	–	6.72e-04	–	0.444
	48	8.11e-05	4.01	3.67e-04	3.62	1.40e-04	3.61	2.97e-04	3.59	5.80e-05	3.54	0.520
3	384	5.36e-06	3.92	2.65e-05	3.79	9.74e-06	3.85	2.13e-05	3.80	4.22e-06	3.78	0.533
	3072	3.51e-07	3.93	1.80e-06	3.88	6.43e-07	3.92	1.44e-06	3.89	2.86e-07	3.88	0.536
	24576	2.26e-08	3.96	1.16e-07	3.96	4.17e-08	3.95	9.52e-08	3.92	1.85e-08	3.95	0.549

Table 3.4: History of convergence of the terms composing the error estimator for the Example 3.3.1 ($\nu = 10^{-1}$). (Fuente: Elaboración propia)

k	N	N_{dof}	e_{L}	order	$\mathsf{e}_{\boldsymbol{u}}$	order	e_p	order
	6	168	1.24e-01	–	8.17e-02	–	2.97e-01	–
	48	1,128	6.00e-02	1.04	3.22e-02	1.35	8.46e-02	1.81
1	384	8,160	2.42e-02	1.31	1.02e-02	1.66	1.86e-02	2.18
	3,072	61,824	8.41e-03	1.52	3.19e-03	1.67	3.87e-03	2.27
	24,576	480,786	2.68e-03	1.65	9.85e-04	1.69	8.94e-04	2.11
	6	330	4.52e-02	–	3.29e-02	–	1.29e-01	–
	48	2,208	1.09e-02	2.05	5.27e-03	2.64	1.25e-02	3.36
2	384	15,936	2.04e-03	2.42	7.62e-04	2.79	1.18e-03	3.41
	3,072	120,576	3.49e-04	2.55	1.19e-04	2.68	1.26e-04	3.23
	24,576	936,960	5.49e-05	2.67	1.81e-05	2.71	1.49e-05	3.08
	6	546	1.11e-02	–	6.69e-03	–	2.81e-02	–
	48	3,648	1.10e-03	3.33	4.82e-04	3.79	9.26e-04	4.92
3	384	26,304	9.73e-05	3.50	3.44e-05	3.81	4.09e-05	4.50
	3,072	198,912	7.99e-06	3.61	2.63e-06	3.71	2.25e-06	4.19
	24,576	1,545,216	6.04e-07	3.73	1.94e-07	3.76	1.36e-07	4.04

Table 3.5: History of convergence of the error terms for the Example 3.3.1 ($\nu = 10^{-2}$). (Fuente: Elaboración propia)

k	N	η_1	order	η_2	order	η_3	order	η_4	order	η_5	order	eff
	6	1.32e-03	–	1.24e-01	–	5.60e-02	–	3.60e-02	–	1.58e-02	–	0.425
	48	3.68e-04	1.85	6.77e-02	0.87	3.12e-02	0.84	1.40e-02	1.36	8.09e-03	0.96	0.703
1	384	7.56e-05	2.28	2.32e-02	1.54	1.04e-02	1.59	3.09e-03	2.18	2.84e-03	1.51	0.800
	3,072	1.51e-05	2.32	7.08e-03	1.71	2.74e-03	1.92	6.67e-04	2.21	8.53e-04	1.73	0.783
	24,576	3.36e-06	2.17	2.14e-03	1.72	9.55e-04	1.52	1.61e-04	2.05	2.43e-04	1.81	0.790
	6	7.35e-04	–	6.69e-02	–	2.64e-02	–	1.48e-02	–	4.94e-03	–	0.524
	48	7.38e-05	3.32	1.63e-02	2.04	7.26e-03	1.86	2.07e-03	2.84	1.09e-03	2.17	1.031
2	384	7.70e-06	3.26	3.12e-03	2.38	1.37e-03	2.41	2.30e-04	3.17	1.98e-04	2.47	1.382
	3,072	9.22e-07	3.06	5.38e-04	2.54	2.30e-04	2.57	2.66e-05	3.11	3.34e-05	2.57	1.506
	24,576	1.21e-07	2.92	8.47e-05	2.67	3.58e-05	2.68	3.37e-06	2.98	5.19e-06	2.68	1.545
	6	1.66e-04	–	1.53e-02	–	6.62e-03	–	2.61e-03	–	8.04e-04	–	0.547
	48	6.78e-06	4.61	1.38e-03	3.47	6.21e-04	3.41	1.51e-04	4.11	7.00e-05	3.52	1.004
3	384	3.68e-07	4.20	1.21e-04	3.52	5.22e-05	3.57	9.21e-06	4.04	6.20e-06	3.50	1.189
	3,072	2.36e-08	3.96	1.01e-05	3.58	4.06e-06	3.69	5.92e-07	3.96	5.17e-07	3.58	1.251
	24,576	1.61e-09	3.87	7.76e-07	3.70	2.93e-07	3.79	3.96e-08	3.90	3.95e-08	3.71	1.282

Table 3.6: History of convergence of the terms composing the error estimator for the Example 3.3.1 ($\nu = 10^{-2}$). (Fuente: Elaboración propia)

3.3.2 A low regularity solution

Based on a numerical experiment presented in [37], we set $\Omega = (-1,1)\times(-1,1)\times(0,1)\setminus(0,1)\times(-1,0)\times(0,1)$, $\nu = 1$ and $\boldsymbol{\beta} = (1,-1,0)$. The source term $\boldsymbol{f}$ and the boundary data $\boldsymbol{u}_D$ are chosen such that the exact solution of the problem is given by $p(x_1,x_2,x_3) := 0$ and $\boldsymbol{u} := \left(\frac{\partial S}{\partial x_1}, \frac{\partial S}{\partial x_2}, 0\right)$, where S is given, in cylindrical coordinates, by $S(r,\phi) = r^{\frac{4}{3}}\sin\left(\frac{4}{3}\phi\right)$. We note that $\boldsymbol{u} \in H^{\frac{4}{3}-\epsilon}(\Omega)^3$, $\epsilon > 0$, due to a singularity located at x_3-axis. In Figure 3.1, we present the orders of convergence for e_h using

uniform and adaptive refinements, $\theta = 0.25$, for $k = 1$.

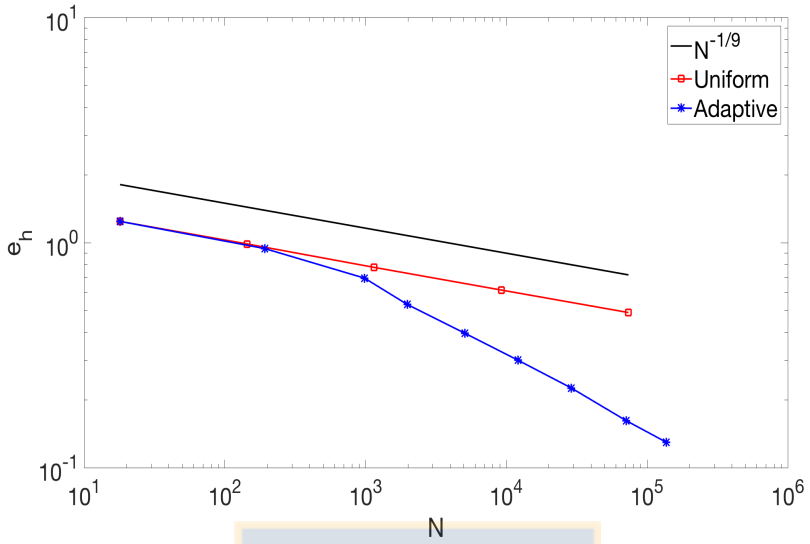

Figure 3.1: History of convergence for e_h with uniform and adaptive ($\theta = 0.25$) refinement, for $k = 1$, in the low regularity example. (Fuente: Elaboración propia)

We observe that the uniform refinement strategy provides an approximate solution that converges with the predicted order of convergence, $\mathcal{O}(h^{1/3})$, because the singularity of the velocity while the adaptive scheme let us achieve a better order of convergence and lower error magnitudes than the uniform case.

In Figure 3.2 we show the final adaptively refined mesh and how the mesh is locally refined near the corner line $x_1 = x_2 = 0$, where the gradient of the velocity has a singularity. We also show the isovalues of the velocity magnitude.

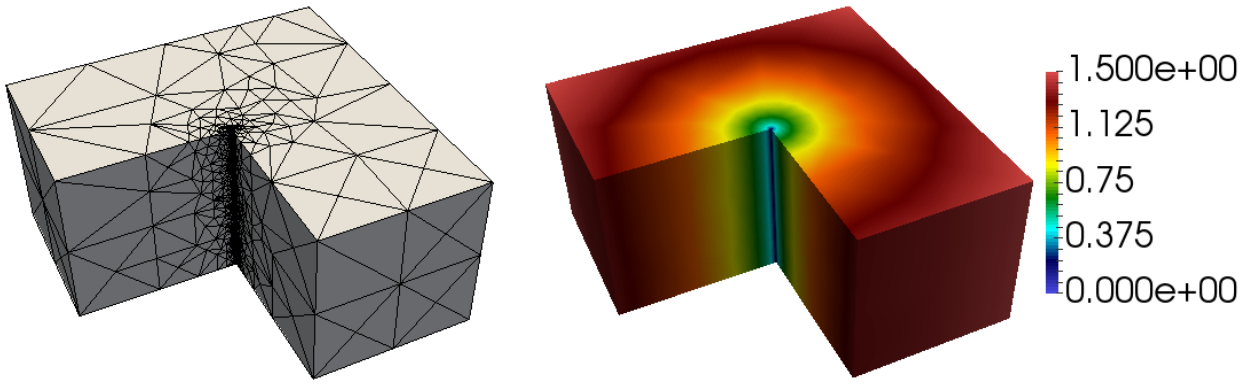

Figure 3.2: Final adaptive mesh (12,114 elements, $\theta = 0.25$) refinement ($k = 1$) and corresponding isovalues of the velocity magnitude, for the low regularity solution. (Fuente: Elaboración propia)

3.3.3 The lid-driven cavity problem

For this test, we consider $\Omega = (0,1)^3$ and set $\nu = 1$, $\boldsymbol{\beta} = (1,0,0)$, $\boldsymbol{f} = \mathbf{0}$ and $\boldsymbol{u}_D = (1,0,0)$, on $x_2 = 1$, and $\mathbf{0}$ on the rest of the boundary of Ω. Note that boundary layers arise at the edges of the top face of the domain, due to the discontinuities on the boundary condition. This fact is captured by our estimator by refining mainly in those edges as can be seen in Figure 3.3, where the initial and an adapted ($\theta = 0.25$) meshes are displayed. Figure 3.4 shows a cross-section at $z = 0.5$ of the same adapted mesh and the isovalues of the first component of the velocity.

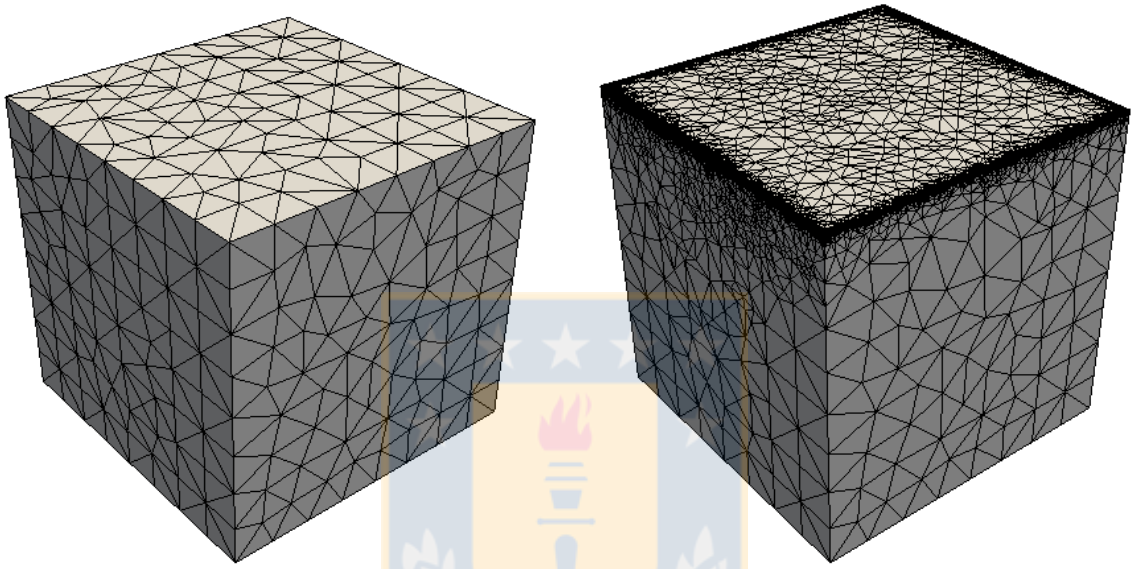

Figure 3.3: Initial mesh (2,255 elements) and final adapted mesh (270,941 elements) for the cavity problem ($k = 1,\ \theta = 0.25$). (Fuente: Elaboración propia)

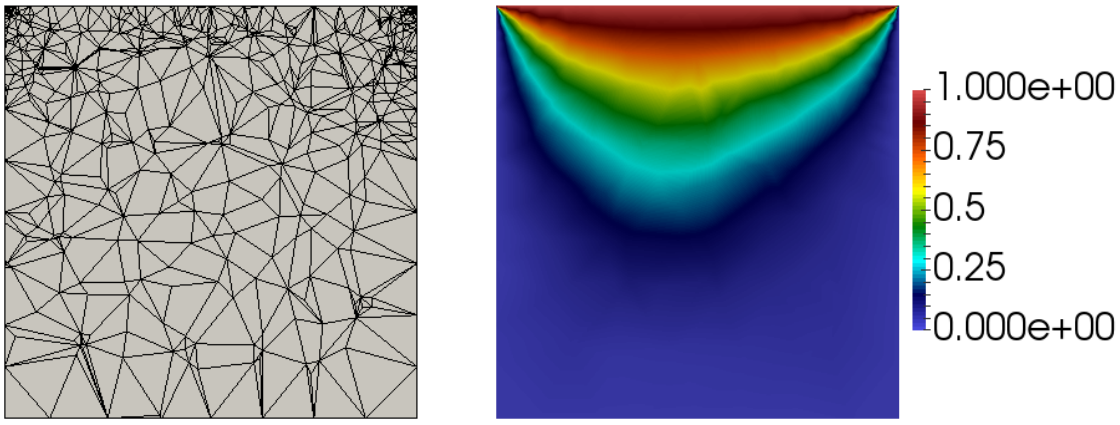

Figure 3.4: A vertical cut at $z = 0.5$ of the adapted mesh (270,941 elements, left) and the isovalues of the first component of the velocity in this mesh (right) at this cut ($k = 1,\ \theta = 0.01$). (Fuente: Elaboración propia)

3.3.4 An application to incompressible Navier–Stokes equations

As we said in the introduction, one of our motivations is to apply the proposed *a posteriori* error estimator to the Navier–Stokes equations, whose solution was constructed using a sequence on Oseen equations associated to a Picard's iteration. We consider $\Omega = (0,1)^3$ and choose the data $\boldsymbol{f}$ and $\boldsymbol{u}_D$ so that the exact solution is given by

$$\boldsymbol{u}(x_1,x_2,x_3) := (\exp(x_1)\sin(x_3), -\exp(x_1)\sin(x_3), \exp(x_1)\cos(x_3) - \exp(x_1)\cos(x_2))$$

and

$$p(x_1,x_2,x_3) := (1/2)\exp(2x_1) + (1/4)(\exp(2)-1).$$

We set $\nu = 1$ and consider the following algorithm to solve the incompressible Navier–Stokes equations:

(i) Solve $\mathrm{HDG}_{Oseen}(\mathbf{0})$ and set $\boldsymbol{\beta}_1 := \boldsymbol{u}_h^{*,0}$, where $\boldsymbol{u}_h^{*,0}$ is the postprocessed velocity (3.6) constructed by using the solution of $\mathrm{HDG}_{Oseen}(\mathbf{0})$.

(ii) For $i = 1, \ldots, I_{\max}$, if $\|\boldsymbol{u}_h^{*,i} - \boldsymbol{u}_h^{*,i-1}\| < \mathrm{tol}$, solve $\mathrm{HDG}_{Oseen}(\boldsymbol{\beta}_i)$ and set $\boldsymbol{\beta}_{i+1} := \boldsymbol{u}_h^{*,i}$, where $\boldsymbol{u}_h^{*,i}$ is the postprocessed velocity (3.6) constructed by using the solution of $\mathrm{HDG}_{Oseen}(\boldsymbol{\beta}_i)$.

Here, $\mathrm{HDG}_{Oseen}(\boldsymbol{\beta})$ is the HDG formulation with data $\boldsymbol{f}$, $\boldsymbol{u}_D$ and convective velocity $\boldsymbol{\beta}$; tol is the tolerance associated to the stopping criteria, $\|\cdot\|$ the Euclidean norm and $I_{\max}$ the maximum number of iterations. Let be $\boldsymbol{u}_h^{*,NS}$ the postprocessed velocity and L_h^{NS}, p_h^{NS} the solution of the Navier–Stokes equations obtained in (ii). Then, we will use L_h^{NS}, $\boldsymbol{u}_h^{*,NS}$, p_h^{NS} and $\boldsymbol{\beta} = \boldsymbol{u}_h^{*,NS}$ to compute our *a posteriori* error estimator for the error with respect to the solution $(\mathrm{L}_h^{NS}, \boldsymbol{u}_h^{*,NS}, p_h^{NS})$.

k	N	N_{sist}	e_{L}	order	$\mathsf{e}_{\boldsymbol{u}}$	order	e_p	order	iter
	6	168	$6.02E-01$	–	$2.10E-01$	–	$1.80E-01$	–	3
	48	1,128	$1.96E-01$	1.62	$6.35E-02$	1.73	$5.24E-02$	1.78	3
1	384	8,160	$5.60E-02$	1.81	$1.77E-02$	1.84	$1.29E-02$	2.02	3
	3,072	61,824	$1.49E-02$	1.91	$4.68E-03$	1.92	$3.18E-03$	2.03	4
	24,576	480,786	$3.84E-03$	1.96	$1.21E-03$	1.96	$7.89E-04$	2.01	4
	6	330	$7.83E-02$	–	$2.64E-02$	–	$2.77E-02$	–	3
	48	2,208	$1.33E-02$	2.56	$4.03E-03$	2.71	$3.79E-03$	2.87	3
2	384	15,936	$1.89E-03$	2.81	$5.51E-04$	2.87	$4.80E-04$	2.98	3
	3,072	120,576	$2.51E-04$	2.92	$7.18E-05$	2.94	$5.97E-05$	3.01	4
	24,576	936,960	$3.22E-05$	2.96	$9.17E-06$	2.97	$7.40E-06$	3.01	4
	6	546	$8.09E-03$	–	$2.59E-03$	–	$3.15E-03$	–	3
	48	3,648	$7.11E-04$	3.51	$2.05E-04$	3.66	$2.22E-04$	3.83	3
3	384	26,304	$5.09E-05$	3.80	$1.43E-05$	3.84	$1.43E-05$	3.96	3
	3,072	198,912	$3.31E-06$	3.94	$9.37E-07$	3.94	$8.97E-07$	3.99	4
	24,576	1,545,216	$2.15E-07$	3.97	$6.12E-08$	3.95	$5.62E-08$	3.99	4

Table 3.7: History of convergence of the error terms for the Example 3.3.4. (Fuente: Elaboración propia)

k	N	η_1	order	η_2	order	η_3	order	η_4	order	η_5	order	eff
	6	$7.21E-01$	–	$9.90E-02$	–	$4.20E-02$	–	$1.03E+00$	–	$1.33E-01$	–	1.915
	48	$2.02E-01$	1.83	$3.73E-02$	1.41	$1.74E-02$	1.27	$3.69E-01$	1.48	$4.27E-02$	1.64	1.998
1	384	$5.24E-02$	1.95	$1.10E-02$	1.77	$5.01E-03$	1.79	$1.06E-01$	1.80	$1.21E-02$	1.82	1.991
	3,072	$1.32E-02$	1.99	$2.92E-03$	1.91	$1.31E-03$	1.93	$2.83E-02$	1.91	$3.20E-03$	1.92	1.979
	24,576	$3.32E-03$	2.00	$7.51E-04$	1.96	$3.34E-04$	1.98	$7.28E-03$	1.96	$8.21E-04$	1.96	1.972
	6	$1.72E-01$	–	$1.87E-02$	–	$8.14E-03$	–	$1.71E-01$	–	$1.33E-02$	–	2.794
	48	$2.45E-02$	2.81	$3.24E-03$	2.52	$1.66E-03$	2.30	$3.11E-02$	2.46	$1.99E-03$	2.75	2.763
2	384	$3.17E-03$	2.95	$4.67E-04$	2.79	$2.48E-04$	2.74	$4.60E-03$	2.76	$2.68E-04$	2.89	2.767
	3,072	$4.00E-04$	2.99	$6.23E-05$	2.91	$3.36E-05$	2.89	$6.24E-04$	2.88	$3.48E-05$	2.95	2.784
	24,576	$5.02E-05$	3.00	$8.01E-06$	2.96	$4.37E-06$	2.94	$8.13E-05$	2.94	$4.42E-06$	2.97	2.798
	6	$2.82E-02$	–	$2.14E-03$	–	$9.76E-04$	–	$2.06E-02$	–	$1.01E-03$	–	3.860
	48	$2.03E-03$	3.80	$1.84E-04$	3.55	$9.63E-05$	3.34	$1.84E-03$	3.48	$7.66E-05$	3.72	3.554
3	384	$1.32E-04$	3.94	$1.30E-05$	3.82	$7.08E-06$	3.76	$1.29E-04$	3.83	$5.19E-06$	3.88	3.379
	3,072	$8.31E-06$	3.99	$8.33E-07$	3.97	$4.55E-07$	3.96	$8.31E-06$	3.96	$3.33E-07$	3.96	3.320
	24,576	$5.21E-07$	4.00	$5.30E-08$	4.01	$2.93E-08$	4.00	$5.31E-07$	3.99	$2.12E-08$	3.98	3.240

Table 3.8: History of convergence of the terms composing the error estimator for the Example 3.3.4. (Fuente: Elaboración propia)

Table 3.7 shows the history of convergence of the error of each variable with all the error terms converging with optimal order of $k+1$, exactly as the error estimates in [22] predicted. In addition, we display the number of iterations, iter, needed to get the solution of Navier–Stokes equations. In Table 3.8, we see that each term of the error estimator converge with order $k+1$ and, as for Oseen equations, the effectivity index remains bounded.

Conclusions and future work

Conclusions

In this thesis we developed HDG methods for a set of partial differential equations of physical interest in fluid mechanics. To be precise, we have designed a high order method for curved geometries and adaptive HDG methods. For the later, we introduced *a posteriori* error analyses applied to linear problems arising from fluid mechanics. In addition, we illustrate the performance of these methods with numerical examples.

The main conclusions of this work are:

1. We proposed a technique for high order approximation of boundary value problems in curved domains with mixed boundary conditions. We have provided numerical evidence suggesting that the technique performs properly if the family of transferring segments on each edge e is normal to e. A practical way to always satisfy this restriction is to define the computational boundary Γ_h by interpolating the true boundary Γ using piecewise linear segments. Moreover, we have extended this technique to elliptic interface problems where the interface is not necessarily polygonal. We have presented numerical results indicating that the orders of convergence are optimal for the errors in the scalar variable u and the flux $\boldsymbol{q}$ if the interface is interpolated by piecewise linear segments.

2. We introduced an HDG method for the velocity gradient-velocity-pressure formulation of the Brinkman problem and designed a local postprocessing of the approximated velocity suited for this problem. We established the corresponding *a priori* error estimates using a projection-based analysis, with projections whose design were inspired by the form of the numerical traces of the HDG method. We also introduced a residual-based *a posteriori* error estimator for the method and proved reliability and local efficiency results that are also valid fo the Stokes problem. In addition, we provided two-dimensional numerical experiments showing the behaviour of our scheme for uniform and adaptive refinement strategies.

3. We established an *a posteriori* error analysis for an HDG method applied to the Oseen problem. We used a weighted function technique to control the L^2-norm of the velocity and prove the reliability result in the absence of a reactive term in the Oseen equation. We also derived a local efficiency estimate. We employed the approximation properties of the Oswald interpolation operator to control the jumps of the velocity for both the Oseen and the Brinkman problems. Finally, we confirmed our theoretical results through numerical experiments in three dimensions.

Future work

The methods developed and results obtained in this thesis have motivated to several ongoing and future work. Some of them are described below:

1. ***A posteriori* error estimates for wave propagation models in diffraction gratings.** We are interested in carrying out an *a posteriori* error analysis for HDG methods applied to equations arising from the simulation of photovoltaic solar cells, characterized by periodic diffraction gratings.

2. ***A posteriori* error analysis for steady state incompressible Navier–Stokes equations.** As a natural extension of the third chapter of this thesis, we are interested in propose an *a posteriori* error estimator for the gradient-velocity-pressure formulation of the Navier–Stokes problem.

3. ***A posteriori* error analysis of HDG methods in fluid mechanics for curved domains.** As a combination between the transferring technique for Dirichlet boundary conditions and extrapolation technique for Neumann boundary conditions with the *a posteriori* error estimates obtained for HDG methods in polygonal domains, we are interested in developing high-order *a posteriori* error estimators for problems defined on curved geometries.

Conclusiones y trabajos futuros

Conclusiones

En esta tesis desarrollamos métodos HDG para un conjunto de ecuaciones diferenciales parciales de interés físico en mecánica de fluidos. Para ser precisos, diseñamos un método de alto orden para geometrías curvas y métodos HDG adaptivos. Para los últimos, introdujimos análisis de error *a posteriori* aplicados a problemas lineales que surgen de la mecánica de fluidos. Además, ilustramos el desempeño de dichos métodos con ejemplos numéricos.

Las principales conclusiones de este trabajo son:

1. Propusimos una técnica para aproximación de alto orden de problemas de valores de contorno en dominios curvos con condiciones de contorno mixtas. Hemos proporcionado evidencia numérica que sugiere que la técnica funciona correctamente si la familia de caminos es normal a la frontera computacional. Una forma práctica de satisfacer siempre esta restricción es definir la frontera computacional Γ_h interpolando la frontera real Γ por segmentos lineales por trozos. Además, extendimos esta técnica a problemas de interfaz elíptica donde la interfaz no es necesariamente poligonal. Ppresentamos resultados numéricos que indican que el orden de convergencia es óptimo para los errores en la variable escalar u y el flujo $\boldsymbol{q}$ si la interfaz es interpolada por segmentos lineales a trozos.

2. Introdujimos un método HDG para la formulación de gradiente de velocidad-velocidad-presión del problema de Brinkman y diseñamos un posprocesamiento local de la velocidad aproximada adecuado para este problema. Establecimos las estimaciones de error *a priori* correspondientes usando un análisis basado en proyecciones, cuyo diseño se inspiró en la forma de las trazas numéricas del método HDG. También introdujimos un estimador de error *a posteriori* basado en residuos y establecimos resultados de confiabilidad y eficiencia local que también son válidos para el problema de Stokes. Además, proporcionamos experimentos numéricos bidimensionales que muestran el comportamiento de nuestro esquema para estrategias de refinamiento uniformes y adaptivas.

3. Establecimos el análisis de error *a posteriori* para un método HDG aplicado al problema de Oseen. En ausencia de un término reactivo en la ecuación de Oseen usamos una técnica de función ponderada para controlar la norma L^2 de la velocidad y probar el resultado de confiabilidad. También derivamos una estimación de eficiencia local. Empleamos las propiedades de aproximación del operador de interpolación Oswald para controlar los saltos de la velocidad para los

problemas de Oseen y Brinkman. Finalmente, confirmamos nuestros resultados teóricos a través de experimentos numéricos en 3 dimensiones.

Trabajos futuros

Los métodos desarrollados y resultados obtenidos en esta tesis han motivado a varios trabajos en curso y futuros. Algunos de ellos se describen a continuación:

1. **Estimaciones de error *a posteriori* para modelos de propagación de ondas en rejillas de difracción**.
   Estamos interesados en llevar a cabo un análisis de error *a posteriori* para métodos HDG aplicados a ecuaciones que surgen de la simulación de celdas solares fotovoltaicas, caracterizadas por rejillas de difracción periódicas.

2. **Análisis de error *a posteriori* para las ecuaciones Navier–Stokes incompresibles en estado estacionario.**
   Como una extensión natural del tercer capítulo de esta tesis, nos interesa proponer un estimador de error *a posteriori* para la formulación gradiente-velocidad-presión del problema de Navier–Stokes.

3. **Análisis de error *a posteriori* de métodos HDG en mecánica de fluidos para dominios curvos.**
   Como una combinación entre la técnica de transferencia para las condiciones de contorno de Dirichlet y la técnica de extrapolación para las condiciones de contorno de Neumann con las estimaciones de error *a posteriori* obtenidas para métodos HDG en dominios poligonales, estamos interesados en desarrollar estimadores de error *a posteriori* de alto orden para problemas definidos en geometrías curvas.

Bibliography

[1] Ainsworth, M. A posteriori error estimation for discontinuous Galerkin finite element approximation. *SIAM J. Numer. Anal. 45* (2007), 1777–1798.

[2] Ainsworth, M., and Fu, G. Fully computable *a posteriori* error bounds for hybridizable discontinuous Galerkin finite element approximations. *J. Sci. Comput. 77* (2018), 443–466.

[3] Ainsworth, M., and Rankin, R. Fully computable error bounds for discontinuous Galerkin finite element approximations on meshes with an arbitrary number of levels of hanging nodes. *SIAM J. Numer. Anal. 47* (2010), 4112–4141.

[4] Araya, R., Solano, M., and Vega, P. Analysis of an adaptive HDG method for the Brinkman problem. *IMA J. Numer. Anal. dry031* (2018).

[5] Araya, R., Solano, M., and Vega, P. *A posteriori* error analysis of an HDG method for the Oseen problem. *Preprint 2018-40, Centro de Investigación en Ingeniería Matemática (CI²MA), Universidad de Concepción, Chile* (2018).

[6] Ayuso, B., and Marini, L. D. Discontinuous Galerkin methods for advection–diffusion–reaction problems. *SIAM J. Numer. Anal. 47* (2009), 1391–1420.

[7] Barrett, J. W., and Elliott, C. M. A finite–element method for solving elliptic equations with Neumann data on a curved boundary using unfitted meshes. *IMA J. Numer. Anal. 4* (1984), 309–325.

[8] Barrett, J. W., and Elliott, C. M. A practical finite element approximation of a semi–definite Neumann problem on a curved domain. *Numer. Math. 51* (1987), 23–36.

[9] Bebendorf, M. A note on the Poincaré inequality for convex domains. *Z. Anal. Anwendungen 22* (2003), 751–756.

[10] Becker, R., Hansbo, P., and Larson, M. G. Energy norm a posteriori error estimation for discontinuous Galerkin methods. *Comput. Methods Appl. Mech. Engrg. 192* (2003), 723–733.

[11] Braess, D., Fraunholz, T., and Hoppe, R. H. W. An equilibrated a posteriori error estimator for the interior penalty discontinuous Galerkin method. *SIAM J. Numer. Anal. 52* (2014), 2121–2136.

[12] Brenner, S. C. Two–level additive Schwarz preconditioners for nonconforming finite elements. In *Domain decomposition methods in scientific and engineering computing (University Park, PA, 1993)*, vol. 180 of *Contemp. Math.* Amer. Math. Soc., Providence, RI, 1994, pp. 9–14.

[13] Brinkman, H. C. A calculation of the viscous force exerted by a flowing fluid on a dense swarm of particles. *App. Sci. Res. A 1* (1947), 27–34.

[14] Burman, E., Claus, S., Hansbo, P., Larson, M. G., and Massing, A. CutFEM: Discretizing geometry and partial differential equations. *Internat. J. Numer. Methods Engrg. 104* (2015), 472–501.

[15] Burman, E., and Ern, A. An unfitted hybrid high–order method for elliptic interface problems. *SIAM J. Numer. Anal. 56* (2018), 1525–1546.

[16] Bustinza, R., Gatica, G. N., and Cockburn, B. An a posteriori error estimate for the local discontinuous Galerkin method applied to linear and nonlinear diffusion problems. *J. Sci. Comput. 22/23* (2005), 147–185.

[17] Bustinza, R., Lombardi, A., and Solano, M. An anisotropic *a priori* error estimate for a convection–dominated diffusion problem using the HDG method. *Preprint 2016-38, Centro de Investigación en Ingeniería Matemática (CI^{2}MA), Universidad de Concepción, Chile* (2016).

[18] Cantin, P., and Ern, A. Vertex-based compatible discrete operator schemes on polyhedral meshes for advection–diffusion equations. *Comput. Methods Appl. Math. 16* (2016), 187–212.

[19] Carstensen, C., Gudi, T., and Jensen, M. A unifying theory of a posteriori error control for discontinuous Galerkin FEM. *Numer. Math. 112* (2009), 363–379.

[20] Castillo, P. An a posteriori error estimate for the local discontinuous Galerkin method. *J. Sci. Comput. 22/23* (2005), 187–204.

[21] Cesmelioglu, A., Cockburn, B., Nguyen, N. C., and Peraire, J. Analysis of HDG methods for Oseen equations. *J. Sci. Comput. 55* (2013), 392–431.

[22] Cesmelioglu, A., Cockburn, B., and Qiu, W. Analysis of a hybridizable discontinuous Galerkin method for the steady–state incompressible Navier–Stokes equations. *Math. Comp. 86* (2017), 1643–1670.

[23] Chen, H., Li, J., and Qiu, W. Robust a posteriori error estimates for HDG method for convection–diffusion equations. *IMA J. Numer. Anal. 36* (2016), 437–462.

[24] Chen, Y., and Cockburn, B. Analysis of variable–degree HDG methods for convection-diffusion equations. Part I: general nonconforming meshes. *IMA J. Numer. Anal. 32* (2012), 1267–1293.

[25] Chen, Y., and Cockburn, B. Analysis of variable–degree HDG methods for convection-diffusion equations. Part II: Semimatching nonconforming meshes. *Math. Comp. 83* (2014), 87–111.

[26] Clément, P. Approximation by finite element functions using local regularization. *Rev. Française Automat. Informat. Recherche Opérationnelle Sér. 9* (1975), 77–84.

[27] Cochez-Dhondt, S., and Nicaise, S. Equilibrated error estimators for discontinuous Galerkin methods. *Numer. Methods Partial Differential Equations 24* (2008), 1236–1252.

[28] Cockburn, B., Dong, B., and Guzmán, J. A superconvergent LDG–hybridizable Galerkin method for second–order elliptic problems. *Math. Comp. 77* (2008), 1887–1916.

[29] Cockburn, B., Dong, B., Guzmán, J., Restelli, M., and Sacco, R. A hybridizable discontinuous Galerkin method for steady–state convection–diffusion–reaction problems. *SIAM J. Sci. Comput. 31* (2009), 3827–3846.

[30] Cockburn, B., and Ern, A. Bridging the hybrid high–order and hybridizable discontinuous Galerkin methods. *ESAIM: M2AN 50* (2016), 635–650.

[31] Cockburn, B., and Gopalakrishnan, J. The derivation of hybridizable discontinuous Galerkin methods for Stokes flow. *SIAM J. Numer. Anal. 47* (2009), 1092–1125.

[32] Cockburn, B., Gopalakrishnan, J., and Lazarov, R. D. Unified hybridization of discontinuous Galerkin, mixed, and continuous Galerkin methods for second order elliptic problems. *SIAM J. Numer. Anal. 47* (2009), 1319–1365.

[33] Cockburn, B., Gopalakrishnan, J., Nguyen, N. C., Peraire, J., and Sayas, F.-J. Analysis of HDG methods for Stokes flow. *Math. Comp. 80* (2011), 723–760.

[34] Cockburn, B., Gopalakrishnan, J., and Sayas, F.-J. A projection–based error analysis of HDG methods. *Math. Comp. 79* (2010), 1351–1367.

[35] Cockburn, B., Gupta, D., and Reitich, F. Boundary–conforming discontinuous Galerkin methods via extensions from subdomains. *SIAM J. Sci. Comput. 42* (2010), 144–184.

[36] Cockburn, B., Guzmán, J., and Wang, H. Superconvergent discontinuous Galerkin methods for second–order elliptic problems. *Math. Comp. 78* (2009), 1–24.

[37] Cockburn, B., Qiu, W., and Solano, M. A priori error analysis for HDG methods using extensions from subdomains to achieve boundary–conformity. *Math. Comp. 83* (2014), 665–699.

[38] Cockburn, B., and Sayas, F.-J. Divergence–conforming HDG methods for Stokes flows. *Math. Comp. 83* (2014), 1571–1598.

[39] Cockburn, B., Sayas, F.-J., and Solano, M. Coupling at a distance HDG and BEM. *SIAM J. Sci. Comput. 34* (2012), A28–A47.

[40] Cockburn, B., and Shu, C.-W. The local discontinuous Galerkin method for time–dependent convection–diffusion systems. *SIAM J. Numer. Anal. 35* (1998), 2440–2463.

[41] Cockburn, B., and Solano, M. Solving Dirichlet boundary–value problems on curved domains by extensions from subdomains. *SIAM J. Sci. Comput. 34* (2012), A497–A519.

[42] Cockburn, B., and Solano, M. Solving convection–diffusion problems on curved domains by extensions from subdomain. *J. Sci Comput. 59* (2014), 512–543.

[43] Cockburn, B., and Zhang, W. A posteriori error estimates for HDG methods. *J. Sci. Comput. 51* (2012), 582–607.

[44] Cockburn, B., and Zhang, W. A posteriori error analysis for hybridizable discontinuous Galerkin methods for second order elliptic problems. *SIAM J. Numer. Anal. 51* (2013), 676–693.

[45] Cockburn, B., and Zhang, W. An a posteriori error estimate for the variable–degree Raviart–Thomas method. *Math. Comp. 83* (2014), 1063–1082.

[46] Creusé, E., and Nicaise, S. A posteriori error estimator based on gradient recovery by averaging for discontinuous Galerkin methods. *J. Comput. Appl. Math. 234* (2010), 2903–2915.

[47] Creusé, E., and Nicaise, S. *A posteriori* error estimator based on gradient recovery by averaging for convection–diffusion–reaction problems approximated by discontinuous Galerkin methods. *IMA J. Numer. Anal. 33* (2013), 212–241.

[48] Daniele, D. P., and Ern, A. A hybrid high–order locking–free method for linear elasticity on general meshes. *Comput. Methods Appl. Mech. Engrg. 283* (2015), 1–21.

[49] Dauge, M. Stationary Stokes and Navier–Stokes systems on two– or three–dimensional domains with corners. Part I. Linearized equations. *SIAM J. Math. Anal. 20* (1989), 74–97.

[50] Deuring, P., Eymard, R., and Mildner, M. L^2-stability independent of diffusion for a finite element–finite volume discretization of a linear convection–diffusion equation. *SIAM J. Numer. Anal. 53* (2015), 508–526.

[51] Devinatz, A., Ellis, R., and Friedman, A. The asymptotic behavior of the first real eigenvalue of second order elliptic operators with a small parameter in the highest derivatives, II. *Indiana Univ. Math. J. 23* (1974), 991–1011.

[52] Di Pietro, D. A., and Ern, A. *Mathematical aspects of discontinuous Galerkin methods*, vol. 69 of *Mathématiques & Applications*. Springer–Verlag, Berlin–Heilderber, 2012.

[53] Dolejší, V., and Feistauer, M. *Discontinuous Galerkin method. Analysis and applications to compressible flow*, vol. 48 of *Springer Series in Computational Mathematics*. Springer, Cham, 2015.

[54] Dolejší, V., Šebestová, I., and Vohralík, M. Algebraic and discretization error estimation by equilibrated fluxes for discontinuous Galerkin methods on nonmatching grids. *J. Sci. Comput. 64* (2015), 1–34.

[55] Ern, A., and Guermond, J.-L. *Theory and Practice of Finite Elements*. Appl. Math. Sci. 159, Springer-Verlag, New York, 2004.

[56] Ern, A., and Guermond, J.-L. Finite element quasi–interpolation and best approximation. *ESAIM: M2AN 51* (2017), 1367–1385.

[57] Ern, A., Nicaise, S., and Vohralí k, M. An accurate $\mathbf{H}(\mathrm{div})$ flux reconstruction for discontinuous Galerkin approximations of elliptic problems. *C. R. Math. Acad. Sci. Paris 345* (2007), 709–712.

[58] Ern, A., Stephansen, A. F., and Vohralík, M. Guaranteed and robust discontinuous Galerkin a posteriori error estimates for convection–diffusion–reaction problems. *J. Comput. Appl. Math. 234* (2010), 114–130.

[59] Ern, A., and Vohralík, M. Flux reconstruction and a posteriori error estimation for discontinuous Galerkin methods on general nonmatching grids. *C. R. Math. Acad. Sci. Paris 347* (2009), 441–444.

[60] Ern, A., and Vohralík, M. Polynomial–degree–robust a posteriori estimates in a unified setting for conforming, nonconforming, discontinuous Galerkin, and mixed discretizations. *SIAM J. Numer. Anal. 53* (2015), 1058–1081.

[61] Fu, G., Jin, Y., and Qiu, W. Parameter–free superconvergent H(div)–conforming HDG methods for the Brinkman equations. *IMA J. Numer. Anal.* (2018), dry001.

[62] Fu, G., Qiu, W., and Zhang, W. An analysis of HDG methods for convection–dominated diffusion problems. *ESAIM: M2AN 49* (2015), 225–256.

[63] Fu, Z., Gatica, L. F., and Sayas, F.-J. Algorithm 949: Matlab tools for HDG in three dimensions. *ACM Trans. Math. Softw. 41* (2015), 20:1–20:21.

[64] Fung, Y. C. *Biomechanics: Circulation.* Plant Gene Research: Basic Knowledge. Springer New York, 1996.

[65] Gatica, G. N., and Sequeira, F. A. Analysis of an augmented HDG method for a class of quasi–Newtonian Stokes flows. *J. Sci. Comput. 65* (2015), 1270–1308.

[66] Gatica, G. N., and Sequeira, F. A. A priori and a posteriori error analyses of an augmented HDG method for a class of quasi–Newtonian Stokes flows. *J. Sci. Comput. 69* (2016), 1192–1250.

[67] Gatica, G. N., and Sequeira, F. A. Analysis of the HDG method for the Stokes–Darcy coupling. *Numer. Methods Partial Differential Equations 33* (2017), 885–917.

[68] Gatica, L. F., and Sequeira, F. A. A priori and a posteriori error analyses of an HDG method for the Brinkman problem. *Comput. Math. Appl. 75* (2018), 1191–1212.

[69] Giorgiani, G., Fernández-Méndez, S., and Huerta, A. Hybridizable discontinuous Galerkin with degree adaptivity for the incompressible Navier–Stokes equations. *Comput. & Fluids 98* (2014), 196–208.

[70] Girault, V., and Raviart, P.-A. *Finite element methods for Navier–Stokes equations. Theory and algorithms*, vol. 5 of *Springer Series in Computational Mathematics*. Springer-Verlag, Berlin, 1986.

[71] Griebel, M., and Klitz, M. Homogenization and numerical simulation of flow in geometries with textile microstructures. *Multiscale Model. Simul. 8* (2010), 1439–1460.

[72] Hansbo, A., and Hansbo, P. An unfitted finite element method, based on Nitsche's method, for elliptic interface problems. *Comput. Methods Appl. Mech. Engrg. 191* (2002), 5537 – 5552.

[73] Hansbo, P., Larson, M. G., and Zahedi, S. A cut finite element method for a Stokes interface problem. *Appl. Numer. Math. 85* (2014), 90 – 114.

[74] Houston, P., Schötzau, D., and Wihler, T. P. Energy norm a posteriori error estimation of *hp*–adaptive discontinuous Galerkin methods for elliptic problems. *Math. Models Methods Appl. Sci. 17* (2007), 33–62.

[75] Huynh, L. N. T., Nguyen, N. C., Peraire, J., and Khoo, B. C. A high–order hybridizable discontinuous Galerkin method for elliptic interface problems. *Int. J. Numer. Meth. Engng. 93* (2013), 183–200.

[76] Jin, Y. Local analysis of HDG methods for convection–dominated diffusion problems. *J. Comput. Appl. Math. 304* (2016), 57–72.

[77] Johansson, A., and Larson, M. G. A high order discontinuous Galerkin Nitsche method for elliptic problems with fictitious boundary. *Numer. Math. 123* (2013), 607–628.

[78] Karakashian, O. A., and Pascal, F. A posteriori error estimates for a discontinuous Galerkin approximation of second–order elliptic problems. *SIAM J. Numer. Anal. 41* (2003), 2374–2399.

[79] Karakashian, O. A., and Pascal, F. Convergence of adaptive discontinuous Galerkin approximations of second–order elliptic problems. *SIAM J. Numer. Anal. 45* (2007), 641–665.

[80] Kaya, T., and Goldak, J. Three–dimensional numerical analysis of heat and mass transfer in heat pipes. *Heat Mass Transfer 43* (2007), 775–785.

[81] Kellogg, R. B., and Osborn, J. E. A regularity result for the Stokes problem in a convex polygon. *J. Funct. Anal. 21* (1976), 397–431.

[82] Kovasznay, L. I. G. Laminar flow behind a two–dimensional grid. *Proc. Camb. Philos. Soc. 44* (1948), 58–62.

[83] Lazarov, R., Repin, S., and Tomar, S. K. Functional a posteriori error estimates for discontinuous Galerkin approximations of elliptic problems. *Numer. Methods Partial Differential Equations 25* (2009), 952–971.

[84] Lenoir, M. Optimal isoparametric finite elements and errors estimates form domains involving curved boundaries. *SIAM J. Numer. Anal. 23* (1986), 562–580.

[85] Li, X. *Principles of fuel cells.* Taylor & Francis, New York, 2005.

[86] Lovadina, C., and Marini, L. D. A posteriori error estimates for discontinuous Galerkin approximations of second order elliptic problems. *J. Sci. Comput. 40* (2009), 340–359.

[87] Nguyen, N. C., Peraire, J., and Cockburn, B. An implicit high–order hybridizable discontinuous Galerkin method for linear convection–diffusion equations. *J. Comput. Phys. 228* (2009), 3232–3254.

[88] Nguyen, N. C., Peraire, J., and Cockburn, B. An implicit high–order hybridizable discontinuous Galerkin method for nonlinear convection–diffusion equations. *J. Comput. Phys. 228* (2009), 8841–8855.

[89] Nguyen, N. C., Peraire, J., and Cockburn, B. A hybridizable discontinuous Galerkin method for Stokes flow. *Comput. Methods Appl. Mech. Engrg. 199* (2010), 582–597.

[90] Nguyen, N. C., Peraire, J., and Cockburn, B. An implicit high–order hybridizable discontinuous Galerkin method for the incompressible Navier–Stokes equations. *J. Comput. Phys. 230* (2011), 1147–1170.

[91] Oseen, C. W. *Über die Stoke'sche Formel und über eine verwandte Aufgabe in der Hydrodynamik.* Arkiv för matematik, astronomi och fysik. Almqvist & Wiksell, 1910.

[92] Oswald, P. On a BPX–preconditioner for P1 elements. *Computing 51* (1993), 125–133.

[93] Peraire, J., Nguyen, N. C., and Cockburn, B. A hybridizable discontinuous Galerkin method for the compressible Euler and Navier–Stokes equations. In *48th AIAA Aerospace Sciences Meeting Including the New Horizons Forum and Aerospace Exposition* (2010).

[94] Peraire, J., Nguyen, N. C., and Cockburn, B. A hybridizable discontinuous Galerkin method for the incompressible Euler and Navier–Stokes equations. In *48th AIAA Aerospace Sciences Meeting Including the New Horizons Forum and Aerospace Exposition* (2010).

[95] Qiu, W., and Shi, K. An HDG method for convection diffusion equation. *J. Sci. Comput. 66* (2016), 346–357.

[96] Qiu, W., and Shi, K. A superconvergent HDG method for the incompressible Navier–Stokes equations on general polyhedral meshes. *IMA J. Numer. Anal. 36* (2016), 1943–1967.

[97] Qiu, W., Solano, M., and Vega, P. A high order HDG method for curved–interface problems via approximation from straight triangulations. *J. Sci. Comput. 69* (2016), 1384–1407.

[98] Reed, W., and Hill, T. Triangular mesh methods for the neutron transport equation. *Technical Report LA-UR-73-479, Los Alamos Scientific Laboratory, United States* (1973).

[99] Rhebergen, S., and Wells, G. N. A hybridizable discontinuous Galerkin method for the Navier–Stokes equations with pointwise divergence-free velocity field. *J. Sci. Comput. 76* (2018), 1484–1501.

[100] Rivière, B., and Wheeler, M. F. A posteriori error estimates for a discontinuous Galerkin method applied to elliptic problems. Log number: R74. *Comput. Math. Appl. 46* (2003), 141–163.

[101] Si, H. Tetgen, a Delaunay–based quality tetrahedral mesh generator. *ACM Trans. Math. Softw. 41* (2015), 11:1–11:36.

[102] Stenberg, R. Postprocessing schemes for some mixed finite elements. *RAIRO Modél. Math. Anal. Numér. 25* (1991), 151–167.

[103] Verfürth, R. A posteriori error estimators for convection–diffusion equations. *Numer. Math. 80* (1998), 641–663.

[104] Verfürth, R. *A posteriori error estimation techniques for finite element methods.* Numerical Mathematics and Scientific Computation. Oxford University Press, Oxford, 2013.

[105] Zhu, L., Giani, S., Houston, P., and Schötzau, D. Energy norm a posteriori error estimation for *hp*–adaptive discontinuous Galerkin methods for elliptic problems in three dimensions. *Math. Models Methods Appl. Sci. 21* (2011), 267–306.